Title
Modeling and Simulation of Multifield Diffusion in Laminated Composites

Author
Klepach, Doron

Publication Date
2010

Peer reviewed|Thesis/dissertation

Modeling and Simulation of Multifield Diffusion in Laminated Composites

by

Doron Klepach

A dissertation submitted in partial satisfaction of the
requirements for the degree of
Doctor of Philosophy

in

Mechanical Engineering

in the

GRADUATE DIVISION
of the
UNIVERSITY OF CALIFORNIA, BERKELEY

Committee in charge:

Professor Tarek Zohdi, Chair
Professor David Steigmann
Professor Michael Frenklach
Professor Jon Wilkening

Fall 2010

Modeling and Simulation of Multifield Diffusion in Laminated Composites

Abstract

Modeling and Simulation of Multifield Diffusion in Laminated Composites

by

Doron Klepach

In this study an analytical and numerical modeling of the interaction between the process of diffusion and the mechanics of a solid are developed. It is then implemented on a fiber composite material, and several cases are simulated and analyzed. Starting with a free energy as a function of the deformation tensor and concentration, $\Psi(\mathbf{F}, \tilde{C})$, a constitutive model is derived for the strain energy function $\Psi_m(\mathbf{F})$, the coupled term of the free energy, $\Psi_{md}(\mathbf{F}, \tilde{C})$, and the diffusion part of the free energy, $\Psi_d(\tilde{C})$. With these terms we define the stress, the coupling terms, and the diffusion flux respectively. These are then used in the balance of mass, the balance of linear momentum and the continuity equation. The equations are discretized using a finite difference scheme for the time variable, and a nonlinear finite element method for the spatial variables. The coupling is implemented using a staggering methodology. The staggering scheme allows for easy implementation and provides a convenient framework. Several phenomena are modeled, for example, strain-dependent diffusivity, concentration based saturation, diffuso-elasticity and nonuniform diffusion induced swelling. The simulations involve various parametric studies including using different elastic strain energy functions, such as Kirchhoff Saint Venant. Moreover, the simulations are conducted for both isotropic and orthotropic materials where we explore such effects as free swelling, and combined mechanical loading and diffusion boundary conditions.

Contents

List of Figures

List of Tables

Acknowledgements

I would like to thank my adviser Prof. Tarek Zohdi for all the help and support throughout my studies and research in the pursuit of my Ph.D. degree. Your help is most appreciated and acknowledged. Also, a great help and advice was given to me by my lab mates Tim Kostka, Likchuan Lee. A special thanks goes to George Mseis, who helped me a lot with introducing me to coding in Fortran and in general help and advice.

I would like to thank the FAA (Research Grant 07-G-005), the U.S. ARMY (Prime Contract W911NF-07-2-0027, Subcontract 2007-CAL-2273-001), and the Powely Fund (Fund 37666, Dept. I.D. 11583) for the financial support toward my research.

Last, a special thanks goes to my family, my parents Jacob and Tammy, my brother Lior, and my wife Noga, for all the support and for believing in me. Of course, I include my son, Elai, who was born during of my Ph.D. studies. Your being gave me energy to keep going, and a better understanding of life.

Symbols

Notation

• Mechanics terms are denoted by $\square$ (no special notation).
• Diffusion terms are denoted by $\tilde{\square}$.

• A,B,C - Capital letters denote Reference configuration unless stated otherwise.
• a,b,c - Small letters usually denote the Current configuration unless stated otherwise.
• In some cases, the reference configuration is denoted by $\hat{\square}_{ref}$.
• The total time derivative is denoted by $\dot{\square}$, i.e. $\dot{a} = \frac{\partial a}{\partial t} + \frac{\partial a}{\partial \boldsymbol{x}} \cdot \boldsymbol{v} = \frac{\partial A}{\partial t}$. Where $a = a(\boldsymbol{x}, t) = A = A(\boldsymbol{X}, t)$.

Symbols

Math

$Div() = \frac{\partial ()}{\partial \mathbf{X}}$ - divergence with respect to $\mathbf{X}$
$div() = \frac{\partial ()}{\partial \mathbf{x}}$ - divergence with respect to $\mathbf{x}$
$Grad() = \frac{\partial ()}{\partial \mathbf{X}_I} \cdot \mathbf{E}_I$ - gradient with respect to $\mathbf{X}$
$grad() = \frac{\partial ()}{\partial \mathbf{x}_i} \cdot \mathbf{e}_i$ - gradient with respect to $\mathbf{x}$

Mechanics

$\boldsymbol{X}$ - position of a material point in the reference configuration.
$\mathbf{x} = \boldsymbol{x}(\boldsymbol{X}, t)$ - position of a material point in the current configuration.
$\mathbf{v} = \boldsymbol{v}(\boldsymbol{x}, t) = \bar{\boldsymbol{V}}(\boldsymbol{X}, t)$ - velocity of a material point.
$\mathbf{a} = \boldsymbol{a}(\boldsymbol{x}, t) = \bar{\boldsymbol{A}}(\boldsymbol{X}, t)$ - acceleration of a material point.
$\mathbf{u} = \boldsymbol{x} - \boldsymbol{X}$ - displacement of a material point.
$\mathbf{F} = Grad(\mathbf{x})$ - the deformation gradient.
$J = det(\mathbf{F}) = \frac{dv}{dV}$ - Jacobian of the deformation gradient
$\rho = \rho(\mathbf{x}, t) = \bar{\rho}(\boldsymbol{X}, t)$ - density of a material point in the current configuration.
$\rho_{ref} = \rho(\mathbf{X}, t) = \bar{\rho}(\boldsymbol{X}, t)$ - density of a material point in the current configuration.
m - mass of a body in the current configuration
$\mathbf{b} = \mathbf{b}(\mathbf{x}, t) = \mathbf{B}(\mathbf{X}, t)$ - body force acting on a material point.

$\mathbf{E}$ - Elasticity tensor.
$\sigma = \sigma(\boldsymbol{x}, t)$ - Cauchy's stress tensor.
$\mathbf{P}$ - First Piola Kirchhoff stress tensor.
$\mathbf{S}$ - Second Piola Kirchhoff stress.
$\mathbf{p}$ - Piola tractions in the reference configuration.
$\mathbf{t}$ - tractions in the current configuration.
$\mathbf{n}$ - unit normal vector in the current configuration
$\mathbf{N}$ - unit normal vector in the reference configuration
da - infinitesimal area element in the current configuration
dA - infinitesimal area element in the reference configuration

Diffusion

$\tilde{c} = \tilde{c}(\boldsymbol{x}, t)$ - concentration of constitute in the current configuration as a function of the current coordinates and time.
$\tilde{C} = \tilde{C}(\boldsymbol{X}, t)$ - concentration of constitute in the reference configuration as a function of the reference coordinates and time.
$\tilde{\boldsymbol{D}}$ - Diffusion coefficient tensor.
$\tilde{\boldsymbol{j}} = \tilde{\boldsymbol{j}}(\boldsymbol{x}, t) = \tilde{\boldsymbol{J}}(\boldsymbol{X}, t)$ - Diffusion flux.

Numerics

$\square_{\mathcal{I}}$ - index number for the nodes in the mesh
N_{en} - number of nodes
N_{el} - number of elements

General

Ψ_m - mechanical strain energy function
Ψ_{md} - internal energy function coupling the mechanics and diffusion
Ψ_d - internal energy function associated with the diffusion

Chapter 1

Introduction

The purpose of this work was to come up with both analytical and numerical models of a solid undergoing a process of *Diffusion* and finite deformations where the two are coupled. With that in hand, the models are used to simulate composite materials undergoing diffusion and deformation.

The coupling of diffusion and mechanics in general, and specifically of fiber composites has been of great interest to many scholars and researchers in the past few decades. A lot of work has been done analytically, numerically and experimentally. In terms of analytical work, The most relevant early work was done by Gibbs [1] and Biot [2] and the foundation for this topic is laid out. Following them, Truesdell [3] Green and Adkins [4], and Adkins ([5],[6]) have made major advancements in the field, where nonlinear diffusion and mechanics were incorporated into the theory. Later on, Aifantis et al. ([7],[8],[9]) did work on stress-assisted diffusion. A theory known as *Mixture theory* can model this coupling and interaction of diffusion and mechanics, and Rajagopal et al. [10] are very active in the development of this theory to solve problems such as the one defined here. In the last decade or so, there were recent theoretical advancements in nonlinear diffusion and mechanics that we found to be most relevant to this research. Baek and Srinivasa [11] came up with a more direct approach that deals with the problem and compared it with mixture theory, finding both theories to be comparable. Suo et al. did work on large deformations in gels [12], that came to good use in the development of the model in this research. In general, a good reference for basic and advanced subjects in diffusion can be found in [13] and [14]. In terms of numerics, a lot of recent studies using nonlinear finite elements were done, where different theories and aspects are examined. The swelling of gels were studied by Suo et al. [15, 16], and studies on fiber-composites were done by [17, 18, 19]. For more complex modeling, including damage and thermal effects, see Zohdi [20] and Duda [21]. We found limited experimental data that includes the material characteristics for coupling between diffusion and deformation. In the case of experimental data on the uncoupled diffusion characteristics in materials, several experimental studies were found to be of interest, and worth mentioning in this context. For studies on diffusion characteristics, coefficients and absorption in composites, see [22, 23, 24, 25, 26, 27, 28]. For degradation, damage and effects of diffusion on the mechanical behavior of composites, see [29, 30, 31, 32, 33, 34, 35]

It is assumed that the reader is familiar with *Continuum Mechanics*, and *Finite Elements*, and therefore, a short review of the subjects are provided, introducing the necessary tools needed for this work.

The layout of the chapters is as follows:

Chapter 2 Defines diffusion and lays out the governing equations for the flux, the mass balance of the of the diffusing substance.

Chapter 3 Consists of a short review of *Continuum Mechanics*, and with the use of chapter 2 defines the balance laws and governing equations for a solid undergoing deformations and diffusion.

Chapter 4 introduces the Constitutive modeling of the strain energy function, and the resulting coupling between mechanics and diffusion. Different models are developed in order to describe physical phenomena.

Chapter 5 provides the numerical formulation for solving the dynamic nonlinear coupled partial differential equations. The method of *Finite Elements* is reviewed in short, and applied. The weak formulation is presented, and a method of defining different materials in the solid is shown. Also an algorithm known as *Staggering Method* is introduced and used in order to solve for the coupling in the equations.

Chapter 6 In this chapter we show the results for several cases chosen. We show the differences between the models defined in Chapter 4 for both homogeneous materials, and non homogeneous materials (fiber composites). The results for stresses, strains and concentrations are shown on the 3-D plots, and scalar quantities such as mass, volume and energy are used to compare between the models.

Chapter 7 A summary of the work done is given, and the results are discussed. We explain briefly the analytical models defined, and the numerical methodologies used. We then go over the results, and discuss them and their significance.

Chapter 2

Diffusion

Diffusion in general occurs as particles move through space due to a difference in concentration, where that space may be occupied by a gas, liquid or solid.

It is important to note here, that even though ***Continuum Mechanics*** is introduced in the next chapter, we define some commonly used terms from *Continuum Mechanics* in this chapter as well (i.e. deformation, reference configuration etc.). The equations and definitions are written in a way that it fits the formulation of *Continuum Mechanics*.

In this chapter we review the classical work that was done in the continuum theory of diffusion, and comment about the changes that need to be made for the new theory. A more extensive review can be found in numerous books and online (i.e. see [13] , [14]). The mathematical formulation of diffusion describes the balance between the rate of change of the concentration with respect to time and the diffusion flux. In other words, flux in - flux out = rate of change in concentration . This approach, uses what is known as *Volume Control*, and does not take into account the deformation of the body. Let us first define the variables that take part in this theory,

$\tilde{c}(\mathbf{x}, t)$ - the concentration of the solute in the solid in the current configuration $[\frac{mole}{m^3}]$ or $[\frac{kg}{m^3}]$
$\tilde{\mathbf{D}}(\mathbf{x}, t)$ - the diffusivity tensor in the current configuration$[\frac{m^2}{sec}]$

$\tilde{\mathbf{j}}(\mathbf{x}, t)$ - the diffusion flux in the current configuration $[\frac{mole}{m^2 sec}]$ or $[\frac{kg}{m^2 sec}]$

$\tilde{C}(\mathbf{X}, t)$ - the concentration of the solute in the solid in the ref. configuration $[\frac{mole}{m^3}]$ or $[\frac{kg}{m^3}]$
$\tilde{\mathbf{D}}_{ref}(\mathbf{X}, t)$ - the diffusivity tensor in the reference configuration$[\frac{m^2}{sec}]$
$\tilde{\mathbf{J}}(\mathbf{X}, t)$ - the diffusion flux in the reference configuration $[\frac{mole}{m^2 sec}]$ or $[\frac{kg}{m^2 sec}]$

The most famous equations describing diffusion are known as ***Fick's laws of diffusion***, we state them here as a basis to the models that are developed.

2.1 Fick's laws of diffusion

Fick's laws of diffusion are a set of two equations. The first is a constitutive law that relates the flux to the concentration, and the second is the equation of continuity of the volume control, where the first law is plugged into that equation. Since there is no mentioning of configurations, we need to address the issue of weather the process takes place in the current or reference configuration. We assume that the process is taking place in the reference configuration.

2.1.1 Fick's first law

The first law describes how the diffusion flux is related to the change of concentration in space (assuming that there are no sources producing particles, i.e. chemical reactions).

$$\tilde{\mathbf{J}} = \tilde{\mathbf{D}} \cdot Grad(\tilde{C}) \qquad or \qquad \tilde{J}_I = \tilde{D}_{IJ} \frac{\partial \tilde{C}}{\partial X_J} \tag{2.1.1}$$

2.1.2 Fick's second law

We first consider a control volume, and mathematically formulate the continuity equation. As mentioned above, this is basically flux in - flux out = rate of change in concentration.

$$\frac{\partial \tilde{C}}{\partial t} = -Div(\tilde{\mathbf{J}}) = Div(\tilde{\mathbf{D}} \cdot grad(\tilde{C})) \qquad or \qquad \frac{\partial \tilde{c}}{\partial t} = -\frac{\partial \tilde{J}_I}{\partial X_I} = \frac{\partial}{\partial X_I}(\tilde{D}_{IJ} \frac{\partial \tilde{C}}{\partial X_J}) \tag{2.1.2}$$

Plugging eqn. (2.1.1) into (2.1.2), we get what is known as the Fick's second law. It describes how the change of concentration with respect to time is related to the divergence of the diffusivity tensor and the gradient of the concentration.

$$\frac{\partial \tilde{C}}{\partial t} = -Div(\tilde{\mathbf{J}}) = Div(\tilde{\mathbf{D}} \cdot grad(\tilde{C})) \qquad or \qquad \frac{\partial \tilde{c}}{\partial t} = -\frac{\partial \tilde{J}_I}{\partial X_I} = \frac{\partial}{\partial X_I}(\tilde{D}_{IJ} \frac{\partial \tilde{C}}{\partial X_J}) \tag{2.1.3}$$

Equation (2.1.3) is the governing field equation for the concentration. Solving that provides the change with time and spatial distribution of the concentration, $\tilde{C}(\mathbf{X}, t)$.

For the case, where the diffusivity tensor is fixed, i.e.

$$\tilde{\mathbf{D}} = \tilde{\mathbf{D}}_0 \qquad or \qquad \tilde{D}_{IJ} = \tilde{D}^0_{IJ} \tag{2.1.4}$$

we get

$$\frac{\partial \tilde{C}}{\partial t} = \tilde{\mathbf{D}}_0 \cdot \Delta(\tilde{C}) \tag{2.1.5}$$

where Δ denotes the *Laplace* operator.

Chapter 3

Continuum Mechanics

In this chapter we introduce the mathematical theory of *Continuum Mechanics* for a solid undergoing deformation and diffusion. It is assumed the the reader is familiar with classic *Continuum Mechanics* (i.e. see [36]), and that the basic concepts are well known. We lay out the equations and models needed to describe the coupled theory in the following manner:

-Kinematics
-Kinetics
-Balance Principles
-Material Models for hyper elasticity

3.1 Kinematics

Consider a body $\mathfrak{B}$ that occupies the region Ω_0 at time t_0. We define the configuration of the body at time t_0 as κ_0, also known as the *Reference Configuration*. At time t, the body occupies the region Ω, and holds a configuration κ, also known as the *Current Configuration* (see Fig. 3.1). A material point $P \in \mathfrak{B}$ can be identified by a position vector $\mathbf{X}$ in the *Reference Configuration* or by $\mathbf{x}$ in the *Current Configuration*. With the use of a mapping function χ we have $\mathbf{x} = \chi(\mathbf{X}, \mathbf{t})$ which gives a one to one mapping of any point P in the body between the *Current Configuration* and the *Reference Configuration*.

3.1.1 Nanson's formula

A very well-known and useful relationship between the reference and current elements of area and their normals known as Nanson's formula. Consider an element of area in the current configuration da with a unit normal $\mathbf{n}$ such that $\mathbf{n}da = d\mathbf{x} \times d\mathbf{y}$, and the same element of area in the reference configuration dA with a unit normal $\mathbf{N}$ such that $\mathbf{n}dA = d\mathbf{X} \times d\mathbf{Y}$. Plugging in that $d\mathbf{x} = \mathbf{F}d\mathbf{X}$ and $d\mathbf{y} = \mathbf{F}d\mathbf{Y}$ gives us

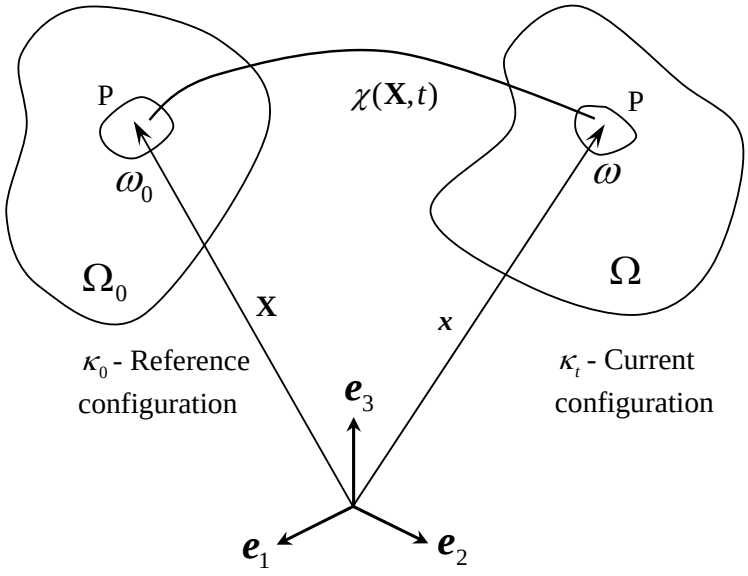

Figure 3.1: Configuration Plot

$$\mathbf{n}da = d\mathbf{x} \times d\mathbf{y} = \mathbf{F}d\mathbf{X} \times \mathbf{F}d\mathbf{Y} = J\mathbf{F}^{-T}d\mathbf{X} \times d\mathbf{Y} = J\mathbf{F}^{-T}\mathbf{N}dA \tag{3.1.1}$$

An illustration of this is shown in Fig. 3.2. With that in hand we can find relations between the current and reference unit normals, $\mathbf{n}$ and $\mathbf{N}$, and the elements of area da and dA. Taking the inner product of each side of the equation with itself gives us

$$\begin{aligned} &\mathbf{n}da \cdot \mathbf{n}da = da^2 \\ &J\mathbf{F}^{-T}\mathbf{N}dA \cdot J\mathbf{F}^{-T}\mathbf{N}dA = J^2dA^2\mathbf{N} \cdot \mathbf{F}^{-1}\mathbf{F}^{-T}\mathbf{N} = J^2dA^2\mathbf{N} \cdot \mathbf{C}^{-1}\mathbf{N} \end{aligned} \tag{3.1.2}$$

which gives us

$$da = JdA\ \sqrt{\mathbf{N} \cdot \mathbf{C}^{-1}\mathbf{N}} \quad or \quad da = JdA\ \sqrt{N_i C_{IJ}^{-1} N_J} \tag{3.1.3}$$

From that we can define the surface Jacobian J_s as

$$J_s \triangleq \frac{da}{dA} = J\ \sqrt{\mathbf{N} \cdot \mathbf{C}^{-1}\mathbf{N}} \quad or \quad J_s \triangleq \frac{da}{dA} = J\ \sqrt{N_i C_{IJ}^{-1} N_J} \tag{3.1.4}$$

3.2 Kinetics

In order to keep this chapter concise, we mention the concept and existence of stress tensor. In the current configuration we assign the Cauchy stress tensor with $\boldsymbol{\sigma}$, and

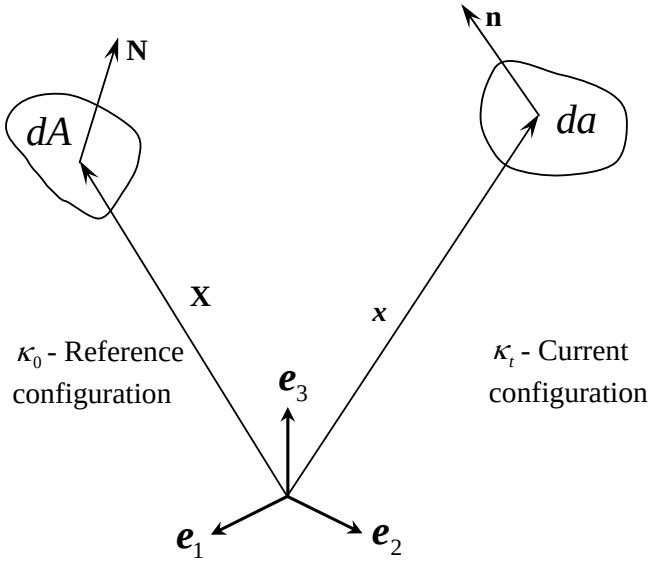

Figure 3.2: Element of area in the Reference and Current configurations

in the reference configuration we assign the First and Second Piola Kirchoff stresses with **P** and **S** respectfully. We state, without proving, the relationship between the stresses by

$$\mathbf{P} = J\boldsymbol{\sigma}\mathbf{F}^{-T} \quad or \quad P_{iA} = J\sigma_{ij}F^{-1}_{Aj} \tag{3.2.1}$$

and

$$\mathbf{P} = \mathbf{FS} \quad or \quad P_{iA} = F_{iB}S_{BA} \tag{3.2.2}$$

We also state the relationship between the traction vector **t** or **p**, the stress tensors and the normals. For the current configuration we have

$$\mathbf{t}(\mathbf{x}, t, \mathbf{n}) = \boldsymbol{\sigma}(\mathbf{x}, t)\mathbf{n} \quad or \quad t_i = \sigma_{ij}n_j \tag{3.2.3}$$

and for the reference configuration we have

$$\mathbf{p}(\mathbf{X}, t, \mathbf{N}) = \mathbf{P}(\mathbf{X}, t)\mathbf{N} \quad or \quad p_i = P_{iA}N_A \tag{3.2.4}$$

3.3 Balance Principles

3.3.1 Mass balance

In the current configuration the mass balance is as follows:

rate change of mass in the body = the flux of mass coming into the body

In our case the diffusion flux $\tilde{\mathbf{j}}$, and the mass flux are the same. The units for the diffusion flux is converted from $[\frac{mole}{m^2 sec}]$ to $[\frac{Kg}{m^2 sec}]$ by multiplying by the atomic weight (for a specific material).

$$\frac{dm}{dt} = \frac{d}{dt}\int_{\Omega} \rho \, d\Omega + \int_{\partial\Omega} \tilde{\mathbf{j}} \cdot \mathbf{n} \, da = 0 \tag{3.3.1}$$

Using *Reynolds Transport Theorem* on the volume integral

$$\frac{d}{dt}\int_{\Omega} \rho \, d\Omega = \int_{\Omega_0} \frac{d(\rho_{ref} J)}{dt} d\Omega_0 \tag{3.3.2}$$

Using *Reynolds Transport Theorem* and *Divergence theorem* on the surface integral

$$\int_{\partial\Omega} \tilde{\mathbf{j}} \cdot \mathbf{n} \, da = \int_{\partial\Omega_0} \tilde{\mathbf{J}} \cdot \mathbf{N} \, dA = \int_{\Omega_0} Div(\tilde{\mathbf{J}}) d\Omega_0 \tag{3.3.3}$$

where $\tilde{\mathbf{J}} = J\mathbf{F}^{-1}\tilde{\mathbf{j}}$ which results in

$$\int_{\Omega_0} \frac{d(\rho_{ref} J)}{dt} d\Omega_0 + \int_{\Omega_0} Div(\tilde{\mathbf{J}}) d\Omega_0 = 0 \tag{3.3.4}$$

Localizing yields

$$\frac{d(\rho_{ref} J)}{dt} + Div(\tilde{\mathbf{J}}) = 0 \tag{3.3.5}$$

with the use of (2.1.3) for the diffusion, we get

$$\frac{d(\rho_{ref} J)}{dt} - \frac{\partial \tilde{C}}{\partial t} = 0 \tag{3.3.6}$$

Since all the variables are in terms of the reference configuration coordinates $\mathbf{X}$ and time, t, the partial time differentiation $(\frac{\partial()}{\partial t})$ is the same as the total time differentiation $(\frac{d()}{dt})$. Integrating with respect to time, and setting $J = 1$ at time $t = t_0 = 0$, we get

$$\rho_{ref}(\mathbf{X}, t)J - \rho_{ref}(\mathbf{X}, t = 0)1 = \tilde{C}(\mathbf{X}, t) - \tilde{C}(\mathbf{X}, t = 0) \tag{3.3.7}$$

Rearranging, and naming $\rho_{ref}(\mathbf{X}, t = 0) = \rho_0$ and $\tilde{C}(\mathbf{X}, t = 0) = \tilde{C}_0$, we get

$$\rho_{ref}(\mathbf{X}, t) = \frac{1}{J}(\rho_0 + \tilde{C}(\mathbf{X}, t) - \tilde{C}_0) \tag{3.3.8}$$

which is the local form of the mass balance in the reference configuration.

3.3.2 Balance of linear momentum

We start off with a body subjected to external body forces **b** and surface tractions **t** as shown in Fig. 3.3

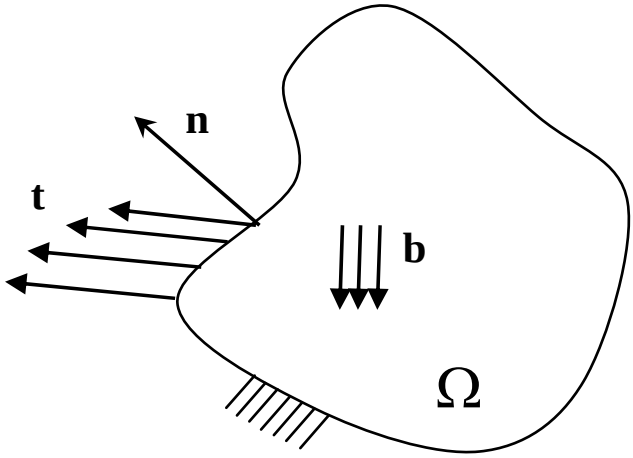

Figure 3.3: Balance of linear momentum for a body in the current configuration

Similar to the balance on a particle, where $\mathbf{F} = M\mathbf{a}$, we have

$$\int_{\partial\Omega} \mathbf{t}\, da + \int_{\Omega} \rho\, \mathbf{b}\, d\Omega = \frac{d}{dt} \int_{\Omega} \rho\, \mathbf{v}\, d\Omega \tag{3.3.9}$$

with the use of the divergence theorem, we get

$$\int_{\partial\Omega} \mathbf{t}\, da = \int_{\partial\Omega} \boldsymbol{\sigma} \cdot \mathbf{n}\, da = \int_{\Omega} div(\boldsymbol{\sigma})\, d\Omega \tag{3.3.10}$$

with the use of the Reynold's theorem, we get

$$\int_{\Omega} div(\boldsymbol{\sigma})\, d\Omega = \int_{\Omega_0} Div(\mathbf{P})\, d\Omega_0 \tag{3.3.11}$$

$$\int_{\Omega} \rho\, \mathbf{b}\, d\Omega = \int_{\Omega_0} \rho_{ref}\, \mathbf{b}_{ref}\, d\Omega_0 \tag{3.3.12}$$

$$\frac{d}{dt} \int_{\Omega} \rho\, \mathbf{v}\, d\Omega = \frac{d}{dt} \int_{\Omega_0} \rho_{ref}\, \mathbf{v}_{ref}\, d\Omega_0 = \int_{\Omega_0} \rho\, \dot{\mathbf{v}}\, d\Omega_0 = \int_{\Omega_0} \rho\, \ddot{\mathbf{u}}\, d\Omega_0 \tag{3.3.13}$$

which gives the *reference form* of the balance of linear momentum

$$\int_{\Omega_0} Div(\mathbf{P})\, d\Omega_0 + \int_{\Omega_0} \rho_{ref}\, \mathbf{b}_{ref} d\Omega_0 = \int_{\Omega_0} \rho_{ref}\, \ddot{\mathbf{u}} d\Omega_0 \tag{3.3.14}$$

localizing this gives

$$Div(\mathbf{P}) + \rho_{ref}\, \mathbf{b}_{ref} = \rho_{ref}\, \ddot{\mathbf{u}} \tag{3.3.15}$$

3.3.3 Balance of angular momentum

The derivation of the final result can be found in numerous books on continuum mechanics. In an effort to keep this chapter concise, we state the final result for this balance, which is

$$\sigma = \sigma^T \tag{3.3.16}$$

or for the reference configuration we have

$$\mathbf{S} = \mathbf{S}^T \tag{3.3.17}$$

3.4 Material Models for hyper elasticity

We introduce here several material models that are relevant to the work done here. These models work well for large deformations, and are extended to include the effects of diffusion further on in here.

3.4.1 Kirchhoff Saint-Venant

Considering an elastic material, one of the most famous models is that of Kirchhoff Saint-Venant. This model is a direct extension the linear Hooke's law. The strain energy is given by

$$\Psi(\mathbf{E}) = \frac{1}{2}\mathbf{E} : \mathbb{E} : \mathbf{E} \qquad or \qquad \Psi(\mathbf{E}) = \frac{1}{2} E_{IJ} \mathbb{E}_{IJKL} E_{KL} \tag{3.4.1}$$

which gives

$$\mathbf{S} = \mathbb{E} : \mathbf{E} \qquad or \qquad S^m_{IJ} = \mathbb{E}_{IJKL} E_{KL} \tag{3.4.2}$$

3.4.2 General isotropic hyper elastic material

For an isotropic hyper-elastic material, it is possible to show that the strain energy is a function of the invariants of $\mathbf{C} = \mathbf{F}^T \cdot \mathbf{F}$, so in general

$$\Psi(\mathbf{C}) = \Psi(I_1(\mathbf{C}), I_2(\mathbf{C}), I_3(\mathbf{C})) \tag{3.4.3}$$

where

$$\begin{aligned} I_1(\mathbf{C}) &= \mathbf{C}\cdot\mathbf{I} = tr(\mathbf{c}) = C_{AA} \\ I_2(\mathbf{C}) &= \frac{1}{2}(I_{\mathbf{C}}^2 - tr(\mathbf{C}^2)) = \frac{1}{2}(I_{\mathbf{C}}^2 - tr(C_{AM}C_{MA})) \\ I_3(\mathbf{C}) &= det(\mathbf{C}) \end{aligned} \tag{3.4.4}$$

With that, is possible to derive a general form of the Second Piola stress. The formulations is as follows

$$\mathbf{S} = 2\frac{\partial\Psi(\mathbf{C})}{\partial\mathbf{C}} = 2[(\frac{\partial\Psi}{\partial I_1} + I_1\frac{\partial\Psi}{\partial I_2\mathbf{C}})\mathbf{I} - \frac{\partial\Psi}{\partial I_2}\mathbf{C} + I_3\frac{\partial\Psi}{\partial I_3}\mathbf{C}^{-1}] \tag{3.4.5}$$

3.4.3 General transversely isotropic hyper elastic material

When considering a material composed of a *matrix* and *fibers* with a reference direction **M**, it can be shown that there are two invariants on top of the three already defined in the last subsection. Theses are defined by

$$\begin{aligned} I_4(\mathbf{C},\mathbf{M}) &= \mathbf{M}\cdot\mathbf{C}\mathbf{M} = M_A C_{AB} M_B \\ I_5(\mathbf{C},\mathbf{M}) &= \mathbf{M}\cdot\mathbf{C}^2\mathbf{M} = M_B C_{BA} C_{AB} M_B \end{aligned} \tag{3.4.6}$$

with this we define the strain energy by

$$\Psi(\mathbf{C},\mathbf{M}\otimes\mathbf{M}) = \Psi(I_1(\mathbf{C}), I_2(\mathbf{C}), I_3(\mathbf{C}), I_4(\mathbf{C},\mathbf{m}), I_5(\mathbf{C},\mathbf{M})) \tag{3.4.7}$$

With that, is possible to derive a general form of the Second Piola stress for the transversely isotropic material. The formulations is as follows

$$\mathbf{S} = 2\frac{\partial\Psi(\mathbf{C})}{\partial\mathbf{C}} = 2[(\frac{\partial\Psi}{\partial I_1} + I_1\frac{\partial\Psi}{\partial I_2\mathbf{C}})\mathbf{I} - \frac{\partial\Psi}{\partial I_2}\mathbf{C} + I_3\frac{\partial\Psi}{\partial I_3}\mathbf{C}^{-1} + \frac{\partial\Psi}{\partial I_4}\mathbf{M}\otimes\mathbf{M} + \frac{\partial\Psi}{\partial I_5}(\mathbf{M}\otimes\mathbf{C}\mathbf{M} + \mathbf{M}\mathbf{C}\otimes\mathbf{M})] \tag{3.4.8}$$

Chapter 4

Constitutive modeling

With the definitions and equations describing the *diffusion* and deformations for a solid body, in order to fully define the mathematical equations, there is a need for constitutive modeling. Given the form of the strain energy function in chapter [3] for a hyper-elastic material we extend that definition to include the effects of diffusion. With the use of *Thermodynamics* in a similar manner to [12] we define and construct the structure of the energy function.

$$\Psi(\mathbf{E}, \tilde{C}) = \Psi_m(\mathbf{E}) + \Psi_{md}(\mathbf{E}, \tilde{C}) + \Psi_d(\tilde{C}) \tag{4.0.9}$$

where $\Psi_m(\mathbf{E})$ stands for the purely mechanical strain energy function, $\Psi_{md}(\mathbf{E}, \tilde{C})$ stand for the internal energy function that couples the mechanics and diffusion, and $\Psi_d(\tilde{C})$ stands for the purely diffusional internal energy function. This leads to the following stresses and chemical potentials definitions

$$\mathbf{S} = \frac{\partial \Psi(\mathbf{E}, \tilde{C})}{\mathbf{E}} \qquad or \qquad S_{IJ} = \frac{\partial \Psi(\mathbf{E}, \tilde{C})}{E_{IJ}} \tag{4.0.10}$$

and

$$\tilde{\mu} = \frac{\partial \Psi(\mathbf{E}, \tilde{C})}{\tilde{C}} \tag{4.0.11}$$

where the total stress $\mathbf{S}$ is a combination of two stresses $\mathbf{S}_m$ and $\mathbf{S}_d$ that are derived from the purely mechanical, and the coupled energy functions $\Psi_m(\mathbf{E})$, and $\Psi_{md}(\mathbf{E}, \tilde{C})$ respectively. The stresses are defined by

$$\mathbf{S} = \mathbf{S}_m + \mathbf{S}_d \quad or \quad S_{IJ} = S^m_{IJ} + S^d_{IJ} \tag{4.0.12}$$

where

$$\mathbf{S}_m = \frac{\partial \Psi_m(\mathbf{E})}{\mathbf{E}} \quad or \quad S^m_{IJ} = \frac{\partial \Psi_m(\mathbf{E})}{E_{IJ}} \tag{4.0.13}$$

and

$$\mathbf{S}_d = \frac{\partial \Psi_{md}(\mathbf{E}, \tilde{C})}{\mathbf{E}} \quad or \quad S^d_{IJ} = \frac{\partial \Psi_{md}(\mathbf{E}, \tilde{C})}{E_{IJ}} \tag{4.0.14}$$

Also, the total chemical potential $\tilde{\mu}$ is a combination of two potentials $\tilde{\mu}_m$ and $\tilde{\mu}_d$ that are derived from the coupled and the purely diffusional energy functions $\Psi_{md}(\mathbf{E}, \tilde{C})$, and $\Psi_d(\tilde{C})$ respectively. The potentials are defined by

$$\tilde{\mu} = \tilde{\mu}_m + \tilde{\mu}_d \tag{4.0.15}$$

where

$$\tilde{\mu}_m = f(\Psi_{md}) \tag{4.0.16}$$

and

$$\tilde{\mu}_d = \frac{\partial \Psi_d(\tilde{C})}{\tilde{C}} \tag{4.0.17}$$

We start with the basic uncoupled equations, and extended the modeling from that. For example, for the mechanics, we pick a Kirchoff - St. Venant material with

$$\Psi_m(\mathbf{E}) = \frac{1}{2}\mathbf{E} : \mathbb{E} : \mathbf{E} \qquad or \qquad \Psi_m(\mathbf{E}) = \frac{1}{2} E_{IJ} \mathbb{E}_{IJKL} E_{KL} \tag{4.0.18}$$

This gives us a linear relation for the second Piola Stress and the Lagrange strain

$$\mathbf{S}_m = \mathbb{E} : \mathbf{E} \qquad or \qquad S^m_{IJ} = \mathbb{E}_{IJKL} E_{KL} \tag{4.0.19}$$

For the diffusion, we start with the a constitutive law similar to the classic Fick's diffusion equations (2.1.1) and (2.1.3)

$$\tilde{\mathbf{J}} = \tilde{\mathbf{D}}_{ref} \cdot Grad(\tilde{\mu}_d) + \mathbf{f}(\tilde{\mu}_m) \quad or \quad \tilde{J}_I = \tilde{D}^{ref}_{IJ} \frac{\partial \tilde{\mu}_d}{\partial X_J} + f_I(\tilde{\mu}_m) \tag{4.0.20}$$

$$\frac{\partial \tilde{C}}{\partial t} = -Div(\tilde{\mathbf{J}}) = Div(\tilde{\mathbf{D}} \cdot Grad(\tilde{\mu}_d) + \mathbf{f}(\tilde{\mu}_m)) \quad or \quad \frac{\partial \tilde{C}}{\partial t} = -\frac{\partial \tilde{J}_I}{\partial X_I} = \frac{\partial}{\partial x_I}(\tilde{D}_{IJ} \frac{\partial \tilde{\mu}}{\partial X_J} + f_I(\tilde{\mu}_m)) \tag{4.0.21}$$

We lay out different constitutive models for the coupling of these equations. One intuitive way of thinking about the constitutive modeling of a solid undergoing deformation and diffusion is to consider a sponge in water. One can think of different changes in the deformation and diffusion that occur. We introduce here several physical phenomena that come out naturally from simple observations and thought experiments.

4.1 Strain dependent diffusivity

Consider a sponge in the reference, stress-free configuration. In one experiment the sponge is just submerged into a tank full of water, and water diffuses into the sponge. In a second experiment the sponge is first compressed and is submerged into a tank of water while being kept compressed. It seems intuitive that the diffusion process is different in the two experiments. For certain materials, the time it takes for the sponge to become fully saturated would differ from the first and the second experiment. In other words, water will diffuse faster or slower in the second experiment than the first. This leads to the assumption that the diffusivity tensor, $\tilde{\mathbf{D}}$ is a function of the deformation in general, and to be more specific, a function of the volume change or surface area change.
We consider the following cases, volume change dependence, and surface area change dependence.

4.1.1 Volume dependent diffusivity

In general, we assume

$$\tilde{\mathbf{D}} = \tilde{\mathbf{D}}(J) \tag{4.1.1}$$

If we consider extreme cases, we get some limits on $\tilde{\mathbf{D}}(J)$. For example, if we compress the sponge into a point, it is reasonable to assume that the diffusivity will decrease to zero, meaning that the sponge will not be able to diffuse any water as it does not have a volume anymore. As the volume increases, the magnitude of the diffusivity will grow, reaching the nominal value $\tilde{\mathbf{D}}_0$ when the volume is the same as the reference configuration ($J = 1$). As the volume increases to values larger than of the reference configuration, the diffusivity grows. In terms of a function, we require that $\tilde{\mathbf{D}}(J = 0) = \mathbf{0}$, $\tilde{\mathbf{D}}(J = 1) = \tilde{\mathbf{D}}_0$. The actual values are material dependent, and can be found experimentally. We also assume that the function is smooth and continuous. One option for this function is the following:

$$\tilde{\mathbf{D}}(J) = \tilde{\mathbf{D}}_0 \frac{e^{aJ} - 1}{e^a - 1} \tag{4.1.2}$$

This is basically a scaling for the e^J such that $\tilde{\mathbf{D}}(J = 0) = \mathbf{0}$, and $\tilde{\mathbf{D}}(J = 1) = \mathbf{D}_0$. The reasoning behind this formulation is that as the volume of the material point approaches zero, the diffusivity should approach zero as well. At the micro level, as the material becomes more and more condensed, there is less ”room” for the solute (i.e. water) to diffuse. For the case where there are no deformations, the diffusivity tensor scale to its initial value $\tilde{\mathbf{D}}_0$. The plot for eqn. (4.1.1) can be seen in Fig. (4.1.2).

4.2 Swelling

When a dry sponge is placed in contact with water (i.e. submerged), it swells up. It is considered here that swelling deformations will not cause any stress at the local level. This is known as ”free swelling”. To be more specific, similar to theories in

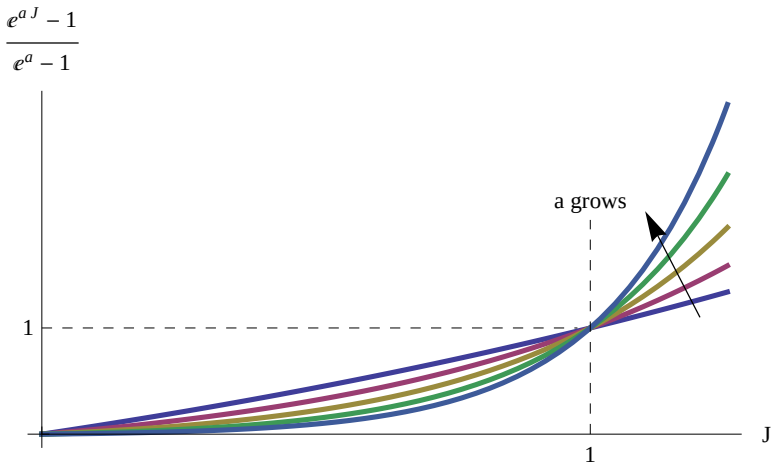

Figure 4.1: Volume dependent Diffusivity

Thermo-elasticity, let us consider that for an isotropic homogeneous solid that is under no mechanical loads, the swelling deformation due to diffusion will not cause any stresses. In terms of the modeling, we have considered two approaches to model this in the theory: *uniform swelling* and *non uniform swelling*. **It is important to mention here, that this is not anisotropic diffusivity, or purely anisotropic mechanical stiffness, it is non uniform swelling that causes diffusion induced non uniform stress**. This model allows for the material to have an isotropic diffusivity tensor and isotropic mechanical stiffness, and therefore isotropic diffusion and isotropic mechanical response, but, at the same time have non uniform swelling and stresses due to the diffusion.

Uniform swelling

This model is taken to be similar to linear thermo-elasticity, but for finite deformations (i.e. see [20])

$$\Psi_m(\mathbf{E}) = \frac{1}{2}\mathbf{E} : \mathbb{E} : \mathbf{E} \quad or \quad \Psi_m(\mathbf{E}) = \frac{1}{2}E_{IJ}\mathbb{E}_{IJKL}E_{KL} \tag{4.2.1}$$

and

$$\Psi_{md}(\mathbf{E}, \mathbf{E}_C) = -\frac{1}{2}\mathbf{E}_C : \mathbb{E} : \mathbf{E} \quad or \quad \Psi_m(\mathbf{E}, \mathbf{E}_C) = -\frac{1}{2}E^C_{IJ}\mathbb{E}_{IJKL}E_{KL} \tag{4.2.2}$$

where $\mathbf{E}_C$ stands for the strains due to the concentration. A simple linear model is

$$\mathbf{E}_C = \beta(\tilde{C} - \tilde{C}_0)\mathbb{E} : \mathbf{I} \tag{4.2.3}$$

where $\tilde{C}_0$ is a material initial concentration that causes a change in the internal energy, and β is a material constant that controls the magnitude of the energy/stress resulting from the

swelling (similar to $\alpha\kappa$ in thermo-elasticity). Differentiating with respect to $\mathbf{E}$ gives us the Second Piola-Kirchoff Stress

$$\frac{\partial \Psi_m}{\partial \mathbf{E}} + \frac{\partial \Psi_{md}}{\partial \mathbf{E}} = \mathbf{S} = \mathbb{E} : (\mathbf{E} - \mathbf{E}_C) = \mathbb{E} : (\mathbf{E} - \beta(\tilde{C} - \tilde{C}_0)\mathbf{I}) \tag{4.2.4}$$

For the potential, $\tilde{\mu}$, we have

$$\frac{\partial \Psi_d}{\partial \tilde{C}} + f(\Psi_{md}) = \tilde{\mu} = a\tilde{C} \tag{4.2.5}$$

where a is a constant taken to be equal to 1.

Nonuniform swelling

In this model, it is assumed the solid swells up differently in different directions. Specifically, it has favored directions to which it will swell up in (i.e. fibers). We define β as a material constant, and $\mathbf{M}$ is a unit vector normal to the plane of isotropy (i.e. $\mathbf{M}$ is in the direction of the fibers in a fiber-composite material). We assume that the material will swell up in any direction normal to the fiber direction, so we use the projection tensor $\mathbf{I} - \mathbf{M} \otimes \mathbf{M}$. With that, we define the internal energy as

$$\Psi_{md}(\mathbf{E}, \tilde{C}) = -\frac{1}{2}\beta(\tilde{C} - \tilde{C}_0)(\mathbf{I} - \mathbf{M} \otimes \mathbf{M}) : \mathbb{E} : \mathbf{E} \quad or \quad \Psi_{md}(\mathbf{E}, \tilde{C}) = -\frac{1}{2}\beta(\tilde{C} - \tilde{C}_0)(\delta_{IJ} - M_I M_J)\mathbb{E}_{IJKL}E_{KL} \tag{4.2.6}$$

Differentiating with respect to $\mathbf{E}$ gives

$$\frac{\partial \Psi_{md}}{\partial \mathbf{E}} = \mathbf{S}_d = -\beta(\tilde{C} - \tilde{C}_0)\mathbb{E} : (\mathbf{I} - \mathbf{M} \otimes \mathbf{M}) \tag{4.2.7}$$

For the potential, $\tilde{\mu}$, we have

$$\frac{\partial \Psi_d}{\partial \tilde{C}} + f(\Psi_{md}) = \tilde{\mu} = a\tilde{C} \tag{4.2.8}$$

where a is a constant taken to be equal to 1.

Generalized nonuniform swelling

One can think of a material that due to its micro-structure will have full anisotropic swelling characteristics. A simple and general case is considered here, where a combination of linear functions is being considered. A more general, nonlinear model can be made up, but this is beyond the scope of this study.

$$\Psi_{md}(\mathbf{E}, \tilde{C}) = -\boldsymbol{\beta} : \tilde{\mathbf{C}}^{\mathbf{d}} : \mathbf{E} \qquad or \qquad \Psi_{md}(\mathbf{E}, \tilde{C}) = -\beta_{IJ}\tilde{C}^d_{IJKL}E_{KL} \tag{4.2.9}$$

where β_{IJ} is a constant tensor with the same sign as E_{IJ}, $\tilde{C}^d_{IJKL} = \tilde{C} - \tilde{C}^0_{IJKL}$ is a fourth order tensor that allows for different stresses components to be induced at different initial

concentrations $\tilde{C}^0_{IJKL}$. Differentiating with respect to $\mathbf{E}$ gives

$$\frac{\partial \Psi_{md}}{\partial \mathbf{E}} = \mathbf{S}_d = -\boldsymbol{\beta} : \tilde{\mathbf{C}}^d \qquad or \qquad \frac{\partial \Psi_{md}}{\partial E_{IJ}} = S^d_{IJ} = -\beta_{KL} : \tilde{C}^d_{KLIJ} \tag{4.2.10}$$

4.3 Saturation

Coming back to the example of a dry sponge placed in water. As time goes the sponge will decrease the rate of absorption up to a point where it becomes fully saturated. That can be modeled by setting the diffusivity as a function of the concentration. Beyond a certain concentration level $\tilde{C}_1$ (which is a material constant), the diffusivity is set to zero so that the diffusion process is stopped. Below a certain concentration level $\tilde{C}_0$ (again, a material constant) it should initially hold its value of $\tilde{D}_0$. In the range $[\tilde{C}_0, \tilde{C}_1]$ the diffusivity should change smoothly. The modeling of these characteristics was done with the following function

$$Grad(\tilde{\mu}(\tilde{C})) = \frac{\partial \tilde{\mu}(\tilde{C})}{\partial \tilde{C}} \frac{\partial \tilde{C}}{\partial \mathbf{X}} = (\tilde{D}_0 - (\tilde{D}_0 - \tilde{D}_1)/(exp(\frac{\frac{\tilde{C}_0+\tilde{C}_1}{2} - \tilde{C}}{\alpha}) + 1)) \frac{\partial \tilde{C}}{\partial \mathbf{X}} \tag{4.3.1}$$

where $\tilde{\mathbf{D}}_1$ can be set to zero for full saturation. α is a material constant smoothing factor that controls the rate of change of the diffusivity with respect to the concentration with in the range $[\tilde{C}_0, \tilde{C}_1]$. The affects of α, and the general behavior of the function can be seen in Fig. (4.2).

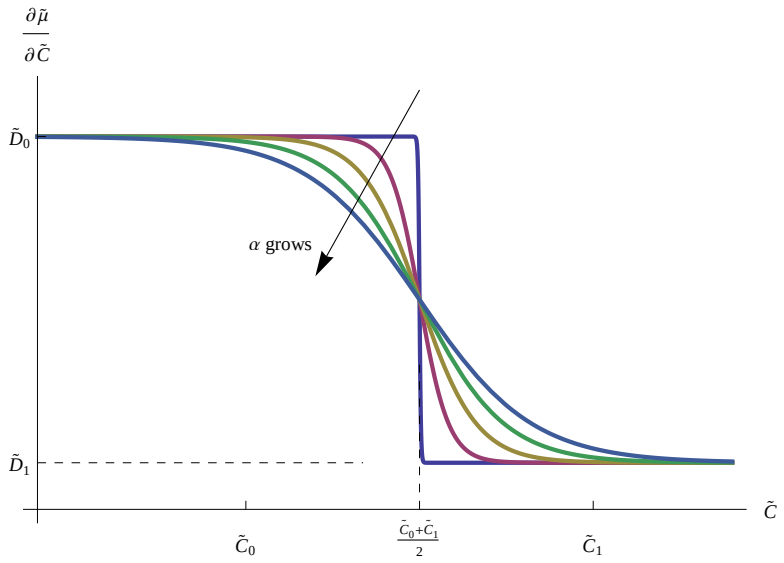

Figure 4.2: Diffusivity for Saturation

With this function in hand, we can come up with the potential $\tilde{\mu}(\tilde{C})$ by integrating with respect to $\tilde{C}$, and resetting the value of $\tilde{\mu}(\tilde{C}=0)$ to be zero. The potential comes out to be

$$\tilde{\mu}(\tilde{C}) = \tilde{C}\tilde{D}_0 - \alpha\left(\tilde{D}_0 - \tilde{D}_1\right)\log\left(e^{(\tilde{C}/\alpha} + e^{(\tilde{C}_0+\tilde{C}_1)/2\alpha}\right) + \tilde{\mu}_0 \tag{4.3.2}$$

where

$$\tilde{\mu}_0 = \alpha\left(\tilde{D}_0 - \tilde{D}_1\right)\log\left(e^{(\tilde{C}_0+\tilde{C}_1)/2\alpha} + 1\right) \tag{4.3.3}$$

is the resetting constant.
As seen in Fig (4.3), the potential grows monotonously up to the point of saturation $\frac{\tilde{C}_0+\tilde{C}_1}{2}$, where it levels at a constant value.

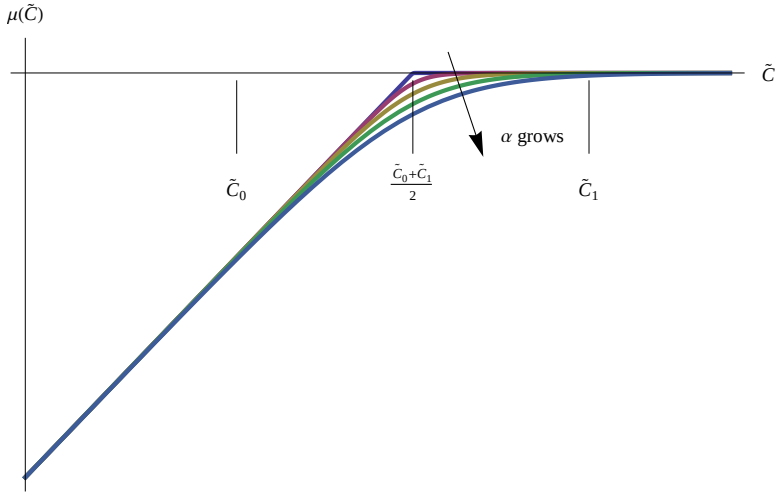

Figure 4.3: Diffusion potential $\tilde{\mu}$ for saturation

4.4 Diffuso-Elasticity

Similar to *Thermo-Elasticity*, we consider here the effects of the diffusing substance on the mechanical properties of the solid. For consistency we name the model "*Diffuso-Elasticity*". It is assumed here that as the concentration increases in the solid, the solid undergoes a softening effect that cause the magnitude of the mechanical constants to decrease. In the case of diffusion, this might not necessarily be the case, as the constants might actually increase with the increase of the concentration. For example consider the bulk modulus that might increase and have a better resistance to compression as the concentration increases. It is also assumed that there is a range of which the change of concentration affects the mechanical properties, so that they only have noticeable change within that range. To model this behavior we used the same function defined in chapter (4.3), but for the elasticity tensor $\mathbb{E}$. As opposed to saturation, we assume here that the

lower values of $\mathbb{E}$ are not zero, so that the solid still has nonzero mechanical properties for high levels of concentrations. This gives us

$$\mathbb{E}(\tilde{C}) = \mathbb{E}_0 - (\mathbb{E}_0 - \mathbb{E}_1)/(exp(\frac{\frac{\tilde{C}_0+\tilde{C}_1}{2} - \tilde{C}}{\alpha}) + 1) \tag{4.4.1}$$

where $\mathbb{E}_0$ is the initial elasticity tensor, and $\mathbb{E}_1$ consists of the lowest values of the elasticity tensor at higher levels of concentration. This model can be generalized so that different material constants such as κ the bulk modulus, ν the Poisson's ratio etc. have different dependencies on the concentration, but this can be done in future work on this subject.

Chapter 5

Numerical formulation

This chapter provides the numerical formulation that was developed for simulation of the balance equations. For references on finite elements see [37, 38, 39], and for references on time discretization and numerical solution of ODEs see [40, 41]. Starting with the equations introduced in the chapter (3), the weak forms are developed, so that the *Finite Element Method* can be used for getting numerical approximations to the analytic equations. In order to numerically solve the coupling between the equations, a staggering method is used. The method is reviewed in this chapter. All the calculations were performed in the reference configuration, so that the mesh does not move with time.

We lay out the methods needed to perform the computations in the following manner:

-Time discretization
-Numerical solvers
-Weak forms of the balance laws
-Combined scheme

5.1 Time discretization

5.1.1 Explicit/Implicit time stepping

Given an equation of the form $\dot{y}(t) = f(t, y(t))$ and initial conditions $y(0) = \xi$ for $0 <= t <= t_f$, we discretize the system in the following way

Setting $\phi = 1$, is known as *Backward Euler*, where we have

$$\begin{aligned} t_{L+1} &= t_L + \Delta t \\ y_{L+1} &= y_L + \Delta t\, f(t_{L+1}, y_{L+1}) \end{aligned} \tag{5.1.1}$$

This method is considered *stable*, which means that it will not amplify an error as the time

Algorithm 1 Algorithm for Time stepping

$t_0 = 0, y_0 \approx \xi$
while $t_n < t_f$ **do**
1. $t_{L+1} = t_L + \phi\Delta t$
2. $y_{L+1} = y_L + \phi\Delta t f(t_{L+1}, y_{L+1})$

end while

steps increase (a more rigorous analysis can be found in [40] and [41]). This equation can be solved using the *fixed point iteration* method provided that f satisfies the Lipschitz condition with respect to y, i.e. $\exists L > 0$ such that $\|f(t,x)\| \leq L\|x - y\|\ \forall x, y \in \mathbb{R}^d, t \in \mathbb{R}$.

For a second order time derivative, we can just expend the algorithm as follows

$$\begin{aligned} t_L &= t_{L-1} + \Delta t_{L-1} \qquad and \qquad t_{L+1} = t_L + \Delta t_L \\ y_L &= y_{L-1} + \Delta t_{L-1}\,\dot{y}_L \qquad and \qquad y_{L+1} = y_L + \Delta t_L\,\dot{y}_{L+1} \end{aligned} \tag{5.1.2}$$

so that

$$\dot{y}_L = \frac{y_L - y_{L-1}}{\Delta t_{L-1}} \qquad and \qquad \dot{y}_{L+1} = \frac{y_{L+1} - y_L}{\Delta t_L} \tag{5.1.3}$$

to get the second order time derivative for y, we use equation (5.1.3), to get

$$\begin{aligned} \ddot{y}_{L+1} &= \frac{\dot{y}_{L+1} - \dot{y}_L}{\Delta t_L} = \left(\frac{y_{L+1} - y_L}{\Delta t_L} - \frac{y_L - y_{L-1}}{\Delta t_{L-1}}\right)/\Delta t_L = \frac{y_{L+1} - y_L}{\Delta t_L^2} - \frac{y_L - y_{L-1}}{\Delta t_L \Delta_{L-1}} \\ &= \frac{y_{L+1}}{\Delta t_L^2} - \frac{1}{\Delta t_L}\left(\frac{1}{\Delta t_L} + \frac{1}{\Delta_{L-1}}\right) y_L + \frac{y_{L-1}}{\Delta t_L \Delta_{L-1}} \end{aligned} \tag{5.1.4}$$

Equations (5.1.4) and (5.1.3) are the equations we will use to discretize time in the numerical solutions.

5.2 Numerical solvers

With the numerical equations set up, a numerical solver needs to be prescribed in order to solve the equations. There are several well-known methods for solving nonlinear coupled algebraic equations (i.e. Newton's method). We introduce here two general methods that were used in this work.

5.2.1 Fixed point iteration

Fixed point iteration is a rather simple to implement nonlinear, numerical solver. Although it has a lower order of convergence ($O(1)$ vs. $O(2)$ in Newton's method), it is assumed to be advantageous for finding solutions to problems involving stability or multi-field coupled problems where the variables are of different order of magnitude. That is

because there is no need to build a stiffness matrix that might be ill conditioned, just iterate using the already specified equations until convergence. As any other method, this method has limitations and does not work for any problem.

Given a equation of the form $x = f(x)$, the algorithm for the method is as follows:

Algorithm 2 Algorithm for fixed point iterations

Guess an initial solution $x = x_0$
Set $i = 1$
while $||f(x_i)|| > TOL$ **do**
1. $x_{i+1} = f(x_i)$
2. $i = i + 1$

end while

The conditions for the method to hold (to converge) are known as the Lipschitz condition (explained in [40] and [41]).

5.2.2 The staggering method

This method can be generalized for N equations, but, for simplicity we show it for two equations, and for the case most suitable for our computations (i.e. it suitable for fixed point iteration)
Given two variables x and y, and two equations that depend on those variables $x = f(x, y)$ and $y = g(x, y)$, the algorithm for the method is as follows:

Algorithm 3 Algorithm for fixed point iterations

Set $i = 1$, $Norm_x = Norm_y = 10^{10}$ (large number)
Guess an initial solution $x_i = x_0, y_i = y_0$
while $||Norm_x|| > TOL_x$ or $||Norm_y|| > TOL_y$ **do**
1. $x_{i+1} = f(x_i, y_i)$
2. $Norm_x = ||x_i - x_{i+1}||$
3. $x_i = x_{i+1}$
4. $y_{i+1} = g(x_i, y_i)$
5. $Norm_y = ||y_i - y_{i+1}||$
6. $y_i = y_{i+1}$

end while

These two methods compose our scheme for solving the coupled, nonlinear algebraic equations.

5.3 Weak forms of the balance laws

Following the standard procedure in Finite elements, we start with the equations introduced in the chapter (2) and (3). The weak forms are developed, so that the *Finite*

Element Method can be used to get numerical approximations to the analytic equations.

The equations to be solved are:
-The mass balance (3.3.8)
-Balance of linear momentum (3.3.14)
-Continuity equation (2.1.3) (similar to Fick's second law)

with the following unknowns:
-The density $\rho_{ref}(\mathbf{X}, t)$
-The displacement $\mathbf{u}(\mathbf{X}, t)$
-The concentration $\tilde{C}(\mathbf{X}, t)$

We now derive the weak form for each equation step by step

5.3.1 Mass Balance

Starting off with eqn. (3.3.8), we have

$$\rho(\mathbf{X}, t) = \frac{1}{J}(\rho_0 + \tilde{C}(\mathbf{X}, t) - \tilde{C}_0) \tag{5.3.1}$$

Since this equation is already analytically defined, we are left with the discretization standard procedure

$$\rho_{\mathcal{I}}(\mathbf{X}, t) = \frac{1}{J}(\rho_{\mathcal{J}}^{ref} + \tilde{C}_{\mathcal{J}}(\mathbf{X}, t) - \tilde{C}_{\mathcal{J}}^{ref}), \qquad i = 1, 2, ..., N_{en} \tag{5.3.2}$$

5.3.2 Balance of linear momentum

Starting with eqn. (3.3.14), we have

$$Div(\mathbf{P}) + \rho_{ref}\,\mathbf{b}_{ref} = \rho_{ref}\,\ddot{\mathbf{u}}_{ref} \qquad or \qquad \frac{\partial P_{iJ}}{\partial X_J} + \rho_{ref}\,b_i^{ref} = \rho_{ref}\,\ddot{u}_i^{ref} \tag{5.3.3}$$

We apply an inner product operation with a vector test function $\mathbf{v}$ on both sides of the equation, and integrate over the entire reference region Ω_0, to get

$$\begin{aligned} &\int_{\Omega_0} [\mathbf{v} \cdot Div(\mathbf{P}) + \rho_{ref}\mathbf{v} \cdot \mathbf{b}_{ref}]\, d\Omega_0 = \int_{\Omega_0} \rho_{ref}\mathbf{v} \cdot \ddot{\mathbf{u}}_{ref}\, d\Omega_0 \quad or \\ &\int_{\Omega_0} [v_i \frac{\partial P_{iJ}}{\partial X_J} + \rho_{ref} v_i b_i^{ref}]\, d\Omega_0 = \int_{\Omega_0} \rho_{ref} v_i \ddot{u}_i^{ref}\, d\Omega_0 \end{aligned} \tag{5.3.4}$$

We use the *product rule* on $\mathbf{v} \cdot Div(\mathbf{P})$

$$Div(\mathbf{v}\cdot\mathbf{P}) = Grad(\mathbf{v})\cdot\mathbf{P} + \mathbf{v}\cdot Div(\mathbf{P}) \qquad or \qquad \frac{\partial(v_i P_{iJ})}{\partial X_J} = \frac{\partial v_i}{\partial X_J}P_{iJ} + v_i\frac{\partial P_{iJ}}{\partial X_J} \tag{5.3.5}$$

which gives

$$\int_{\Omega_0}\mathbf{v}\cdot Div(\mathbf{P})\,d\Omega_0 = \int_{\Omega_0} Div(\mathbf{v}\cdot\mathbf{P})\,d\Omega_0 - \int_{\Omega_0} Grad(\mathbf{v})\cdot\mathbf{P}\,d\Omega_0 \tag{5.3.6}$$

using the *Divergence theorem* leads to

$$\int_{\Omega_0}\mathbf{v}\cdot Div(\mathbf{P})\,d\Omega_0 = \int_{\partial\Omega_0}\mathbf{v}\cdot\mathbf{p}\,dA_0 - \int_{\Omega_0} Grad(\mathbf{v})\cdot\mathbf{P}\,d\Omega_0 \quad or \quad \int_{\Omega_0}\frac{\partial(v_i P_{iJ})}{\partial X_J}\,d\Omega_0 = \int_{\partial\Omega_0} v_i p_i\,dA_0 - \int_{\Omega_0}\frac{\partial v_i}{\partial X_J}P_{iJ}\,d\Omega_0 \tag{5.3.7}$$

where $\mathbf{p} = \mathbf{P}\cdot\mathbf{N}$ is the Piola traction in the reference configuration. We invoke that on the boundary, wherever the displacement is known (Γ_u), the test function $\mathbf{v}$ is set to be zero, and therefore the area integral is reduced to

$$\int_{\partial\Omega_0}\mathbf{v}\cdot\mathbf{p}\,dA_0 = \int_{\Gamma_p}\mathbf{v}\cdot\mathbf{p}\,d\Gamma_p \quad or \quad \int_{\partial\Omega_0} v_i p_i\,dA_0 = \int_{\Gamma_p} v_i p_i\,d\Gamma_p \tag{5.3.8}$$

Γ_p is the boundary where the tractions are specified, and $\partial\Omega_0 = \Gamma_p \cup \Gamma_u$. This leads to the following equation

$$\int_{\Gamma_p}\mathbf{v}\cdot\mathbf{p}\,d\Gamma_p - \int_{\Omega_0} Grad(\mathbf{v})\cdot\mathbf{P}\,d\Omega_0 + \int_{\Omega_0}\rho_{ref}\mathbf{v}\cdot\mathbf{b}_{ref}\,d\Omega_0 = \int_{\Omega_0}\rho_{ref}\mathbf{v}\cdot\ddot{\mathbf{u}}_{ref}\,d\Omega_0 \tag{5.3.9}$$

Equation (5.3.9) is the weak form of eqn. (5.3.3), and its solution can be approximated with the use of the *Finite Element method* and *time discretization*. With the use of the *Backward Euler* time-scheme from section (5.1), we approximate $\ddot{u}_I(\mathbf{X}, t)$ with

$$\ddot{u}_i(\mathbf{X}, t) = \frac{1}{\Delta t_L^2}u_i^{L+1} - \frac{1}{\Delta t_L}\left(\frac{1}{\Delta t_L} + \frac{1}{\Delta_{L-1}}\right)u_i^L + \frac{1}{\Delta t_L\Delta_{L-1}}u_i^{L-1} \tag{5.3.10}$$

to get

$$\begin{aligned}&\int_{\Gamma_p} v_i p_i\,d\Gamma_p - \int_{\Omega_0}\frac{\partial v_i}{\partial X_J}P_{iJ}\,d\Omega_0 + \int_{\Omega_0}\rho_{ref}\,v_i\,b_i^{ref}\,d\Omega_0 = \\ &\int_{\Omega_0}\rho_{ref}\,v_i\left[\frac{1}{\Delta t_L^2}u_i^{L+1} - \frac{1}{\Delta t_L}\left(\frac{1}{\Delta t_L} + \frac{1}{\Delta_{L-1}}\right)u_i^L + \frac{1}{\Delta t_L\Delta_{L-1}}u_i^{L-1}\right]d\Omega_0\end{aligned} \tag{5.3.11}$$

where $u_i^{L+1} = u_i(\mathbf{X}, t_{L+1})$. We follow the Galerkin procedure, and approximate the displacements, u_i^{L+1}, u_i^L and u_i^{L-1}, and the test function v_i with

$$\begin{aligned} &u_i^{L+1}(\mathbf{X}) \approx \sum_{\mathcal{J}=1}^{N} a_{i\mathcal{J}}^{L+1}\phi_{\mathcal{J}}(\mathbf{X}),\ \ u_i^{L}(\mathbf{X}) \approx \sum_{\mathcal{J}=1}^{N} a_{i\mathcal{J}}^{L}\phi_{\mathcal{J}}(\mathbf{X}),\ \ u_i^{L-1}(\mathbf{X}) \approx \sum_{\mathcal{J}=1}^{N} a_{i\mathcal{J}}^{L-1}\phi_{\mathcal{J}}(\mathbf{X}) \\ &v_i(\mathbf{X}) \approx \sum_{\mathcal{I}=1}^{N} b_{i\mathcal{I}}\phi_{\mathcal{I}}(\mathbf{X}) \end{aligned} \tag{5.3.12}$$

where N is the number of nodes in the discretization, $a_{i\mathcal{J}}^{L+1}$, $a_{i\mathcal{J}}^{L}$, $a_{i\mathcal{J}}^{L-1}$, and $b_{i\mathcal{I}}$ are unknown constants, and $\phi_{\mathcal{I}}(\mathbf{X})$ are the spatial shape functions. We are assuming that the functions are smooth enough so that we can switch the order between integration and summation. This leads to the following

$$\begin{aligned} &\int_{\Omega_0} \rho_{ref} v_i [\frac{1}{\Delta t_L^2} u_i^{L+1} - \frac{1}{\Delta t_L}(\frac{1}{\Delta t_L} + \frac{1}{\Delta_{L-1}}) u_i^L + \frac{1}{\Delta t_L \Delta_{L-1}} u_i^{L-1}]\, d\Omega_0 = \\ &\sum_{\mathcal{I}=1}^{N} b_{i\mathcal{I}} \sum_{\mathcal{J}=1}^{N} \int_{\Omega_0} \rho_{ref}\phi_{\mathcal{I}}(\mathbf{X})[\frac{1}{\Delta t_L^2} a_{i\mathcal{J}}^{L+1} - \frac{1}{\Delta t_L}(\frac{1}{\Delta t_L} + \frac{1}{\Delta_{L-1}}) a_{i\mathcal{J}}^{L} + \frac{1}{\Delta t_L \Delta_{L-1}} a_{i\mathcal{J}}^{L-1}]\phi_{\mathcal{J}}(\mathbf{X})\, d\Omega_0 = \\ &\sum_{\mathcal{I}=1}^{N} b_{i\mathcal{I}} \sum_{\mathcal{J}=1}^{N} [\frac{1}{\Delta t_L^2} M_{\mathcal{I}\mathcal{J}}^{L+1} a_{i\mathcal{J}}^{L+1} - \frac{1}{\Delta t_L}(\frac{1}{\Delta t_L} + \frac{1}{\Delta_{L-1}}) M_{\mathcal{I}\mathcal{J}}^{L} a_{i\mathcal{J}}^{L} + \frac{1}{\Delta t_L \Delta_{L-1}} M_{\mathcal{I}\mathcal{J}}^{L-1} a_{i\mathcal{J}}^{L-1}] \end{aligned} \tag{5.3.13}$$

where $M_{\mathcal{I}\mathcal{J}}^{L+1} = \int_{\Omega_0} \rho_{ref}^{L+1} \phi_{\mathcal{I}}(\mathbf{X})\phi_{\mathcal{J}}(\mathbf{X})\, d\Omega_0$ is known as the mass matrix at time $L+1$, $M_{\mathcal{I}\mathcal{J}}^{L} = \int_{\Omega_0} \rho_{ref}^{L} \phi_{\mathcal{I}}(\mathbf{X})\phi_{\mathcal{J}}(\mathbf{X})\, d\Omega_0$ is the mass matrix at time L, and $M_{\mathcal{I}\mathcal{J}}^{L-1} = \int_{\Omega_0} \rho_{ref}^{L-1} \phi_{\mathcal{I}}(\mathbf{X})\phi_{\mathcal{J}}(\mathbf{X})\, d\Omega_0$ is the mass matrix at time $L-1$. The indexes $i = 1, 2, 3$, and $\mathcal{I} = 1, 2, ...N$ can be combined to a new index $\mathcal{I} = 1, 2, ...3N$. So eqn. (5.3.14) can be written in matrix form as follows

$$\begin{aligned} &\int_{\Omega_0} \rho_{ref} v_i [\frac{1}{\Delta t_L^2} u_i^{L+1} - \frac{1}{\Delta t_L}(\frac{1}{\Delta t_L} + \frac{1}{\Delta_{L-1}}) u_i^L + \frac{1}{\Delta t_L \Delta_{L-1}} u_i^{L-1}]\, d\Omega_0 = \\ &\mathbf{b}[\frac{1}{\Delta t_L^2} \mathbf{M}^{L+1}\mathbf{a}^{L+1} - \frac{1}{\Delta t_L}(\frac{1}{\Delta t_L} + \frac{1}{\Delta_{L-1}}) \mathbf{M}^{L}\mathbf{a}^{L} + \frac{1}{\Delta t_L \Delta_{L-1}} \mathbf{M}^{L-1}\mathbf{a}^{L-1}] \end{aligned} \tag{5.3.14}$$

where $\mathbf{M}^{L+1} = M_{\mathcal{I}\mathcal{J}}^{L+1}$ etc., and $\mathbf{a}^{L+1} = a_{\mathcal{J}}^{L+1}$. For the L.H.S. of (5.3.9), we get

$$\begin{aligned}
&\int_{\Gamma_p} \mathbf{v}\cdot\mathbf{p}\, d\Gamma_p - \int_{\Omega_0} Grad(\mathbf{v})\cdot\mathbf{P}\, d\Omega_0 + \int_{\Omega_0} \rho_{ref}\mathbf{v}\cdot\mathbf{b}_{ref}\, d\Omega_0 = \\
&\sum_{\mathcal{I}=1}^{N} b_{i\mathcal{I}} \int_{\Gamma_p} \phi_{\mathcal{I}}(\mathbf{X}) p_i\, d\Gamma_p - \sum_{\mathcal{I}=1}^{N} b_{i\mathcal{I}} \int_{\Omega_0} \frac{\partial \phi_{\mathcal{I}}(\mathbf{X})}{\partial X_K} P_{iK}\, d\Omega_0 + \sum_{\mathcal{I}=1}^{N} b_{i\mathcal{I}} \int_{\Omega_0} \rho_{ref}\phi_{\mathcal{I}} b_i^{ref}\, d\Omega_0 = \\
&\mathbf{b}\int_{\Gamma_p} \mathbf{p}_\phi\, d\Gamma_p - \mathbf{b}\int_{\Omega_0} \mathbf{D}[\boldsymbol{\phi}]\mathbf{P}\, d\Omega_0 + \mathbf{b}\int_{\Omega_0} \rho_{ref}\mathbf{b}_\phi^{ref}\, d\Omega_0
\end{aligned} \tag{5.3.15}$$

where $\mathbf{p}_\phi = \phi_{\mathcal{I}}(\mathbf{X}) p_i$, $\mathbf{D}[\boldsymbol{\phi}] = \frac{\partial \phi_{\mathcal{I}}(\mathbf{X})}{\partial X_K}$, and $\mathbf{b}_\phi^{ref} = \phi_{\mathcal{I}} b_i^{ref}$. This leads to the discrete form of the balance of linear momentum

$$\begin{aligned}
&\mathbf{b}\int_{\Gamma_p} \mathbf{p}_\phi\, d\Gamma_p - \mathbf{b}\int_{\Omega_0} \mathbf{D}[\boldsymbol{\phi}]\mathbf{P}\, d\Omega_0 + \mathbf{b}\int_{\Omega_0} \rho_{ref}\mathbf{b}_\phi^{ref}\, d\Omega_0 = \\
&\mathbf{b}[\frac{1}{\Delta t_L^2}\mathbf{M}^{L+1}\mathbf{a}^{L+1} - \frac{1}{\Delta t_L}(\frac{1}{\Delta t_L} + \frac{1}{\Delta_{L-1}})\mathbf{M}^L\mathbf{a}^L + \frac{1}{\Delta t_L \Delta_{L-1}}\mathbf{M}^{L-1}\mathbf{a}^{L-1}]
\end{aligned} \tag{5.3.16}$$

or

$$\begin{aligned}
&\mathbf{b}\Bigg(\int_{\Gamma_p} \mathbf{p}_\phi\, d\Gamma_p - \int_{\Omega_0} \mathbf{D}[\boldsymbol{\phi}]\mathbf{P}\, d\Omega_0 \\
&+ \int_{\Omega_0} \rho_{ref}\mathbf{b}_\phi^{ref}\, d\Omega_0 - [\frac{1}{\Delta t_L^2}\mathbf{M}^{L+1}\mathbf{a}^{L+1} - \frac{1}{\Delta t_L}(\frac{1}{\Delta t_L} + \frac{1}{\Delta_{L-1}})\mathbf{M}^L\mathbf{a}^L + \frac{1}{\Delta t_L \Delta_{L-1}}\mathbf{M}^{L-1}\mathbf{a}^{L-1}]\Bigg) = 0
\end{aligned} \tag{5.3.17}$$

Since $\mathbf{b}$ is arbitrary, the expression inside the parenthesis holds for any $\mathbf{b}$. This leads to the following formulation

$$\mathbf{a}^{L+1} = \Delta t_L^2 [\mathbf{M}^{L+1}]^{-1}(\mathbf{f}^{ext} + \mathbf{f}^{int}) \tag{5.3.18}$$

where

$$\mathbf{f}^{ext} = \int_{\Gamma_p} \mathbf{p}_\phi\, d\Gamma_p + \int_{\Omega_0} \rho_{ref}\mathbf{b}_\phi^{ref}\, d\Omega_0 \tag{5.3.19}$$

and

$$\mathbf{f}^{int} = -\int_{\Omega_0} \mathbf{D}[\phi]\,\mathbf{P}\,d\Omega_0 + [\frac{1}{\Delta t_L}(\frac{1}{\Delta t_L} + \frac{1}{\Delta_{L-1}})\mathbf{M}^L\mathbf{a}^L - \frac{1}{\Delta t_L \Delta_{L-1}}\mathbf{M}^{L-1}\mathbf{a}^{L-1}] \tag{5.3.20}$$

For computational convenience and efficiency, we replace $\mathbf{P}$ with $\mathbf{F}\cdot\mathbf{S}$, and combine $\mathbf{D}[\phi]$ with $\mathbf{F}$ to create $\mathbf{B}$ (see [38], pp. 202-203 for more details).

5.3.3 Diffusion equation

Starting with eqn. (4.0.21), we have

$$\frac{\partial \tilde{C}}{\partial t} = -Div(\tilde{\mathbf{J}}) = Div(\tilde{\mathbf{D}}\cdot Grad(\tilde{\mu})) \quad or \quad \frac{\partial \tilde{C}}{\partial t} = -\frac{\partial \tilde{J}_I}{\partial X_I} = \frac{\partial}{\partial x_I}(\tilde{D}_{IJ}\frac{\partial \tilde{\mu}}{\partial X_J}) \tag{5.3.21}$$

We apply an inner product operation with a scalar test function v on both sides of the equation, and integrate over the entire reference region Ω_0, to get

$$\int_{\Omega_0} v\frac{\partial \tilde{C}}{\partial t}\,d\Omega_0 = \int_{\Omega_0} v\,Div(\tilde{\mathbf{D}}\cdot Grad(\tilde{\mu}))\,d\Omega_0 \quad or \quad \int_{\Omega_0} v\frac{\partial \tilde{C}}{\partial t}\,d\Omega_0 = \int_{\Omega_0} v\frac{\partial}{\partial x_I}(\tilde{D}_{IJ}\frac{\partial \tilde{\mu}}{\partial X_J})\,d\Omega_0 \tag{5.3.22}$$

We use the *product rule* on $v\,Div(\tilde{\mathbf{D}}\cdot Grad(\tilde{\mu}))$

$$\begin{aligned} &Div(v\,\mathbf{D}\cdot Grad(\tilde{\mu})) = Grad(v)\cdot\mathbf{D}\cdot Grad(\tilde{\mu}) + v\,Div(\mathbf{D}\cdot Grad(\tilde{\mu})) \quad or \\ &\frac{\partial}{\partial X_I}(v\tilde{D}_{IJ}\frac{\partial \tilde{\mu}}{\partial X_J}) = \frac{\partial v}{\partial X_I}\tilde{D}_{IJ}\frac{\partial \tilde{\mu}}{\partial X_J} + v\frac{\partial}{\partial X_I}(\tilde{D}_{IJ}\frac{\partial \tilde{\mu}}{\partial X_J}) \end{aligned} \tag{5.3.23}$$

which gives

$$\int_{\Omega_0} v\,Div(\mathbf{D}\cdot Grad(\tilde{\mu}))\,d\Omega_0 = \int_{\Omega_0} Div(v\,\mathbf{D}\cdot Grad(\tilde{\mu}))\,d\Omega_0 - \int_{\Omega_0} Grad(v)\cdot\mathbf{D}\cdot Grad(\tilde{\mu})\,d\Omega_0 \tag{5.3.24}$$

using the *Divergence theorem* leads to

$$\begin{aligned} &\int_{\Omega_0} v\,Div(\mathbf{D}\cdot Grad(\tilde{\mu}))\,d\Omega_0 = \int_{\partial\Omega_0} v\tilde{\mathbf{J}}\cdot\mathbf{N}\,dA_0 - \int_{\Omega_0} Grad(v)\cdot\mathbf{D}\cdot Grad(\tilde{\mu})\,d\Omega_0 \quad or \\ &\int_{\Omega_0} v\frac{\partial}{\partial X_I}(\tilde{D}_{IJ}\frac{\partial \tilde{\mu}}{\partial X_J})\,d\Omega_0 = \int_{\partial\Omega_0} v\tilde{J}_I N_I\,dA_0 - \int_{\Omega_0} \frac{\partial v}{\partial X_I}\tilde{D}_{IJ}\frac{\partial \tilde{\mu}}{\partial X_J}\,d\Omega_0 \end{aligned} \tag{5.3.25}$$

We invoke that on the boundary, wherever the concentration is known ($\Gamma_{\tilde{C}}$), the test function v is set to be zero, and therefore the area integral is reduced to

$$\int_{\partial\Omega_0} v\tilde{\mathbf{J}}\cdot\mathbf{N}\,dA_0 = \int_{\Gamma_{\tilde{J}}} v\tilde{\mathbf{J}}\cdot\mathbf{N}\,d\Gamma_{\tilde{J}} \quad or \quad \int_{\partial\Omega_0} v\tilde{J}_I N_I\,dA_0 = \int_{\Gamma_{\tilde{J}}} v\tilde{J}_I N_I\,d\Gamma_{\tilde{J}} \tag{5.3.26}$$

$\Gamma_{\tilde{J}}$ is the boundary where the flux is prescribed, and $\partial\Omega_0 = \Gamma_{\tilde{J}} \cup \Gamma_{\tilde{C}}$. This leads to the following equation

$$\int_{\Omega_0} v\frac{\partial\tilde{C}}{\partial t}\,d\Omega_0 = \int_{\Gamma_{\tilde{J}}} v\tilde{\mathbf{J}}\cdot\mathbf{N}\,d\Gamma_{\tilde{J}} - \int_{\Omega_0} Grad(v)\cdot\mathbf{D}\cdot Grad(\tilde{\mu})\,d\Omega_0 \tag{5.3.27}$$

Equation (5.3.27) is the weak form of eqn. (5.3.21), and its solution can be approximated with the use of the *Finite Element method* and *time discretization*. With the use of the *Backward Euler* time-scheme from section (5.1), we approximate $\frac{\partial\tilde{C}(\mathbf{X},t)}{\partial t}$ with

$$\frac{\partial\tilde{C}(\mathbf{X},t)}{\partial t} = \frac{1}{\Delta t_L}(\tilde{C}^{L+1} - \tilde{C}^L) \tag{5.3.28}$$

to get

$$\int_{\Omega_0} v\frac{1}{\Delta t_L}(\tilde{C}^{L+1} - \tilde{C}^L)\,d\Omega_0 = \int_{\Gamma_{\tilde{J}}} v\tilde{\mathbf{J}}\cdot\mathbf{N}\,d\Gamma_{\tilde{J}} - \int_{\Omega_0} Grad(v)\cdot\mathbf{D}\cdot Grad(\tilde{\mu})\,d\Omega_0 \tag{5.3.29}$$

where $\tilde{c}^{L+1} = \tilde{C}(\mathbf{X}, t_{L+1})$. We follow the Galerkin procedure, and approximate the concentrations, $\tilde{C}^{L+1}$, $\tilde{C}^L$, and the test function v with

$$\begin{aligned} &\tilde{C}^{L+1}(\mathbf{X}) \approx \sum_{\mathcal{J}=1}^{N} c_{\mathcal{J}}^{L+1}\phi_{\mathcal{J}}(\mathbf{X}),\ \ \tilde{c}^L(\mathbf{X}) \approx \sum_{\mathcal{J}=1}^{N} c_{\mathcal{J}}^{L}\phi_{\mathcal{J}}(\mathbf{X}) \\ &v(\mathbf{X}) \approx \sum_{\mathcal{I}=1}^{N} b_{\mathcal{I}}\phi_{\mathcal{I}}(\mathbf{X}) \end{aligned} \tag{5.3.30}$$

where N is the number of nodes in the discretization, $c_{\mathcal{J}}^{L+1}$, $c_{\mathcal{J}}^{L}$, and $b_{i\mathcal{I}}$ are unknown constants, and $\phi_{\mathcal{I}}(\mathbf{X})$ are the spatial shape functions. We are assuming that the functions are smooth enough so that we can switch the order between integration and summation. This leads to the following

$$\int_{\Omega_0} v\frac{1}{\Delta t_L}(\tilde{C}^{L+1}-\tilde{C}^{L})\,d\Omega_0 = \sum_{i=\mathcal{I}}^{N} b_{\mathcal{I}} \sum_{\mathcal{J}=1}^{N} \int_{\Omega_0} \phi_{\mathcal{I}}(\mathbf{X})\frac{1}{\Delta t_L}(c_{\mathcal{J}}^{L+1}-c_{\mathcal{J}}^{L})\phi_{\mathcal{J}}(\mathbf{X})\,d\Omega_0 = \sum_{\mathcal{I}=1}^{N} b_{\mathcal{I}} \sum_{\mathcal{J}=1}^{N} \frac{1}{\Delta t_L} M^{c}_{\mathcal{I}\mathcal{J}}(c_{i\mathcal{J}}^{L+1}-c_{\mathcal{J}}^{L}) \tag{5.3.31}$$

where $M^{c}_{\mathcal{I}\mathcal{J}} = \int_{\Omega_0} \phi_{\mathcal{I}}(\mathbf{X})\phi_{\mathcal{J}}(\mathbf{X})\,d\Omega_0$ is known as the mass matrix. Equation (5.3.32) can be written in matrix form as follows

$$\int_{\Omega_0} v\frac{1}{\Delta t_L}(\tilde{C}^{L+1}-\tilde{C}^{L})\,d\Omega_0 = \mathbf{b}\frac{1}{\Delta t_L}\mathbf{M}^{c}(\mathbf{c}^{L+1}-\mathbf{c}^{L}) \tag{5.3.32}$$

where $\mathbf{M}^{c} = M^{c}_{\mathcal{I}\mathcal{J}}$, and $\mathbf{c}^{L+1} = c_{\mathcal{J}}^{L+1}$. For the R.H.S. of (5.3.27), we get

$$\begin{aligned} &\int_{\Gamma_{\tilde{J}}} v\tilde{\mathbf{J}}\cdot\mathbf{N}\,d\Gamma_{\tilde{J}} - \int_{\Omega_0} Grad(v)\cdot\mathbf{D}\cdot Grad(\tilde{\mu})\,d\Omega_0 = \\ &\sum_{\mathcal{I}=1}^{N} b_{\mathcal{I}} \int_{\Gamma_{\tilde{J}}} \phi_{\mathcal{I}}(\mathbf{X})\tilde{J}_B N_B\,d\Gamma_p - \sum_{\mathcal{I}=1}^{N} b_{\mathcal{I}} \int_{\Omega_0} \frac{\partial\phi_{\mathcal{I}}(\mathbf{X})}{\partial X_K} D_{KL}\frac{\partial\mu_(\mathbf{X})}{\partial X_L}\,d\Omega_0 = \\ &\mathbf{b}\int_{\Gamma_{\tilde{J}}} \tilde{\mathbf{J}}_{\phi}\,d\Gamma_p - \mathbf{b}\int_{\Omega_0} \mathbf{D}[\boldsymbol{\phi}]\mathbf{D}\cdot Grad(\mu)\,d\Omega_0 \end{aligned} \tag{5.3.33}$$

where $\tilde{\mathbf{J}}_{\phi} = \phi_{\mathcal{I}}(\mathbf{X})\tilde{J}_B N_B$, $\mathbf{D}[\boldsymbol{\phi}] = \frac{\partial\phi_{\mathcal{I}}(\mathbf{X})}{\partial X_K}$. This leads to the discrete form of the diffusion equation

$$\mathbf{b}\frac{1}{\Delta t_L}\mathbf{M}^{c}(\mathbf{c}^{L+1}-\mathbf{c}^{L}) = \mathbf{b}\int_{\Gamma_{\tilde{J}}} \tilde{\mathbf{J}}_{\phi}\,d\Gamma_p - \mathbf{b}\int_{\Omega_0} \mathbf{D}[\boldsymbol{\phi}]\mathbf{D}\cdot Grad(\mu)\,d\Omega_0 \tag{5.3.34}$$

or

$$\mathbf{b}\left(\frac{1}{\Delta t_L}\mathbf{M}^{c}(\mathbf{c}^{L+1}-\mathbf{c}^{L}) - \mathbf{b}\int_{\Gamma_{\tilde{J}}} \tilde{\mathbf{J}}_{\phi}\,d\Gamma_p + \mathbf{b}\int_{\Omega_0} \mathbf{D}[\boldsymbol{\phi}]\mathbf{D}\cdot Grad(\mu)\,d\Omega_0\right) = 0 \tag{5.3.35}$$

Since $\mathbf{b}$ is arbitrary, the expression inside the parenthesis holds for any $\mathbf{b}$. This leads to the following formulation

$$\mathbf{c}^{L+1} = \mathbf{c}^{L} + \Delta t_L [\mathbf{M}]^{-1} \mathbf{f}^{c} \tag{5.3.36}$$

where

$$\mathbf{f}^{c} = \int_{\Gamma_{\tilde{j}}} \tilde{\mathbf{j}}_{\phi}\, d\Gamma_p - \int_{\Omega_0} \mathbf{D}[\boldsymbol{\phi}]\, \mathbf{D} \cdot Grad(\mu)\, d\Omega_0 \tag{5.3.37}$$

5.4 Combined scheme

With all the schemes and algorithms mentioned in this chapter, we now combine all of them to solve our coupled, time-dependent, nonlinear partial differential equations. We are solving the field equations for the mass balance (3.3.5),the balance of linear momentum (3.3.15), and the diffusion equation (4.0.21) numerically. The scheme goes as follows

Algorithm 4 Algorithm for the combined scheme

Set initial conditions $a_{\mathcal{I}}^{L=0} = a_{\mathcal{I}}^{0}$, $c_{\mathcal{K}}^{L=0} = c_{\mathcal{K}}^{0}$ ($\mathcal{I} = 1, 2, ...3N$ and $\mathcal{K} = 1, 2, ...N$)
Compute $M_{\mathcal{I}\mathcal{J}}^{c}$, $M_{\mathcal{I}\mathcal{J}}^{L-1}$, $M_{\mathcal{I}\mathcal{J}}^{L}$
Set $L = 0$, $t_L = 0$
for $L = 1$ to num time steps **do**
1. $t_{L+1} = t_L + \Delta t_L$
2. Compute time dependent boundary conditions (i.e. displacement B.C.)
3. Guess $a_{\mathcal{I}}^{L+1,i} = a_{\mathcal{I}}^{L}$ and $c_{\mathcal{K}}^{L+1,i} = c_{\mathcal{K}}^{L}$
4. $Norm_u = 10^{10}$, $Norm_c = 10^{10}$
while $||Norm_u|| > TOL_u$ or $||Norm_c|| > TOL_c$ **do**
i. Compute $M_{\mathcal{I}\mathcal{J}}^{L+1,i+1}$, $f_{\mathcal{J}}^{int,i+1}$, $f_{\mathcal{J}}^{ext,i+1}$, $f_{\mathcal{K}}^{c,i+1}$
ii Set $u_{\mathcal{I}}^{L+1,i+1} = \Delta t_L^2 [M_{\mathcal{I}\mathcal{J}}^{L+1,i+1}]^{-1} (f_{\mathcal{J}}^{int,i+1} + f_{\mathcal{J}}^{ext,i+1})$
iii. $Norm_u = \|u_{\mathcal{I}}^{L+1,i} - u_{\mathcal{I}}^{L+1,i+1}\|$
iv. $u_{\mathcal{I}}^{L+1,i} = u_{\mathcal{I}}^{L+1,i+1}$
iv. Compute $M_{\mathcal{I}\mathcal{J}}^{L+1,i+1}$, $f_{\mathcal{J}}^{int,i+1}$, $f_{\mathcal{J}}^{ext,i+1}$, $f_{\mathcal{K}}^{c,i+1}$
v. Set $c_{\mathcal{K}}^{L+1,i+1} = c_{\mathcal{K}}^{L} - \Delta t_L [M_{\mathcal{I}\mathcal{J}}^{c}]^{-1} f_{\mathcal{K}}^{c,i+1}$
vi. $Norm_c = \|c_{\mathcal{K}}^{L+1,i} - c_{\mathcal{K}}^{L+1,i+1}\|$
vi. $c_{\mathcal{K}}^{L+1,i} = c_{\mathcal{K}}^{L+1,i+1}$
end while
5. $a_{\mathcal{I}}^{L-1} = a_{\mathcal{I}}^{L}$, $M_{\mathcal{I}\mathcal{J}}^{L-1} = M_{\mathcal{I}\mathcal{J}}^{L}$
6. $a_{\mathcal{I}}^{L} = a_{\mathcal{I}}^{L+1}$, $M_{\mathcal{I}\mathcal{J}}^{L} = M_{\mathcal{I}\mathcal{J}}^{L+1}$, $c_{\mathcal{K}}^{L} = c_{\mathcal{K}}^{L+1}$, $t_L = t_{L+1}$
end for

Chapter 6

Examples & Results

With the combined numerical scheme at hand, we use it to simulate different cases and specific examples, and compare one to another, and observe the behavior of the models.

For the examples in this chapter we consider the cases in table 6.1. For convenience we define case numbers for each case so that a case number defines the main idea behind the model and the equation that defines it. We also provide the material constants needed for each model

Case #	Eqn	Desription	Material Const.
case 1	(2.1.4)	Fixed diffusivity	$\tilde{\mathbf{D}}_0$, β, $\tilde{C}_0$, $\mathbb{E}_0$
case 2	(4.1.2)	Strain dependent diffusivity	$\tilde{\mathbf{D}}_0$, β, $\tilde{C}_0$, a, $\mathbb{E}_0$
case 3	(4.2.10)	Saturation	$\tilde{\mathbf{D}}_0$, $\tilde{\mathbf{D}}_1$, β, $\tilde{C}_0$, $\tilde{C}_1$, α, $\mathbb{E}_0$
case 4	(4.3.1)	Diffusion induced nonuniform strain	$\tilde{\mathbf{D}}_0$, β, $\tilde{C}_0$, $\mathbf{M}$, $\mathbb{E}_0$

Table 6.1: Cases of modeling the coupling of diffusion with mechanics

In the next few sections, we consider the case of free swelling. Where the body is not subjected to any mechanical loads. The body is subjected to a change in the concentration on all the boundaries, and due to the diffusion presses into the body, it swells up. More specifically, the concentration boundary conditions are set as follows: the body has an initial concentration $\tilde{C}_0$ in the entire body at time $t = 0$. For a short amount of time up to $t = t_r$ the concentration on the boundary is linearly ramped up to a value of $\tilde{C}_f$, and it is kept at that value until the end of the simulation at time $t = t_f$ (see Fig. 6.1). This is basically done to avoid a "jump" between the initial and the boundary conditions. This mimics a solid with an initial concentration submerged into a infinite bath with a different concentration. We are following the concentration in the body as well as the Von Mises stress and the displacements. Note that the model for free swelling does not induce stresses in a homogeneous body at steady state, however, transient stresses will be induced during the redistribution of the diffusing phase in the body. By contrast, if a body has coupling terms that are non homogeneous, stresses will be induced even at steady state. This is because the deformations are inhomogeneous at steady state, and therefore stresses are

produced.

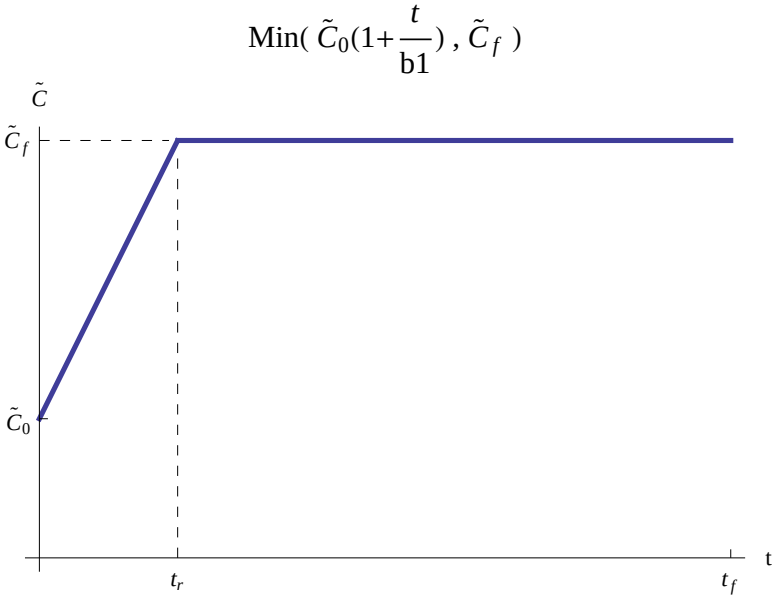

Figure 6.1: Ramping up concentration boundary conditions

Due to the symmetry of the problem in the case of free swelling, only one eighth of the cubic was modeled with a mesh of $10 \times 10 \times 10$ elements (see Fig. 6.2). The size of the cube is $0.1 \times 0.1 \times 0.1 meters$.

This gives the same results as of running the computations on the entire body of size $0.2 \times 0.2 \times 0.2 meters$, with a mesh of $20 \times 20 \times 20$ elements, thus reducing the computational cost.

6.1 Free Swelling of a homogeneous material

In this section we are considering a homogeneous material, that is subjected to a change in concentration on the boundaries, as described previously.

6.1.1 Case 1: Fixed diffusivity

In this example we consider the following constitutive models:

$$\begin{aligned} \tilde{\mathbf{D}} &= \tilde{\mathbf{D}}_0 \\ \mathbf{S} &= \mathbb{E} : (\mathbf{E} - \beta(\tilde{C} - \tilde{C}_0)\mathbf{I}) \end{aligned} \tag{6.1.1}$$

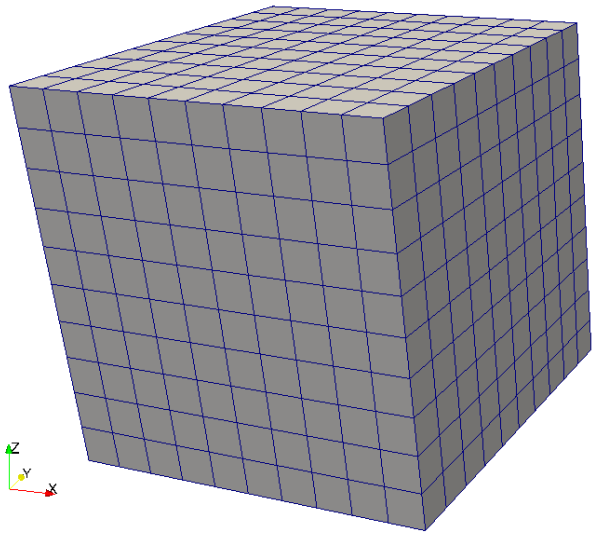

Figure 6.2: Meshed solid cube

Figure 6.3 shows how the non-dimensional Von Mises stress (divided by the yield stress), change during the change of concentration in the body. Because this is a homogeneous material, the body reaches a steady-state, where the stresses die down and the body has a homogeneous distribution of the concentration. Since the model has uniform strains induced by diffusion and the material is isotropic, we can see that the surfaces constructed by constant values of Von Mises stress are spherical, as expected.
Figure 6.4 shows how the magnitude of the displacements changes during the change of concentration in the body. As mentioned before, this is an isotropic homogeneous material, so the swelling causes spherical deformations. This can be seen by surfaces constructed by constant values of the magnitude of the deformation that produce spheres with different radii.

6.1.2 Case 2: Strain dependent diffusivity

In this example we consider the following constitutive models:

$$\begin{aligned} \tilde{\mathbf{D}}(J) &= \tilde{\mathbf{D}}_0 \frac{e^J - 1}{e - 1} \\ \mathbf{S} &= \mathbb{E} : (\mathbf{E} - \beta(\tilde{C} - \tilde{C}_0)\mathbf{I}) \end{aligned} \tag{6.1.2}$$

Figure 6.5 shows how the non-dimensional Von Mises stress (divided by the yield stress), change during the change of concentration in the body. The shape of the body, and values of the Von Mises stresses are very similar to those shown in subsection 6.1.1. That is because

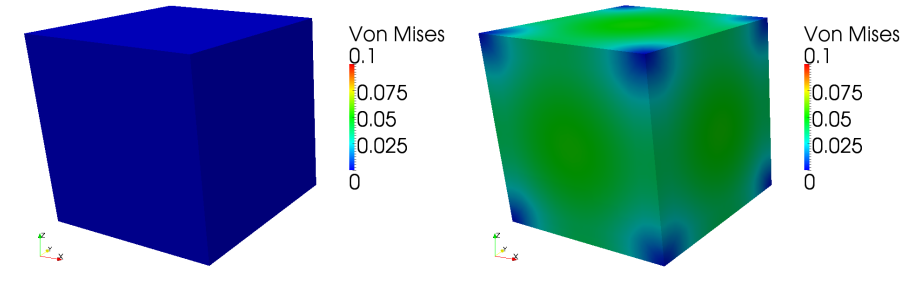

(a) $t = 0$

(b) $t = 2$

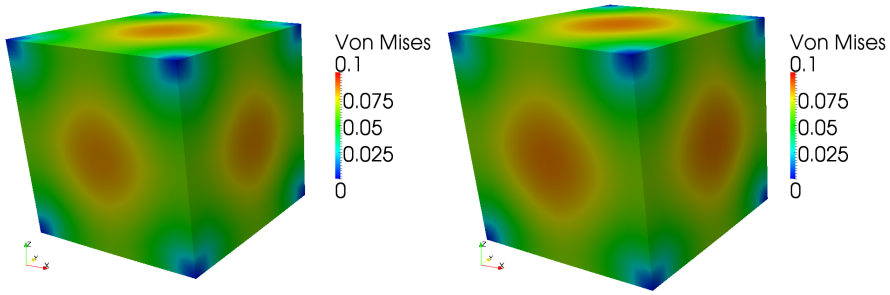

(c) $t = 8$

(d) $t = 25$

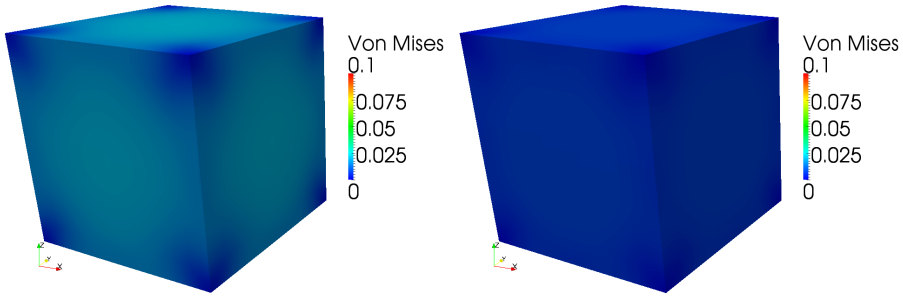

(e) $t = 28$

(f) $t = 30$

Figure 6.3: Plots of the Von Mises stress for Case 1 at different time steps. Each time step is 0.02 seconds (displacements are magnified by a factor of 50)

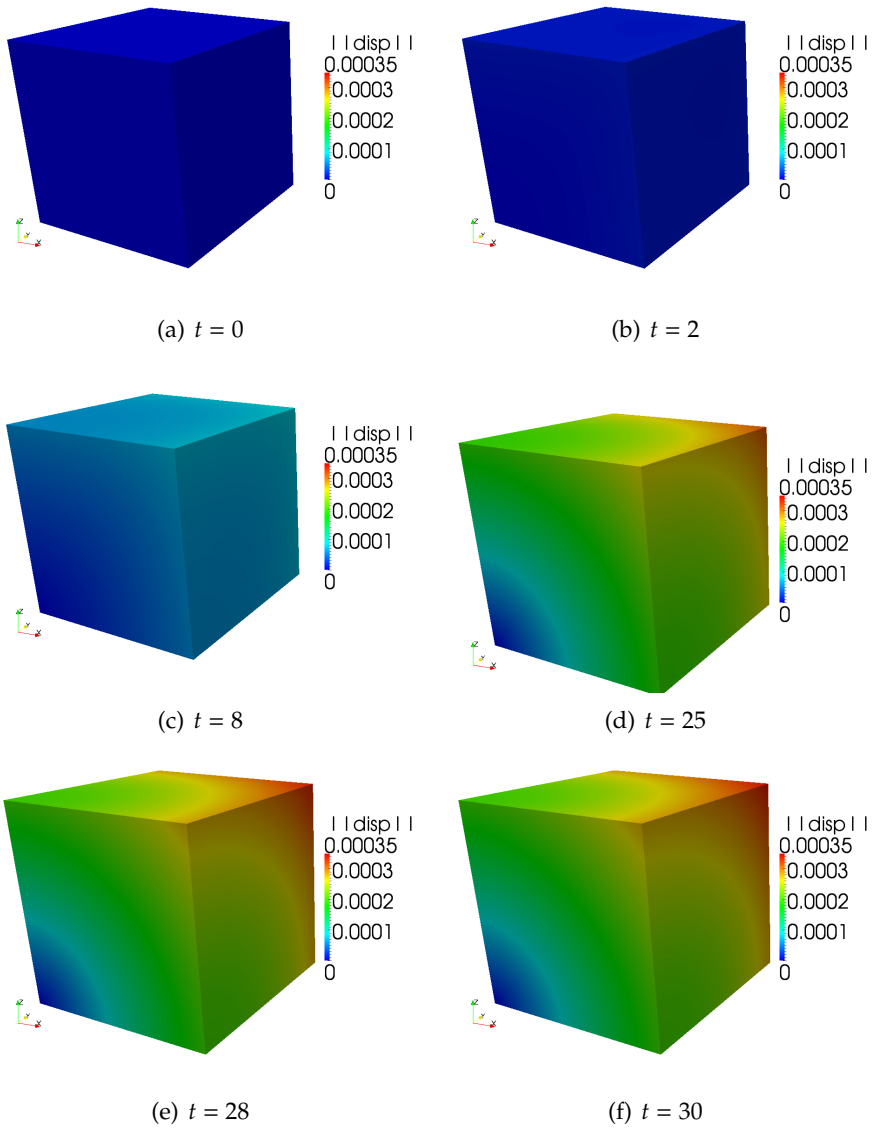

(a) $t = 0$ (b) $t = 2$

(c) $t = 8$ (d) $t = 25$

(e) $t = 28$ (f) $t = 30$

Figure 6.4: Plots of the magnitude of the displacement for Case 1 at different time steps. Each time step is 0.02 seconds (displacements are magnified by a factor of 50). Note: only one eighth of the cube is plotted

both models have the same term for uniform swelling.

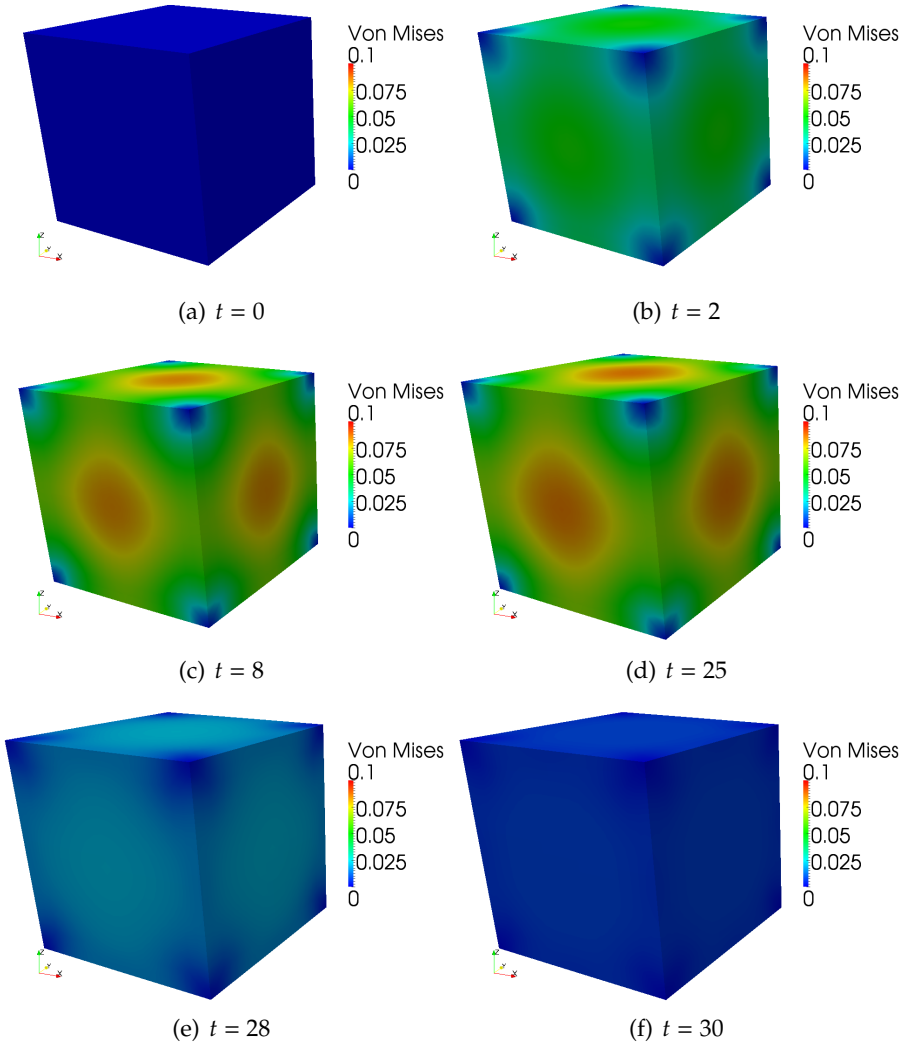

(a) $t = 0$ (b) $t = 2$

(c) $t = 8$ (d) $t = 25$

(e) $t = 28$ (f) $t = 30$

Figure 6.5: Plots of the Von Mises stress Case 2 at different time steps. Each time step is 0.02 seconds (displacements are magnified by a factor of 50)

Figure 6.6 shows how the magnitude of the displacement change during the change of concentration in the body. The values of the magnitude of the displacements are very similar to those shown in subsection 6.1.1. That is because both models have the same term for uniform swelling.

6.1.3 Case 3: Saturation

In this example we consider the following constitutive models:

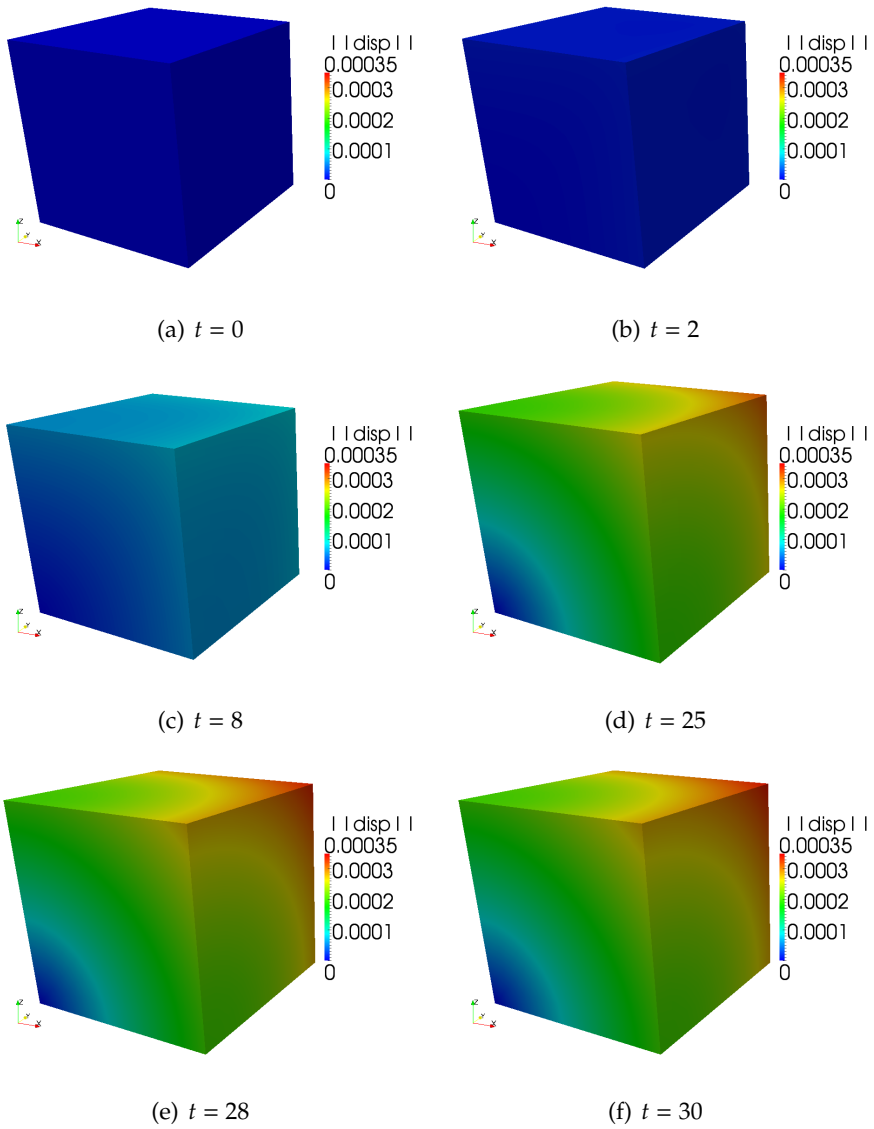

(a) $t = 0$ (b) $t = 2$

(c) $t = 8$ (d) $t = 25$

(e) $t = 28$ (f) $t = 30$

Figure 6.6: Plots of the magnitude of the displacement Case 2 at different time steps. Each time step is 0.02 seconds (displacements are magnified by a factor of 50). Note: only one eighth of the cube is plotted

$$\begin{aligned}\tilde{\mathbf{D}}(\tilde{C}) &= \tilde{\mathbf{D}}_0 - \frac{\tilde{\mathbf{D}}_0}{Exp((\frac{\tilde{C}_0+\tilde{C}_1}{2} - \tilde{C})/\alpha) + 1} \\ \mathbf{S} &= \mathbb{E} : (\mathbf{E} - \beta(1 - \frac{1}{Exp((-\frac{\tilde{C}_0+\tilde{C}_1}{2} + \tilde{C})/\alpha) + 1})\mathbf{I})\end{aligned} \tag{6.1.3}$$

Figure 6.7 shows how the non-dimensional Von Mises stress (divided by the yield stress), change during the change of concentration in the body. The shape of the body is very similar to those shown in subsection 6.1.1, but the values one order of magnitude smaller. Figure 6.8 shows how the magnitude of the displacement change during the change of concentration in the body. The values of the magnitude of the displacements are about one order of magnitude smaller than those shown in subsection 6.1.1.

6.1.4 Case 4: Diffusion induced non uniform strain

In this example we consider the following constitutive models:

$$\begin{aligned}\tilde{\mathbf{D}} &= \tilde{\mathbf{D}}_0 \\ \mathbf{S} &= \mathbb{E} : (\mathbf{E} - \beta(\tilde{C} - \tilde{C}_0)(\mathbf{I} - \mathbf{M} \otimes \mathbf{M}))\end{aligned} \tag{6.1.4}$$

Figure 6.9 shows how the non-dimensional Von Mises stress (divided by the yield stress), change during the change of concentration in the body. Because this is a homogeneous material, the body reaches a steady-state, where the stresses die down and the body has a homogeneous distribution of the concentration. Since the model has nonuniform strains induced by diffusion, even though the material is isotropic, we can see that the surfaces constructed by constant values of Von Mises stress are not spherical, as expected. The body swells up and deforms due to diffusion in two directions only, causing it to deform in the third direction due to Poisson's effect.
Figure 6.10 shows how the magnitude of the displacement change during the change of concentration in the body. Due to the nonuniform deformations induced by diffusion, the maximum magnitude of the displacements in this case is almost twice as large as the values shown in Case 1 and 2.

With all the above cases shown, we show several scalar physical quantities that can be used to compare and show differences between the cases. These are computed for the entire body.

Figure 6.11 (a) shows the change of non dimensional total mass of the body (divided by its initial mass) as a function of time. The plots of Cases 1, 2, and 4 lie one on top of the other. The curves rise as the concentration ramps up on the boundaries, and then gradually approach a final value that corresponds to the final level of concentration in the body. For Case 3 (saturation), we see that the curve does not rise in a linear manner, it seems to rise to a constant value which is the saturation point of the body. It then remains

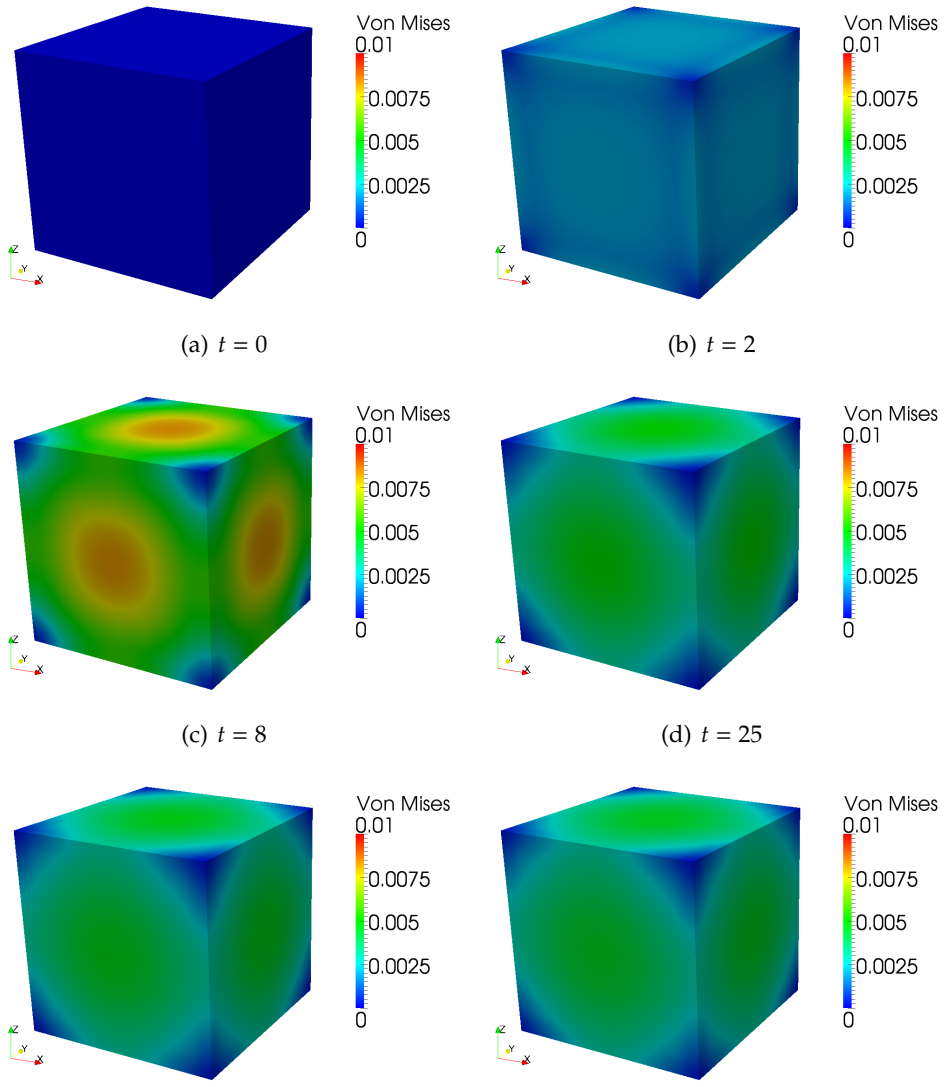

(a) $t = 0$ (b) $t = 2$

(c) $t = 8$ (d) $t = 25$

(e) $t = 28$ (f) $t = 30$

Figure 6.7: Plots of the Von Mises stress Case 3 at different time steps. Each time step is 0.02 seconds (displacements are magnified by a factor of 50)

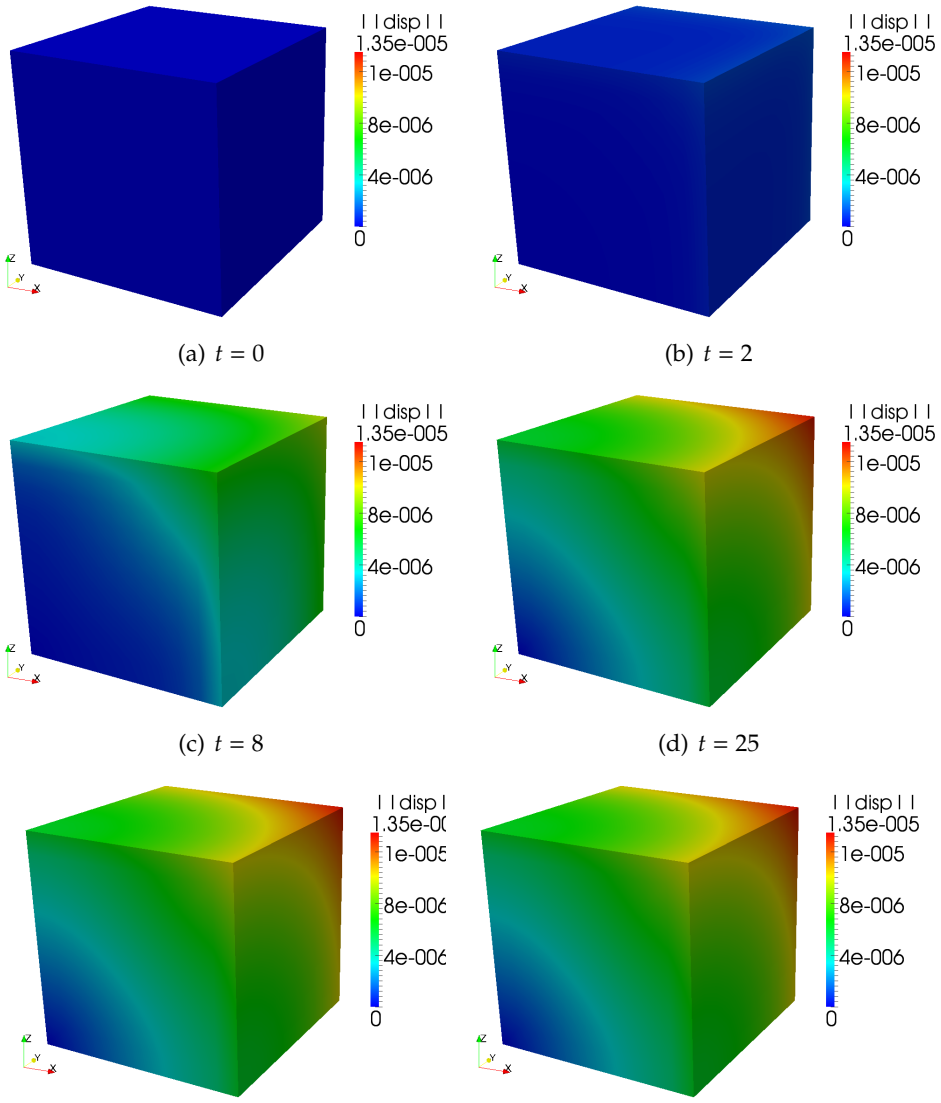

(a) $t = 0$ (b) $t = 2$

(c) $t = 8$ (d) $t = 25$

(e) $t = 28$ (f) $t = 30$

Figure 6.8: Plots of the magnitude of the displacement Case 3 at different time steps. Each time step is 0.02 seconds (displacements are magnified by a factor of 50). Note: only one eighth of the cube is plotted

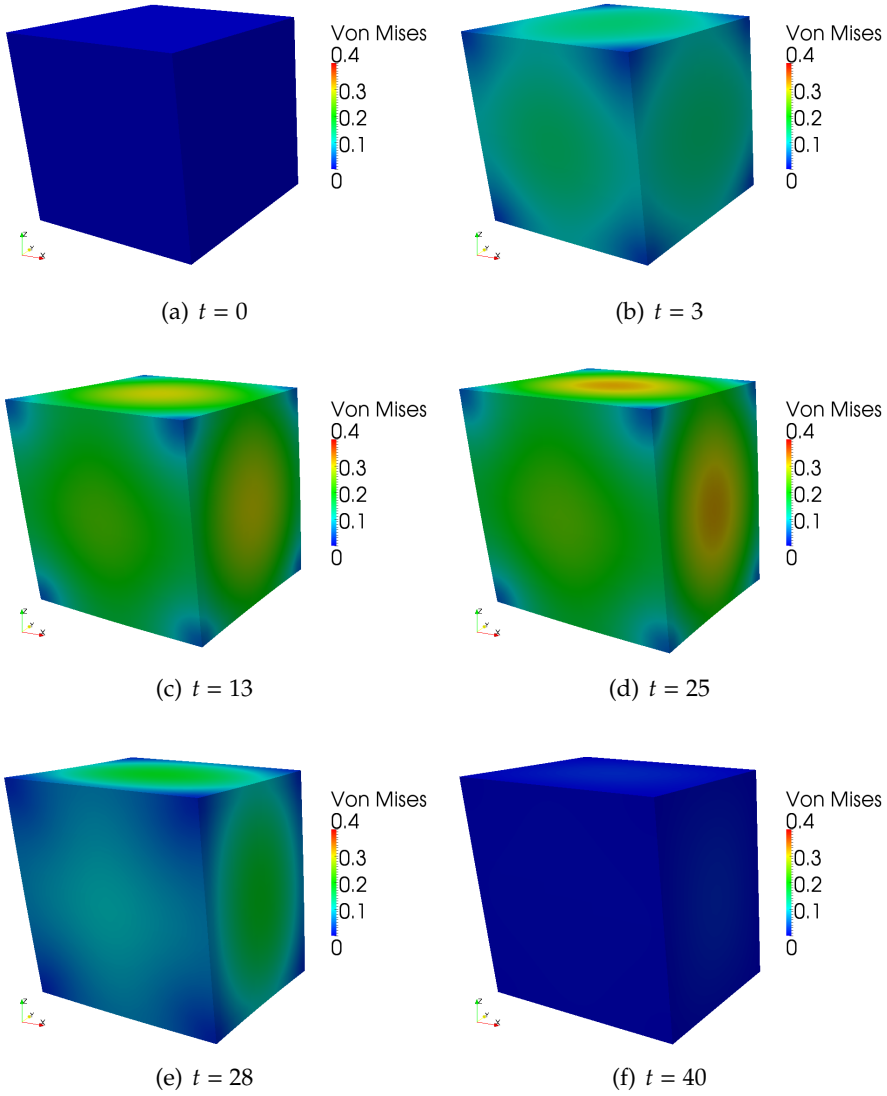

(a) $t = 0$ (b) $t = 3$

(c) $t = 13$ (d) $t = 25$

(e) $t = 28$ (f) $t = 40$

Figure 6.9: Plots of the Von Mises stress Case 4 at different time steps. Each time step is 0.02 seconds (displacements are magnified by a factor of 50)

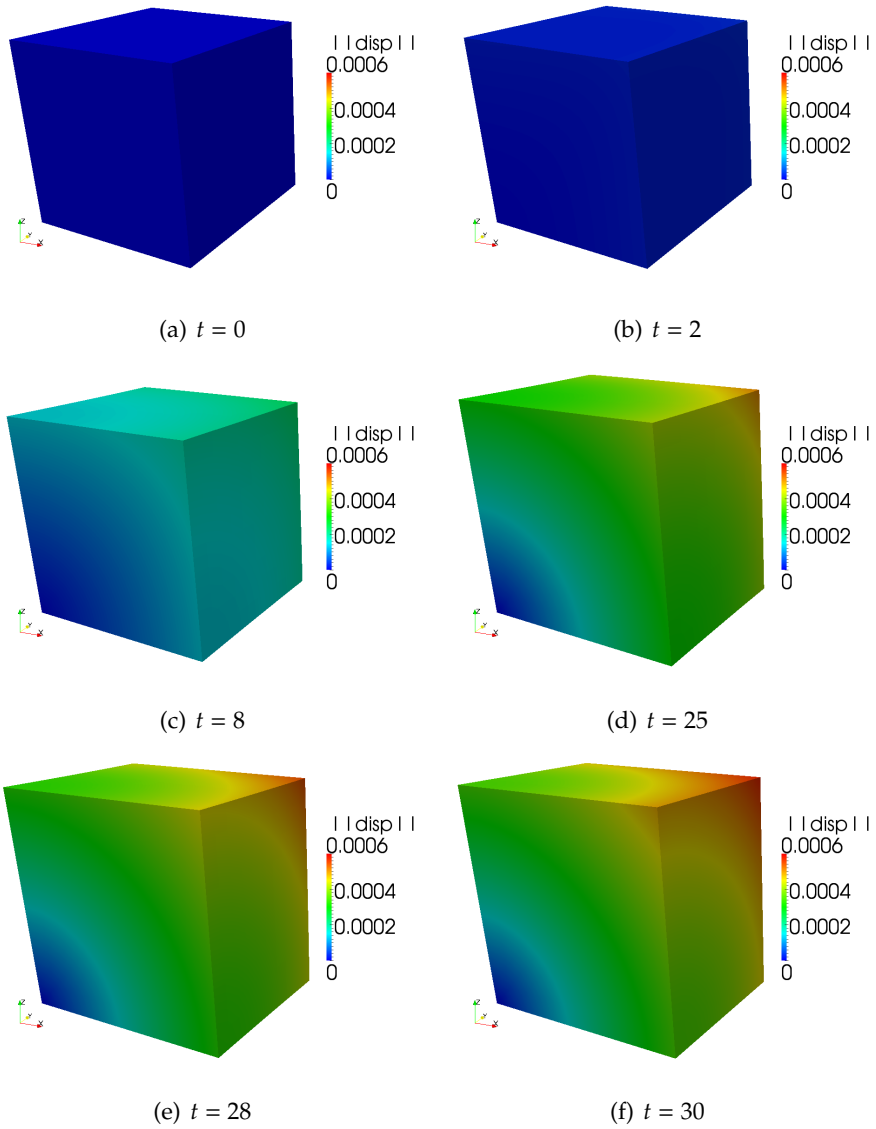

(a) $t = 0$ (b) $t = 2$

(c) $t = 8$ (d) $t = 25$

(e) $t = 28$ (f) $t = 30$

Figure 6.10: Plots of the magnitude of the displacement Case 4 at different time steps. Each time step is 0.02 seconds (displacements are magnified by a factor of 50). Note: only one eighth of the cube is plotted

at that value for the rest of the simulation.

Figure 6.11 (b) shows the change of non dimensional total volume of the body (divided by its initial volume) as a function of time. The plots of Cases 1 and 2 lie one on top of the other. The curves rise as the concentration ramps up on the boundaries. For Case 3 (saturation), we see that the curve rises in a similar manner to Case 1 and 2, but for different values. It rises asymptotically to a constant value which is the saturation point of the body. For Case 4 (Nonuniform diffusion induced strain), there is a very small change in the volume. That is due to the fact that the direction of the vector **M** is such that the deformation induced by diffusion is constrained by the boundary conditions.

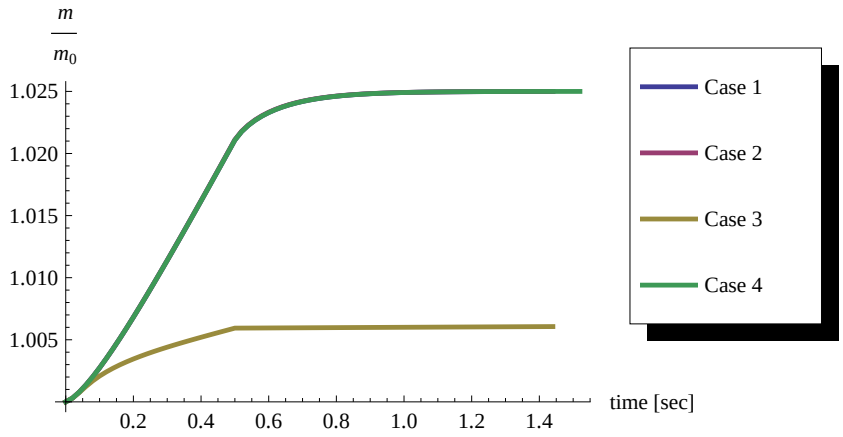

(a) Nondimensional mass as a function of time

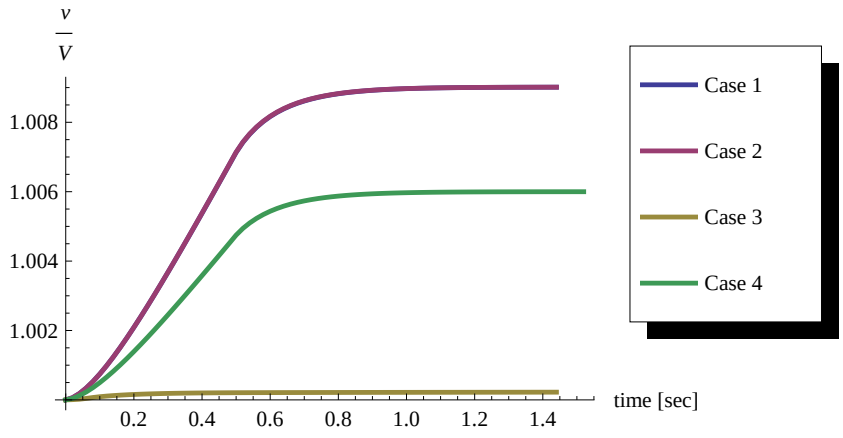

(b) Nondimensional volume as a function of time

Figure 6.11: Plots of the non dimensional mass and volume as functions of time

Figure 6.12 (a) shows the change of the strain energy of the body, Ψ_m, as a function of time. The plots of Cases 1 and 2 lie one on top of the other. The curves rise as the

concentration ramps up on the boundaries. For Case 3 (saturation), we see that the curve rises in a similar manner. It seems to rise asymptotically to a constant value which is the saturation point of the body. For Case 4 (Nonuniform diffusion induced strain), there is a very small change in the energy. That is due to the fact that the direction of the vector **M** is such that the deformation induced by diffusion is constrained by the boundary conditions.

Figure 6.12 (b) shows the change of coupled energy term of the body, Ψ_{md}, as a function of time. The behavior is very similar to figure 6.12 (a).

Figure 6.12 (c) shows the change of diffusion energy of the body, Ψ_d, as a function of time. The plots of Cases 1, 2 and 4 lie one on top of each other. The curves rise as the concentration ramps up on the boundaries and set at a final value. For Case 3 (saturation), we see that the curve does not rise in a similar manner, it seems to rise to a constant value which is the saturation point of the body. It then remains at that value for the rest of the simulation.

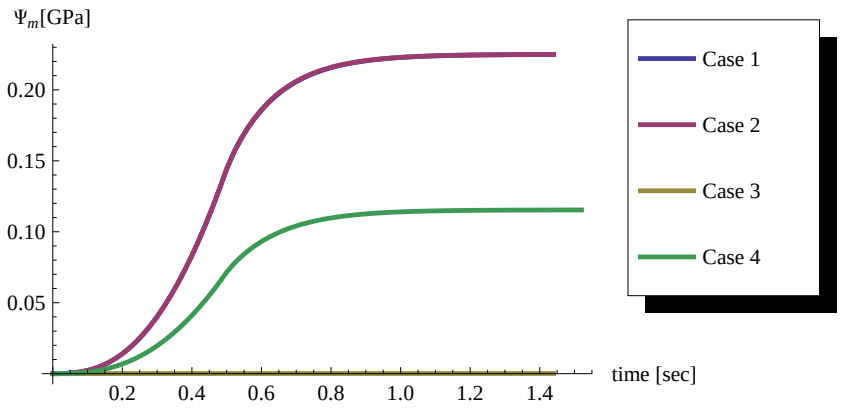

(a) The strain energy Ψ_m as a function of time

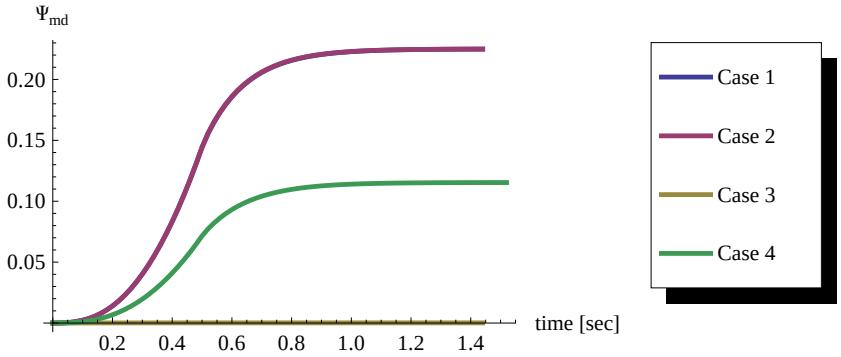

(b) The coupled term of internal energy Ψ_{md} as a function of time

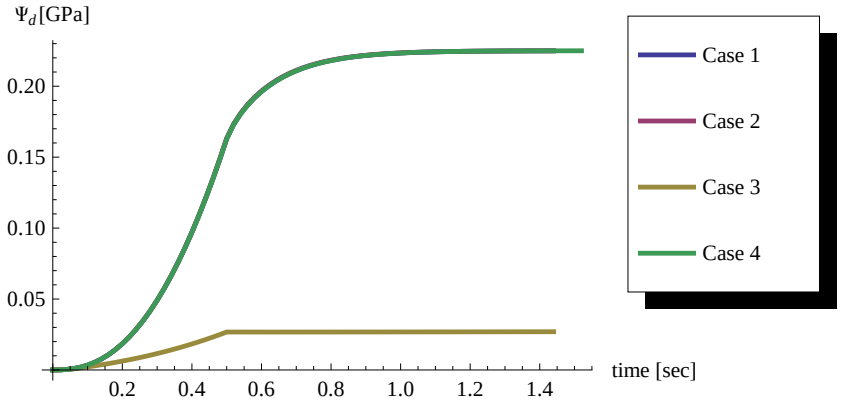

(c) The diffusion part of the internal energy Ψ_d as a function of time

Figure 6.12: Components of the internal energy in the body: Ψ_m, Ψ_{md} and Ψ_d

6.2 Free swelling of a fiber composite material

As described in section (6.1), we consider the same settings of cases, boundary conditions, etc. The difference is that instead of the homogeneous solid, we consider a fiber composite material. the matrix and the fibers have different mechanical and diffusivity properties. To illustrate the effects, one fiber is positioned in the middle which by the symmetry accounts for four fibers in the matrix.

6.2.1 Case 1: Fixed diffusivity

We consider the following constitutive models for both the fibers and the matrix:

$$\begin{aligned} \tilde{\mathbf{D}} &= \tilde{\mathbf{D}}_0 \\ \mathbf{S} &= \mathbb{E} : \mathbf{E} - \beta(\tilde{C} - \tilde{C}_0)\mathbf{I} \end{aligned} \tag{6.2.1}$$

With an isotropic model for the matrix, and a transverse isotropic for the fiber. For the deformation induced by diffusion, the parameters are set to be the same for the matrix and the fibers. The following plots show several parameters at different time steps.

Figure 6.23 shows how the non-dimensional Von Mises stress (divided by the yield stress), change during the change of concentration in the body. Even though this is a non-homogeneous material, the body reaches a steady-state, where the stresses die down and the body has a homogeneous distribution of the concentration. That is due to the fact that the parameters for the diffusion are set to be the same for the matrix and the fibers. Since this is a non-homogeneous material, the dynamic deformation is more complex than a that of a homogeneous material.

Figure 6.24 shows how the magnitude of the displacement change during the change of concentration in the body. As mentioned before, because the diffusion parameters are set to be the same, the final configuration of the body is similar to that shown for a homogeneous material. So, even though the mechanical parameters are different, for a homogeneous concentration at steady state, the deformation due to diffusion is the same for the matrix and the fibers.

Figures 6.15 and 6.16 show the values of the strain energy Ψ_m on a virtual cut plane in the body, for different time steps. We can see that the highest values are in the fibers, as they are stiffer that the matrix in this case. We can also see how the fibers move with the change in concentration. The fibers displace further from each other as the concentration values increase, and cause deformations and stresses in the matrix.

6.2.2 Case 2: Strain dependent diffusivity

We consider the following constitutive models for both the fibers and the matrix:

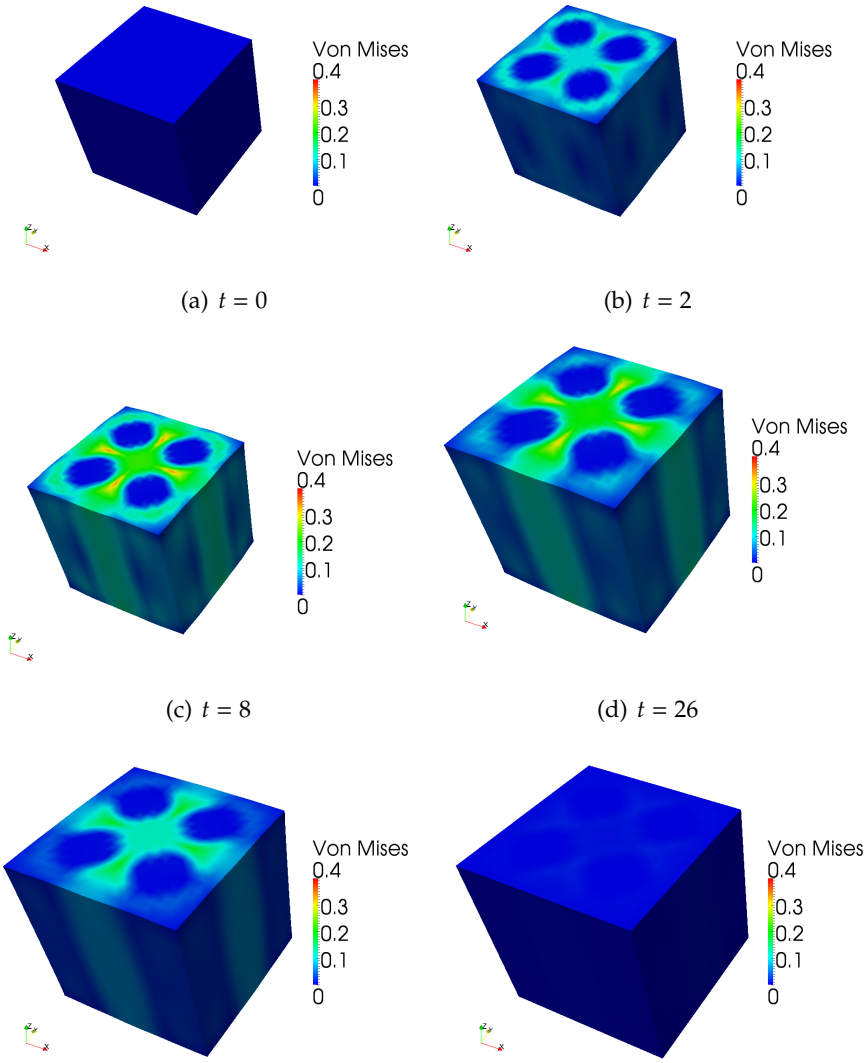

(a) $t = 0$ (b) $t = 2$

(c) $t = 8$ (d) $t = 26$

(e) $t = 28$ (f) $t = 39$

Figure 6.13: Fiber composite swelling, Case 1: Plots of the Von Mises stress at different time steps. Each time step is 0.02 seconds (displacements are magnified by a factor of 200)

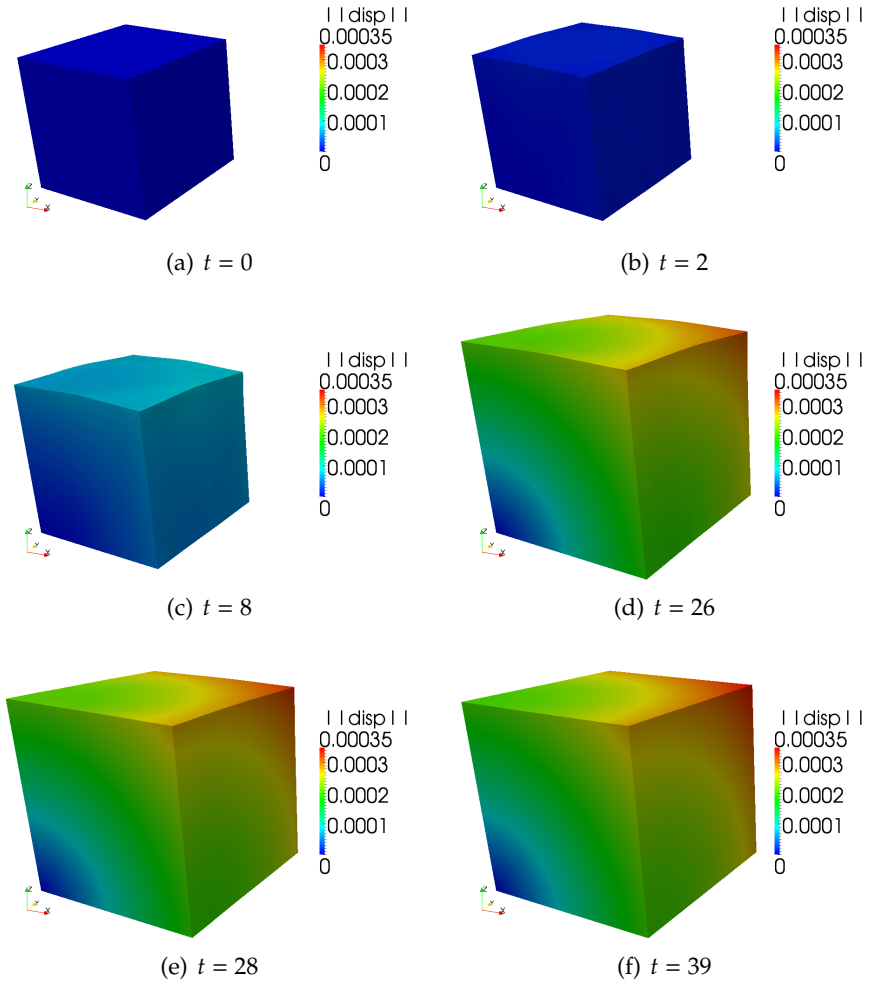

(a) $t = 0$ (b) $t = 2$

(c) $t = 8$ (d) $t = 26$

(e) $t = 28$ (f) $t = 39$

Figure 6.14: Fiber composite swelling, Case 1: Plots of the magnitude of the displacement at different time steps. Each time step is 0.02 seconds (displacements are magnified by a factor of 200). Note: only one eighth of the cube is plotted

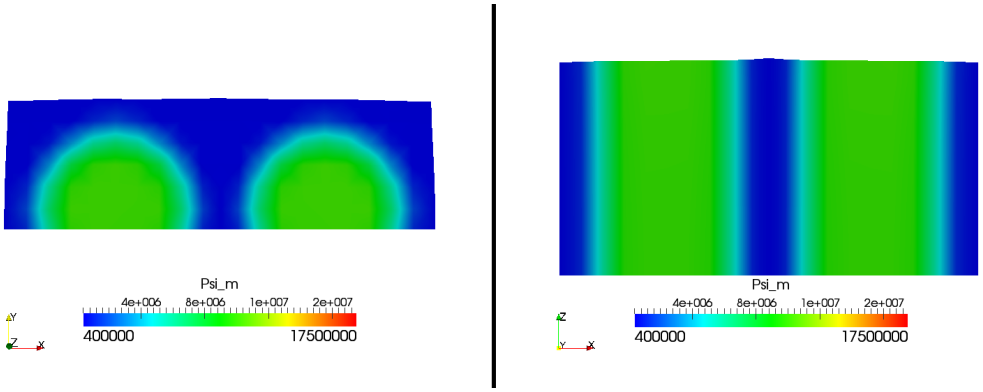

(a) $t = 19$

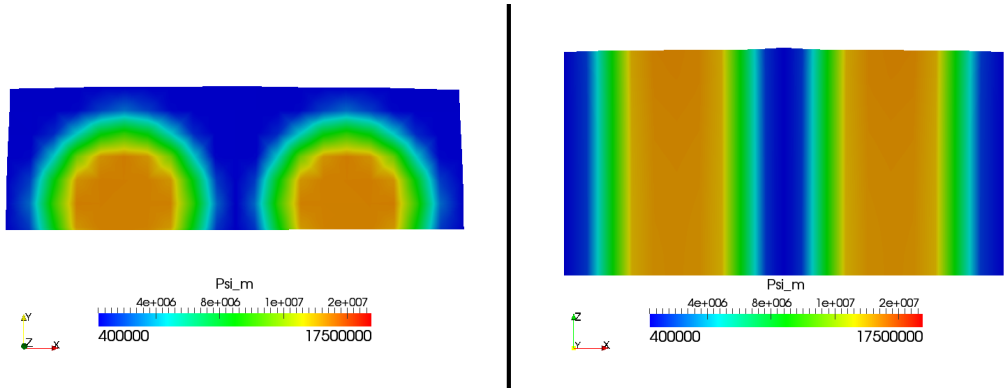

(b) $t = 23$

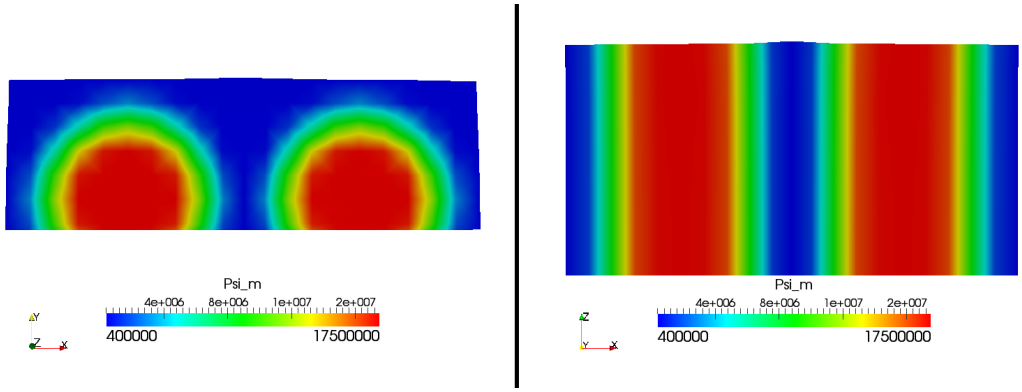

(c) $t = 26$

Figure 6.15: Fiber composite swelling, Case 1, part 1 of 2: Plots of the strain energy, Ψ_m, at different time steps. Each time step is 0.02 seconds (displacements are magnified by a factor of 200)

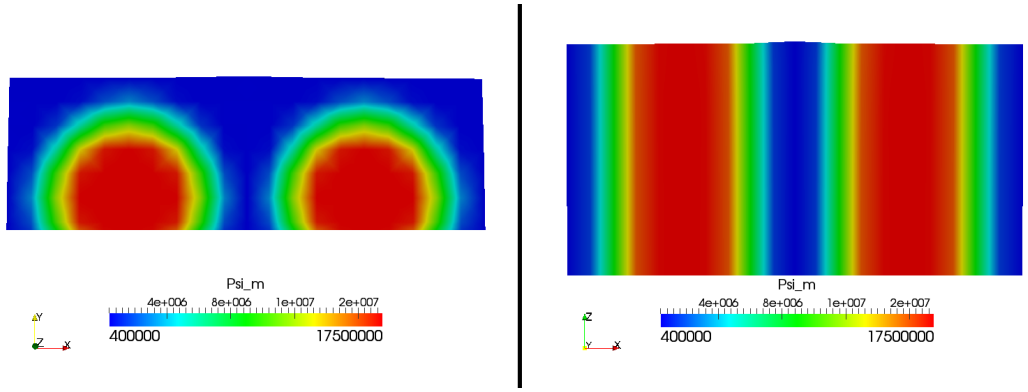

(a) $t = 28$

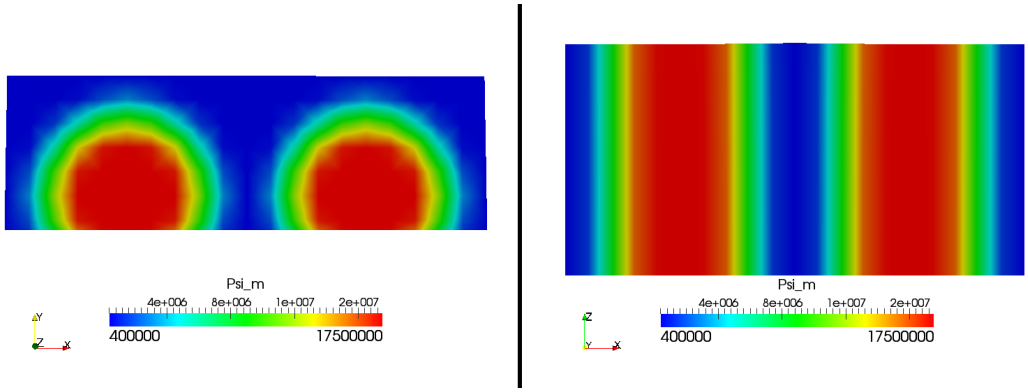

(b) $t = 33$

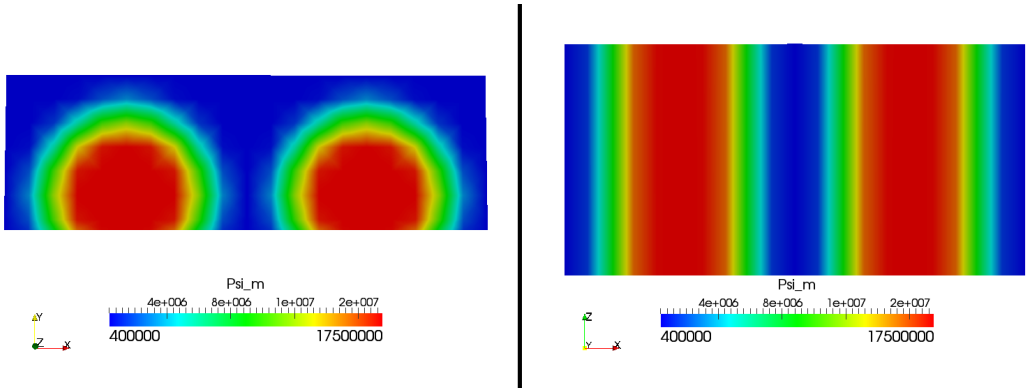

(c) $t = 39$

Figure 6.16: Fiber composite swelling, Case 1, part 2 of 2: Plots of the strain energy, Ψ_m, at different time steps. Each time step is 0.02 seconds (displacements are magnified by a factor of 200)

$$\begin{aligned} \tilde{\mathbf{D}} &= \tilde{\mathbf{D}}_0 \frac{e^J - 1}{e - 1} \\ \mathbf{S} &= \mathbb{E} : \mathbf{E} - \beta(\tilde{C} - \tilde{C}_0)\mathbf{I} \end{aligned} \tag{6.2.2}$$

With an isotropic model for the matrix, and a transverse isotropic for the fiber. The following plots show several parameters at different time steps.

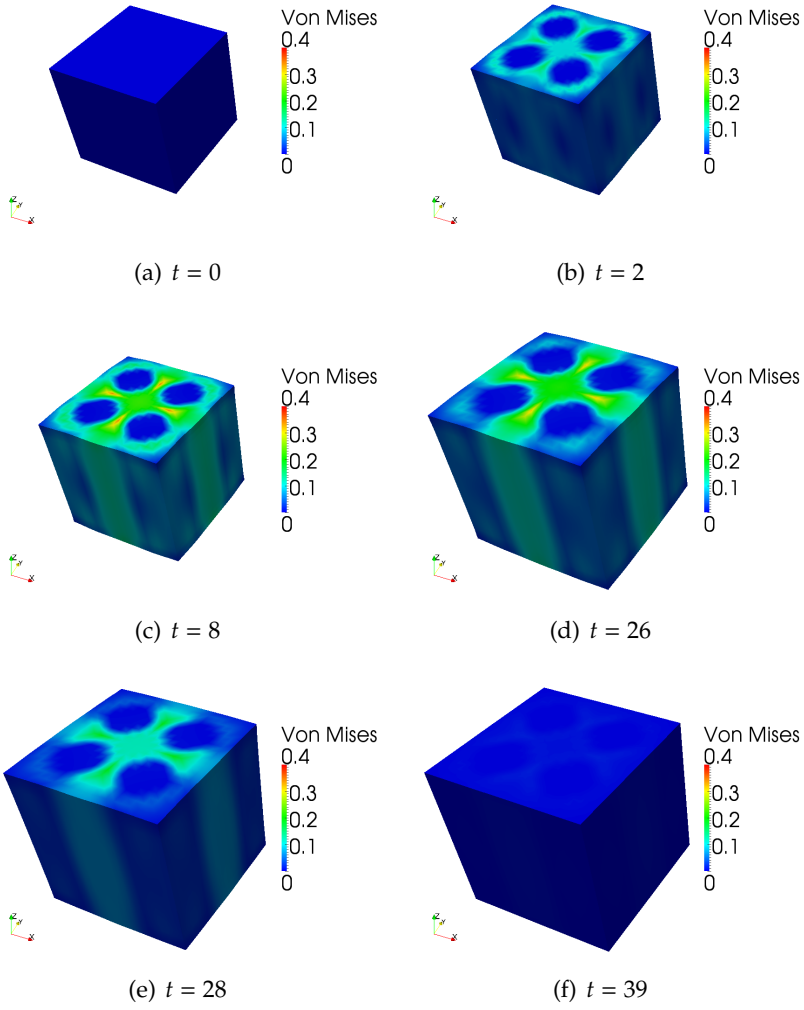

(a) $t = 0$ (b) $t = 2$

(c) $t = 8$ (d) $t = 26$

(e) $t = 28$ (f) $t = 39$

Figure 6.17: Fiber composite swelling, Case 2: Plots of the Von Mises stress at different time steps. Each time step is 0.02 seconds (displacements are magnified by a factor of 200)

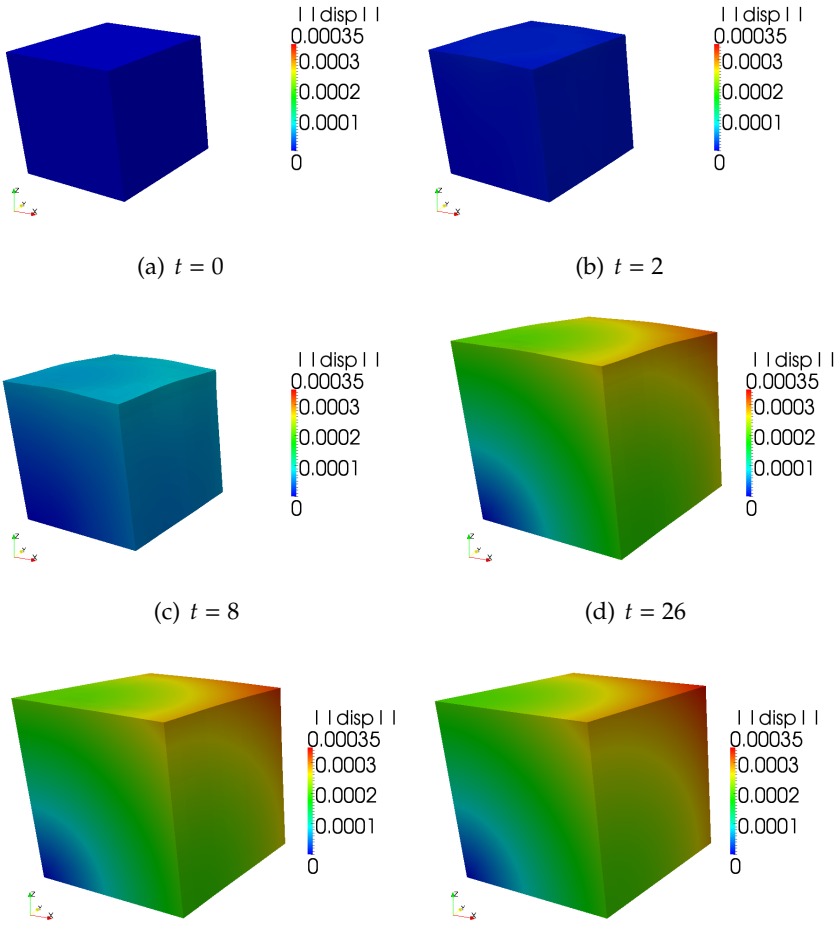

(a) $t = 0$ (b) $t = 2$

(c) $t = 8$ (d) $t = 26$

(e) $t = 28$ (f) $t = 39$

Figure 6.18: Fiber composite swelling, Case 2: Plots of the magnitude of the displacement at different time steps. Each time step is 0.02 seconds (displacements are magnified by a factor of 200). Note: only one eighth of the cube is plotted

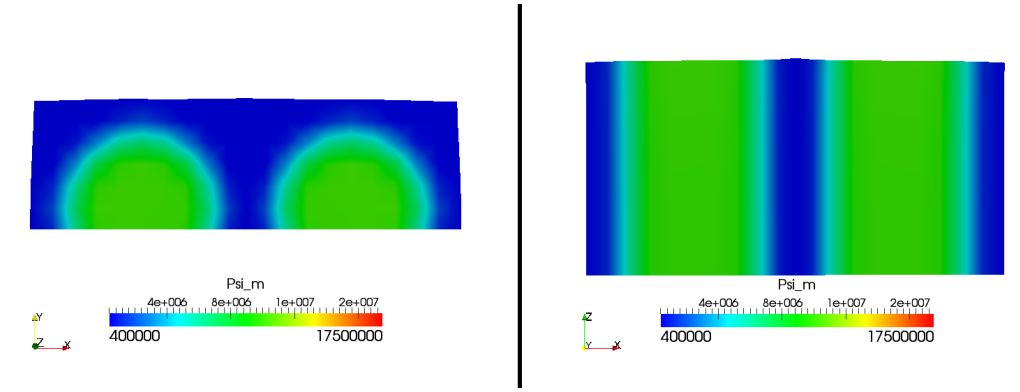

(a) $t = 19$

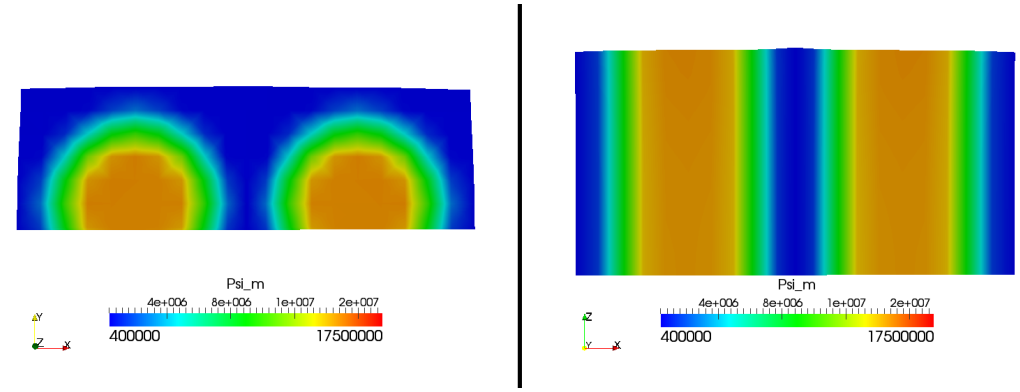

(b) $t = 23$

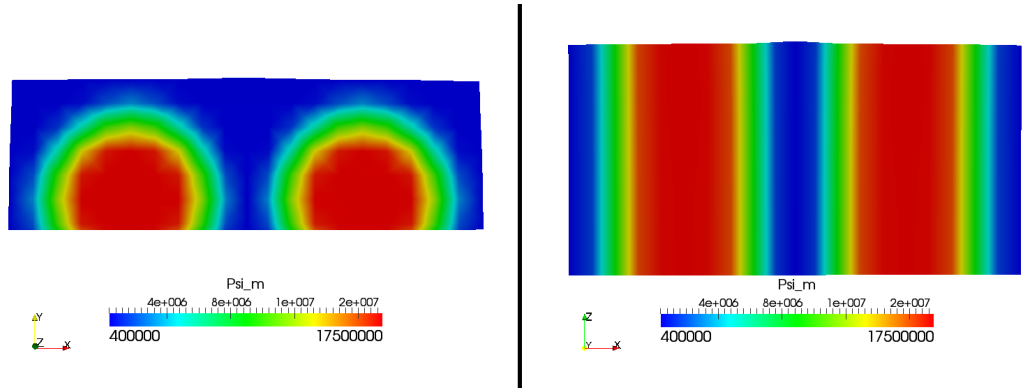

(c) $t = 26$

Figure 6.19: Fiber composite swelling, Case 2, part 1 of 2: Plots of the strain energy, Ψ_m, at different time steps. Each time step is 0.02 seconds (displacements are magnified by a factor of 200)

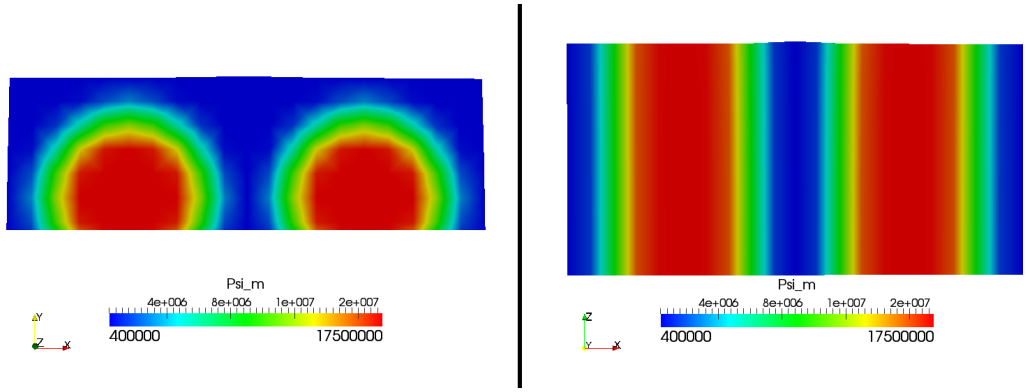

(a) $t = 28$

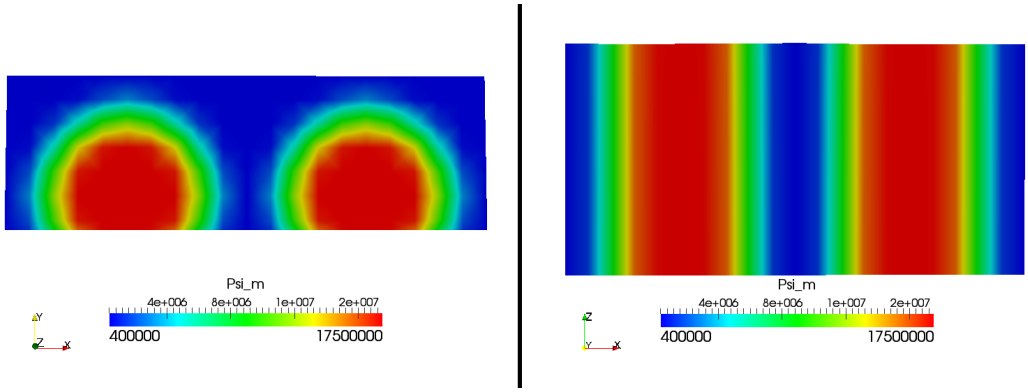

(b) $t = 33$

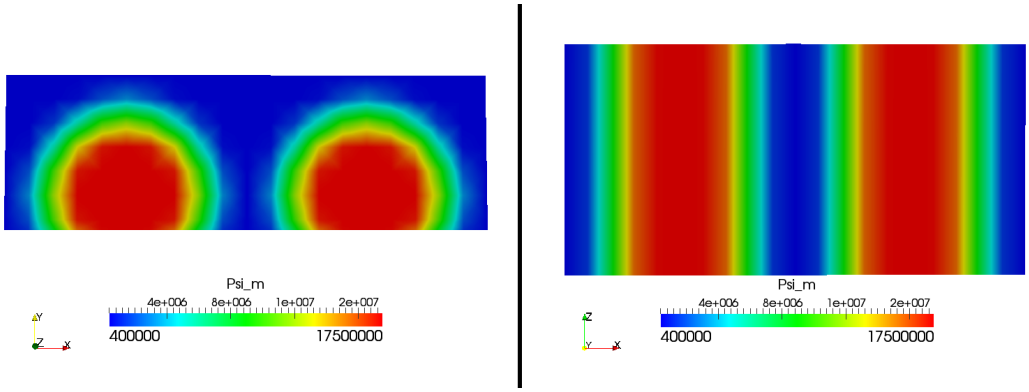

(c) $t = 39$

Figure 6.20: Fiber composite swelling, Case 2, part 2 of 2: Plots of the strain energy, Ψ_m, at different time steps. Each time step is 0.02 seconds (displacements are magnified by a factor of 200)

6.2.3 Case 3: Saturation

We consider the following constitutive models for both the fibers and the matrix:

$$\begin{aligned}\tilde{\mathbf{D}}(\tilde{C}) &= \tilde{\mathbf{D}}_0 - \frac{\tilde{\mathbf{D}}_0}{Exp((\frac{\tilde{C}_0+\tilde{C}_1}{2} - \tilde{C})/\alpha) + 1} \\ \mathbf{S} &= \mathbb{E} : (\mathbf{E} - \beta(1 - \frac{1}{Exp((-\frac{\tilde{C}_0+\tilde{C}_1}{2} + \tilde{C})/\alpha) + 1})\mathbf{I})\end{aligned} \tag{6.2.3}$$

6.2.4 Case 4: Nonuniform diffusion induced strain

We consider the following constitutive models for both the fibers and the matrix:

$$\begin{aligned}\tilde{\mathbf{D}} &= \tilde{\mathbf{D}}_0 \\ \mathbf{S} &= \mathbb{E} : (\mathbf{E} - \beta(\tilde{C} - \tilde{C}_0)(\mathbf{I} - \mathbf{M} \otimes \mathbf{M}))\end{aligned} \tag{6.2.4}$$

With an isotropic model for the matrix, and a transverse isotropic model for the fiber. The following plots show several parameters at different time steps.

6.2.5 Free swelling of a fiber composite with Case 1 for the matrix and case 4 for the fibers

For the matrix, we consider an isotropic material, and the following constitutive model for the diffusion:

$$\begin{aligned}\tilde{\mathbf{D}} &= \tilde{\mathbf{D}}_0 \\ \mathbf{S} &= \mathbb{E} : (\mathbf{E} - \beta(\tilde{C} - \tilde{C}_0)\mathbf{I})\end{aligned} \tag{6.2.5}$$

and for the fibers, we consider a transverse-isotropic material, and the following constitutive model for the diffusion:

$$\begin{aligned}\tilde{\mathbf{D}} &= \tilde{\mathbf{D}}_0 \\ \mathbf{S} &= \mathbb{E} : (\mathbf{E} - \beta(\tilde{C} - \tilde{C}_0)(\mathbf{I} - \mathbf{M} \otimes \mathbf{M}))\end{aligned} \tag{6.2.6}$$

where $\mathbf{M}$ is the fiber direction. This means that for the deformation induced by diffusion, the parameters are set to be different for the matrix and the fibers.
Figure 6.27 shows how the non-dimensional Von Mises stress (divided by the yield stress), change during the change of concentration in the body. Because this is a inhomogeneous material, with a constitutive equation for diffusion, and mechanical properties that are

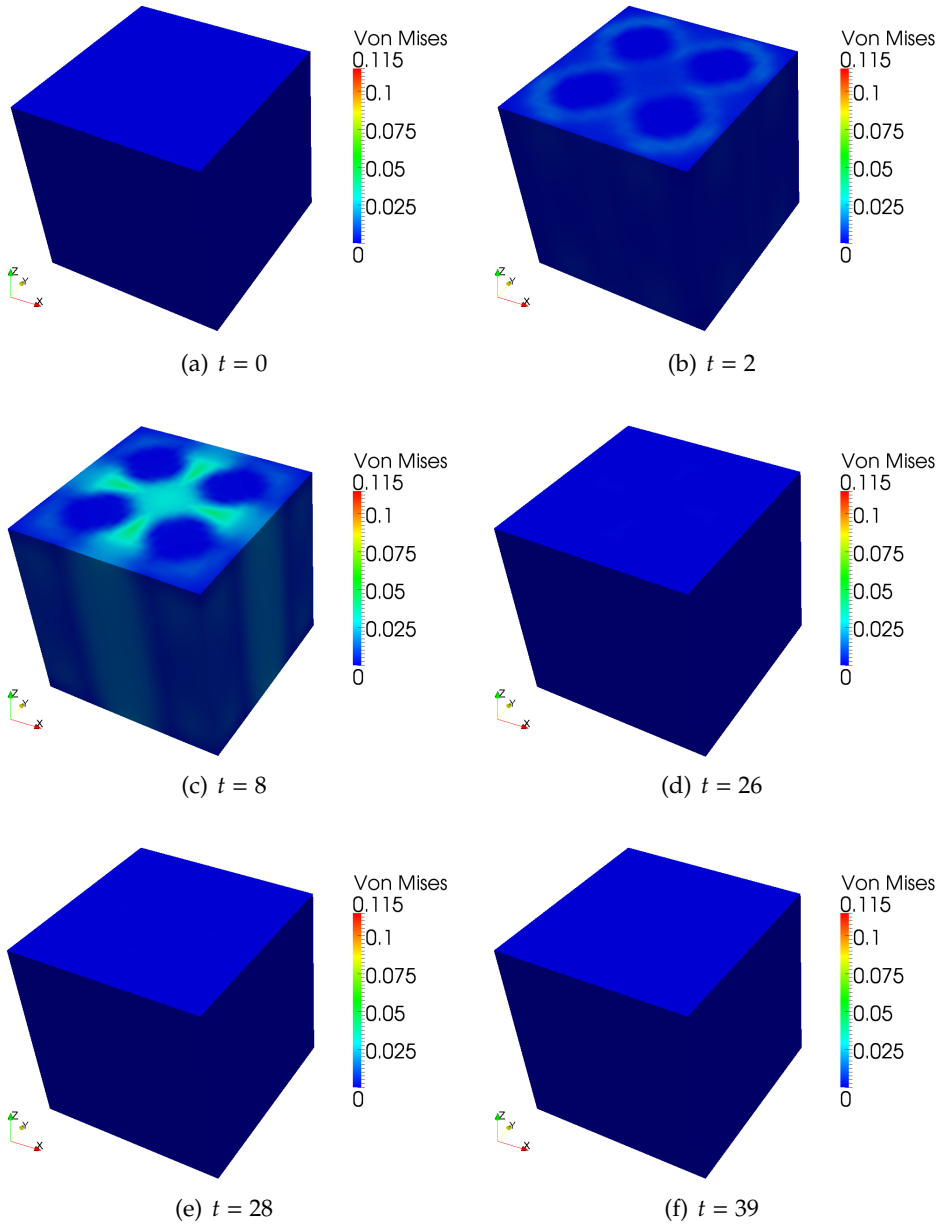

(a) $t = 0$ (b) $t = 2$

(c) $t = 8$ (d) $t = 26$

(e) $t = 28$ (f) $t = 39$

Figure 6.21: Fiber composite swelling, Case 3: Plots of the Von Mises stress at different time steps. Each time step is 0.02 seconds (displacements are magnified by a factor of 200)

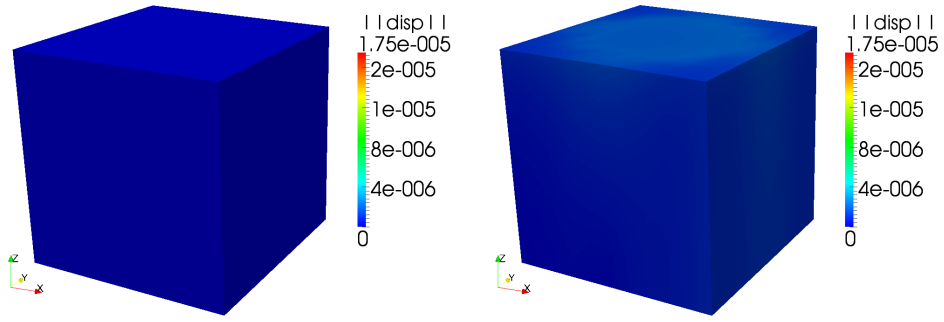

(a) $t = 0$

(b) $t = 2$

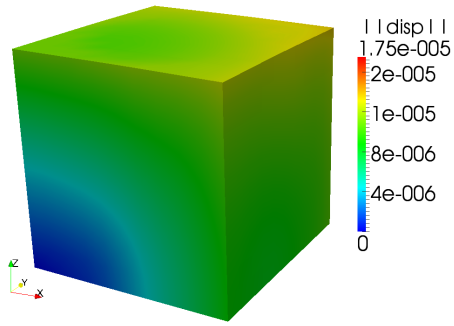

(c) $t = 8$

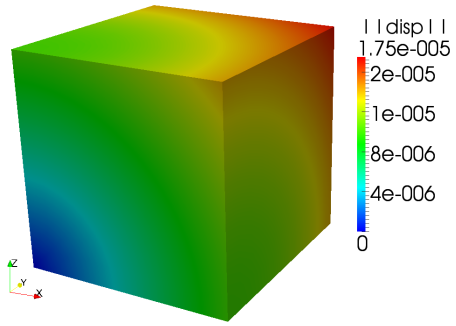

(d) $t = 26$

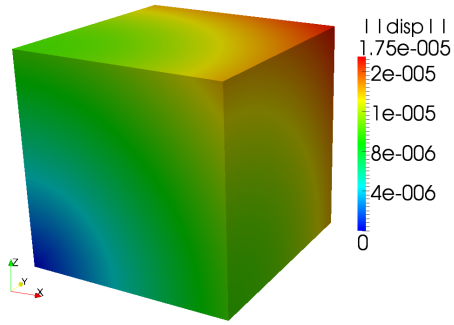

(e) $t = 28$

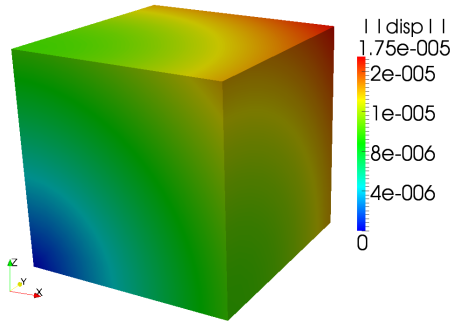

(f) $t = 39$

Figure 6.22: Fiber composite swelling, Case 3: Plots of the magnitude of the displacement at different time steps. Each time step is 0.02 seconds (displacements are magnified by a factor of 200). Note: only one eighth of the cube is plotted

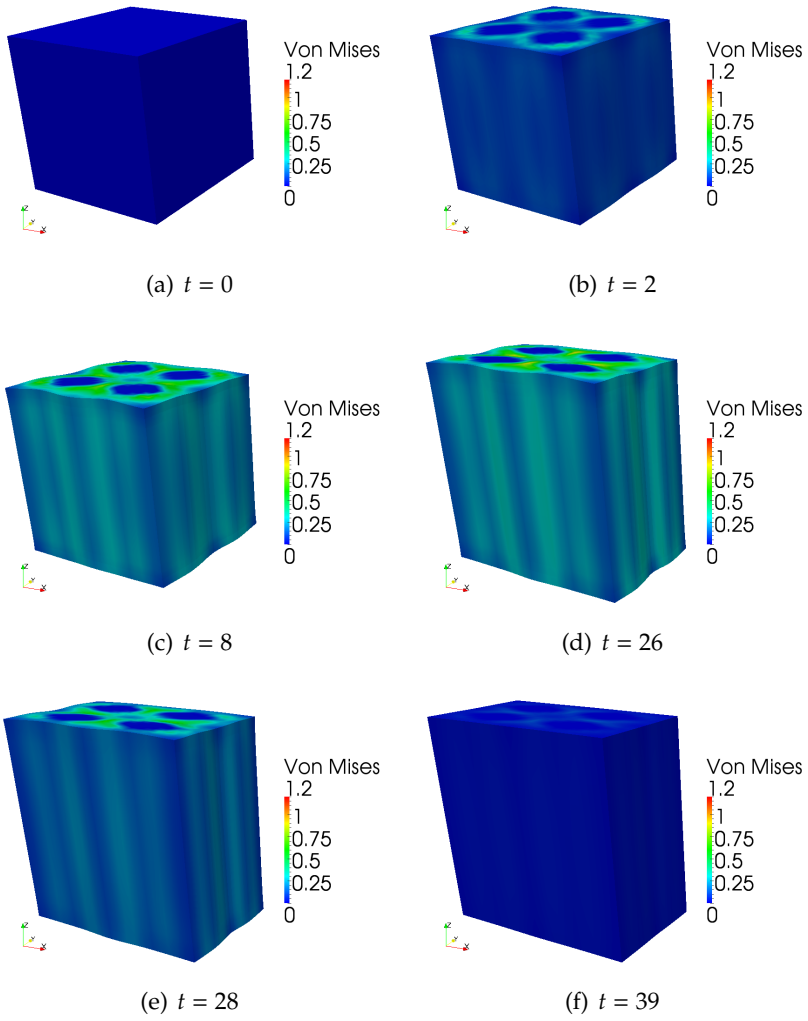

(a) $t = 0$ (b) $t = 2$

(c) $t = 8$ (d) $t = 26$

(e) $t = 28$ (f) $t = 39$

Figure 6.23: Fiber composite swelling, Case 4: Plots of the Von Mises stress at different time steps. Each time step is 0.02 seconds (displacements are magnified by a factor of 200)

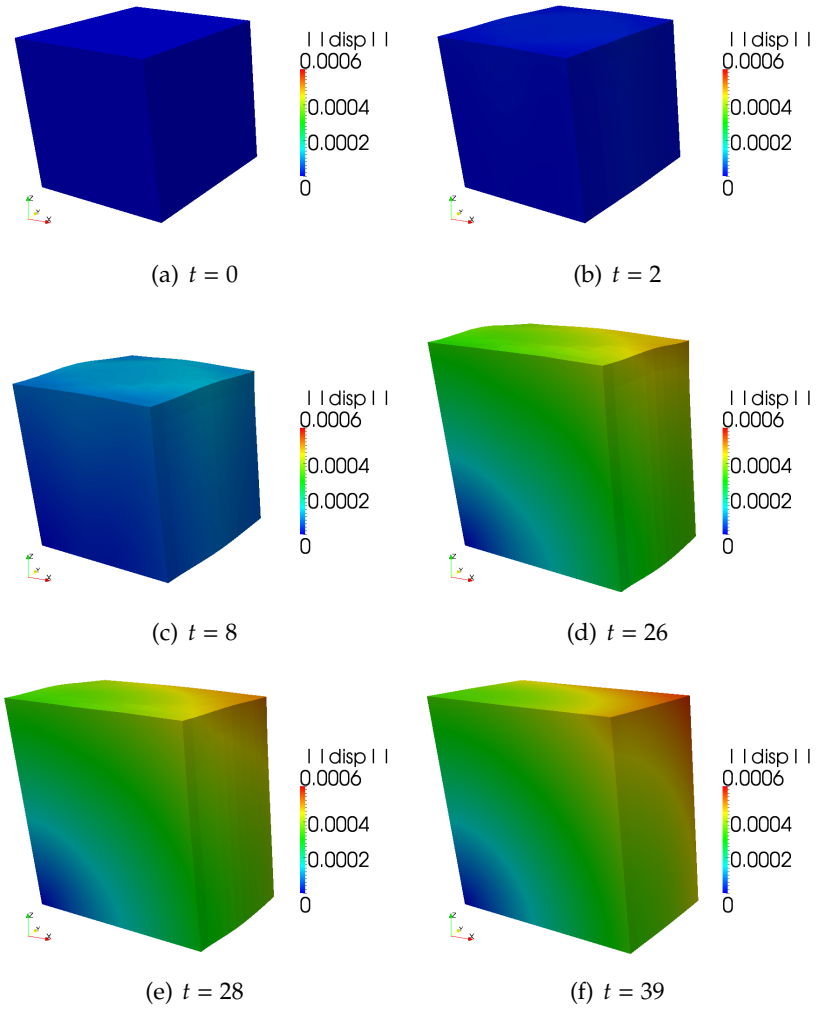

(a) $t = 0$ (b) $t = 2$

(c) $t = 8$ (d) $t = 26$

(e) $t = 28$ (f) $t = 39$

Figure 6.24: Fiber composite swelling, Case 4: Plots of the magnitude of the displacement at different time steps. Each time step is 0.02 seconds (displacements are magnified by a factor of 200). Note: only one eighth of the cube is plotted

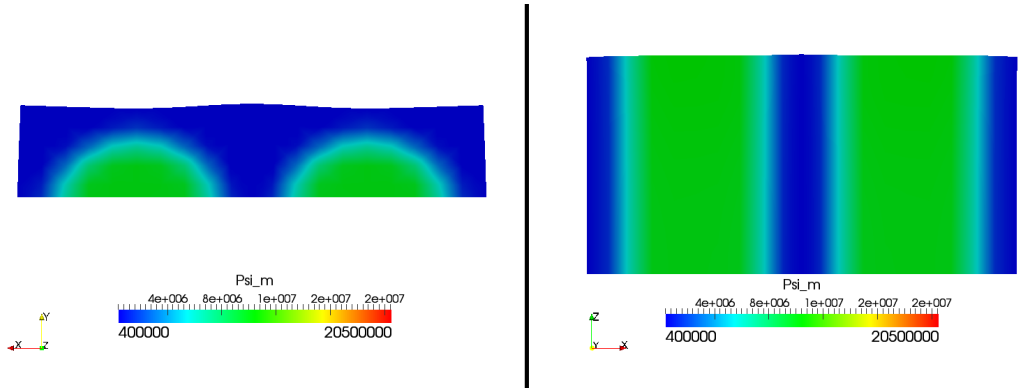

(a) $t = 19$

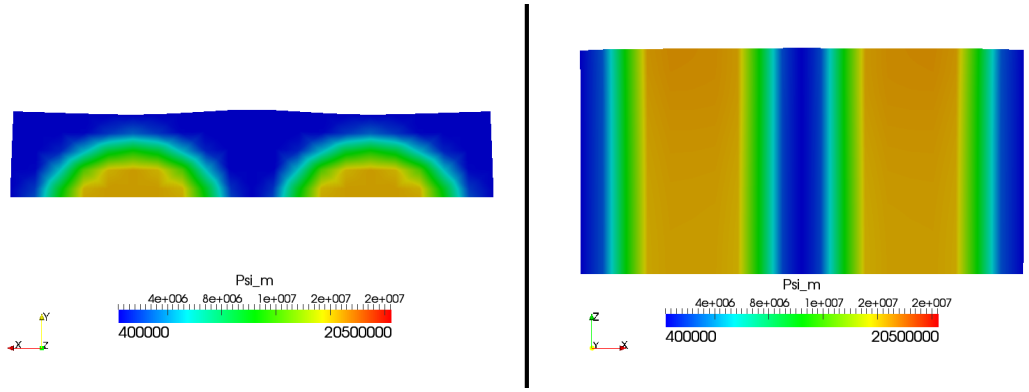

(b) $t = 23$

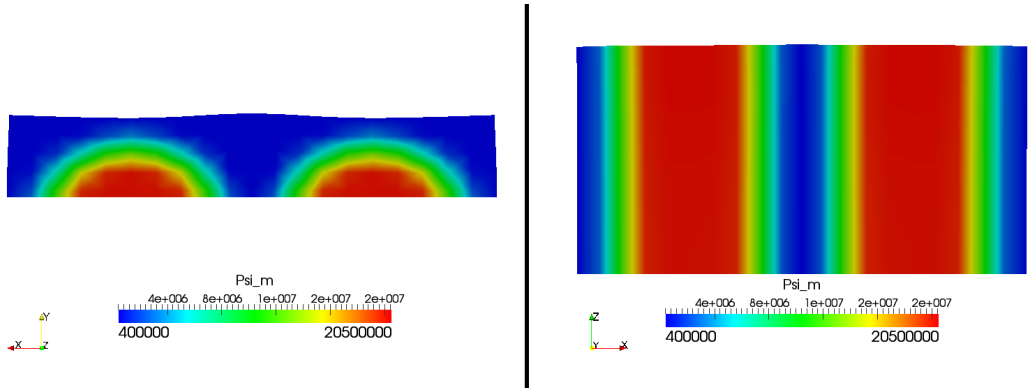

(c) $t = 26$

Figure 6.25: Fiber composite swelling, Case 4, part 1 of 2: Plots of the strain energy, Ψ_m, at different time steps. Each time step is 0.02 seconds (displacements are magnified by a factor of 200)

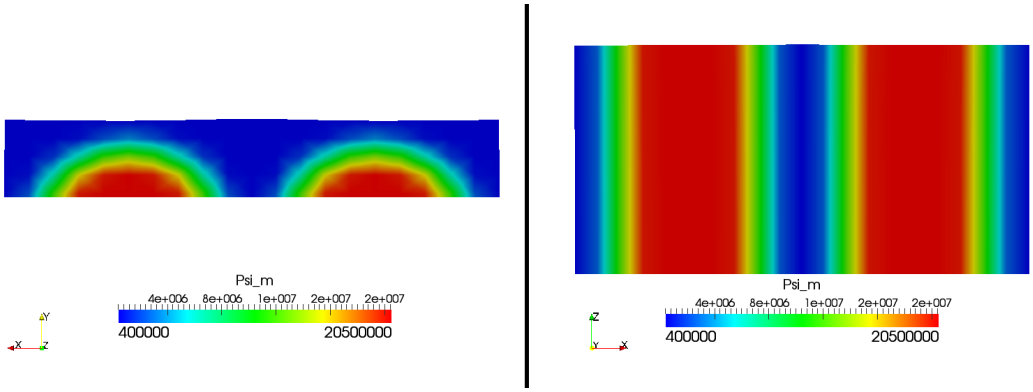

(a) $t = 28$

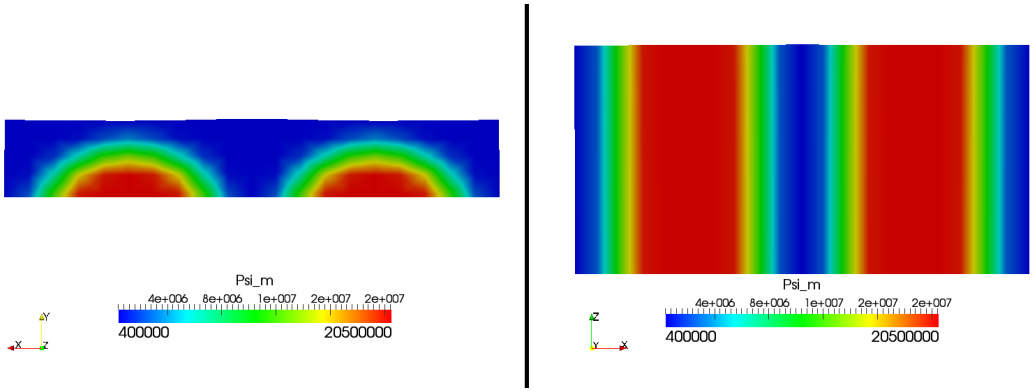

(b) $t = 33$

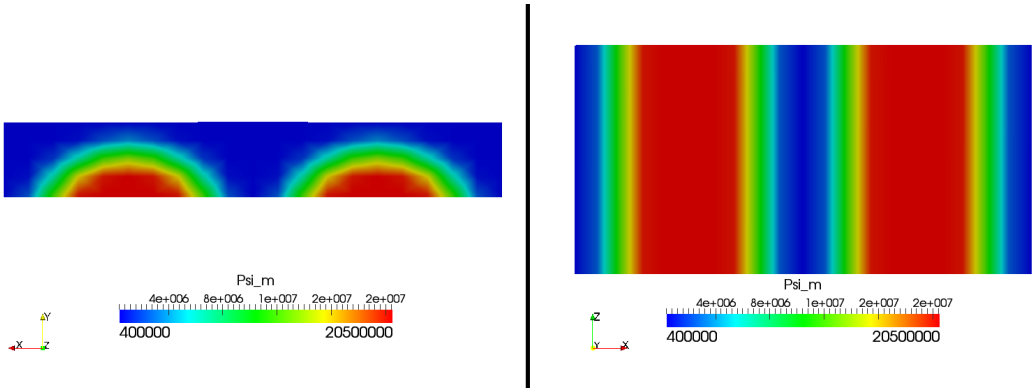

(c) $t = 39$

Figure 6.26: Fiber composite swelling, Case 4, part 2 of 2: Plots of the strain energy, Ψ_m, at different time steps. Each time step is 0.02 seconds (displacements are magnified by a factor of 50)

different for the matrix and the fibers, the body does not reach a stress free configuration in a process of free swelling.

To see where the high stresses are we made a virtual cut in the $X - Z$ plane with the origin at $\{0, 0.06, 0\}$ as shown in Figure 6.28.
With that we can see in Figure 6.29 that the high stresses occur close to the intersection between the fibers and the matrix.
Figure 6.30 shows how the magnitude of the displacement change during the change of concentration in one eighth of the body.

6.3 Uniaxial Compression with diffusion of a homogeneous diffuso-elastic material

In this section, we compare the different models for a case of combined loading. Specifically, the loading boundary conditions are as follows:

The cube is held fixed at $Z = 0$, and the edge where $Z = L_3$ (L_3 is the length of the cube in the e_3 direction), the cube is glued to a rigid surface that is displaced. On those two edges the concentration is then ramped up. Figure 6.31 shows the actual results for the four cases that were computed. It shows that the boundary conditions are identical for all four cases.
where the cases are given in the following sub-sections

6.3.1 Case 1: Fixed diffusivity with Diffuso-Elasticity

We consider the following constitutive models:

$$\begin{aligned} \tilde{\mathbf{D}} &= \tilde{\mathbf{D}}_0 \\ \mathbf{S} &= \mathbb{E} : (\mathbf{E} - \beta(\tilde{C} - \tilde{C}_0)\mathbf{I}) \\ \mathbb{E} &= \mathbb{E}_0 - \frac{\mathbb{E}_0 - \mathbb{E}_1}{Exp((-\frac{\tilde{C}_0+\tilde{C}_1}{2} + \tilde{C})/\alpha) + 1} \end{aligned} \tag{6.3.1}$$

6.3.2 Case 2: Strain dependent diffusivity

In this example we consider the following constitutive models:

$$\begin{aligned} \tilde{\mathbf{D}}(J) &= \tilde{\mathbf{D}}_0 \frac{e^J - 1}{e - 1} \\ \mathbf{S} &= \mathbb{E} : (\mathbf{E} - \beta(\tilde{C} - \tilde{C}_0)\mathbf{I}) \\ \mathbb{E} &= \mathbb{E}_0 - \frac{\mathbb{E}_0 - \mathbb{E}_1}{Exp((-\frac{\tilde{C}_0+\tilde{C}_1}{2} + \tilde{C})/\alpha) + 1} \end{aligned} \tag{6.3.2}$$

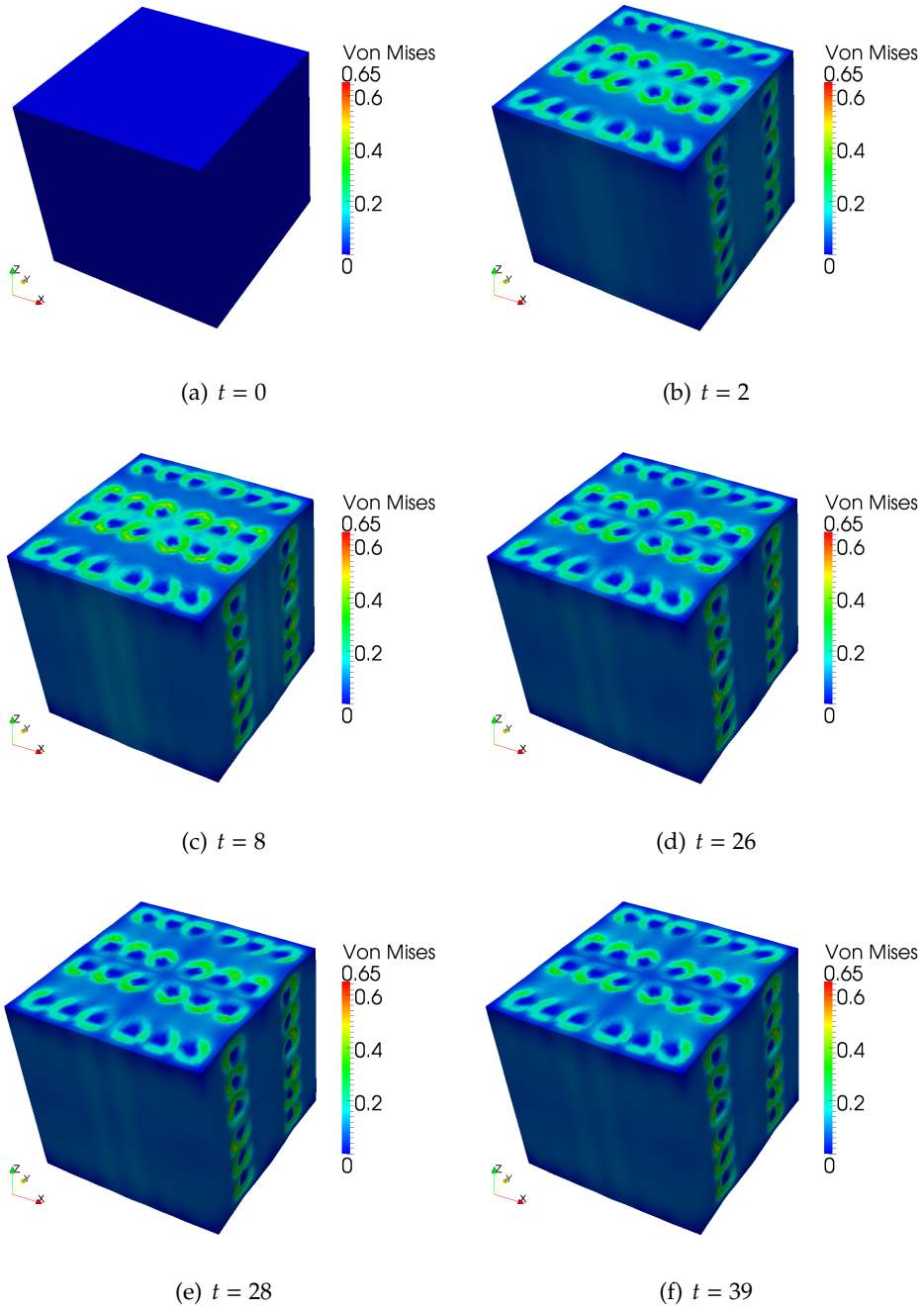

(a) $t = 0$ (b) $t = 2$

(c) $t = 8$ (d) $t = 26$

(e) $t = 28$ (f) $t = 39$

Figure 6.27: Fiber composite swelling, Case 1 and 4: Plots of the Von Mises stresses at different time steps. Each time step is 0.02 seconds (displacements are magnified by a factor of 200)

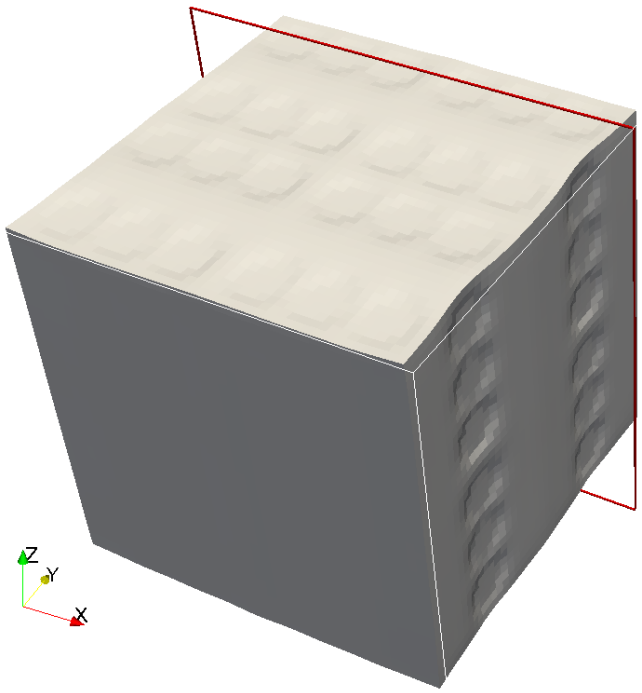

Figure 6.28: Plane cut in the fiber composite

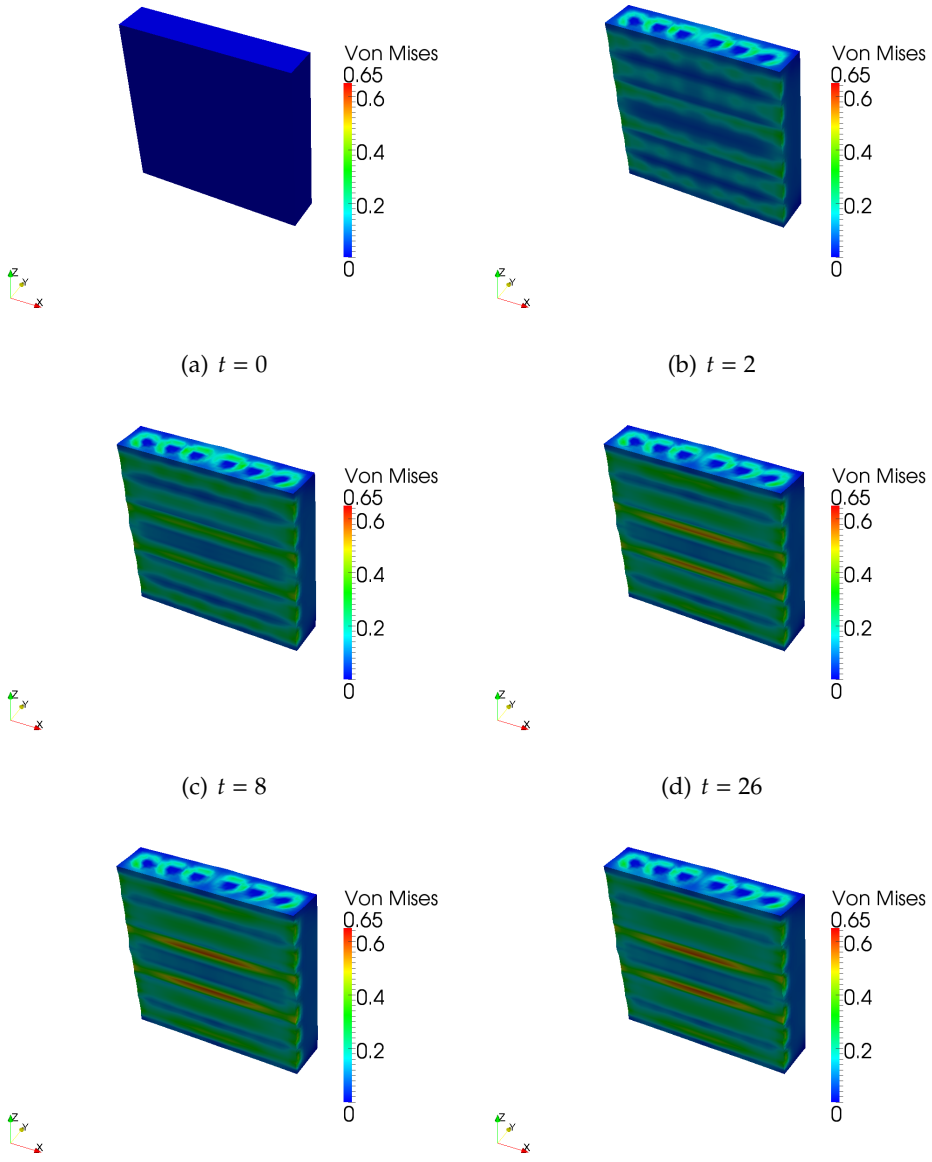

(a) $t = 0$ (b) $t = 2$

(c) $t = 8$ (d) $t = 26$

(e) $t = 28$ (f) $t = 39$

Figure 6.29: Fiber composite swelling on a plane cut, Case 1 and 4: Plots of the Von Mises stress at different time steps. Each time step is 0.02 seconds (displacements are magnified by a factor of 200)

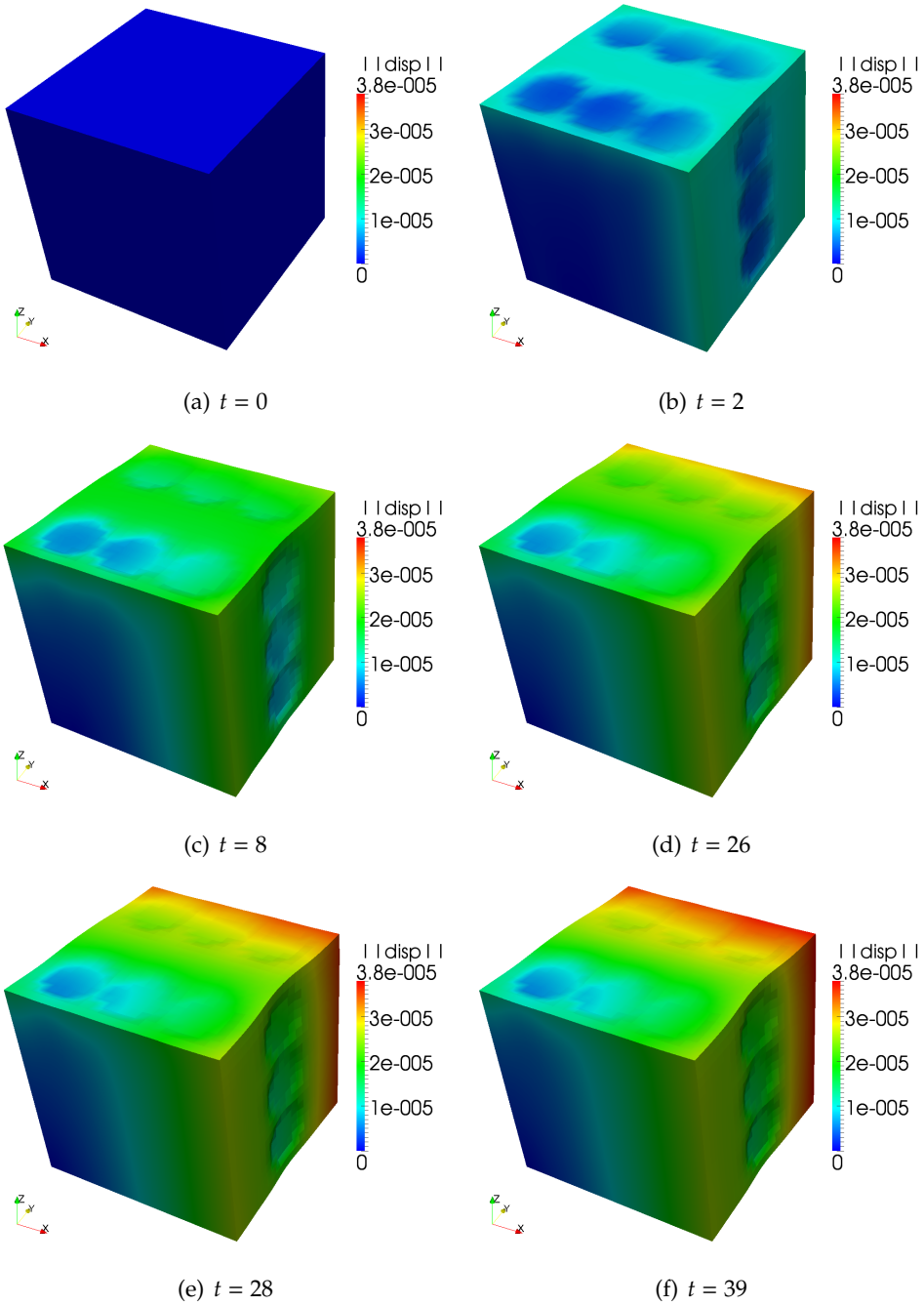

(a) $t = 0$ (b) $t = 2$

(c) $t = 8$ (d) $t = 26$

(e) $t = 28$ (f) $t = 39$

Figure 6.30: Fiber composite swelling, Case 1 and 4: Plots of the magnitude of the displacement at different time steps. Each time step is 0.02 seconds (displacements are magnified by a factor of 200). Note: only one eighth of the cube is plotted

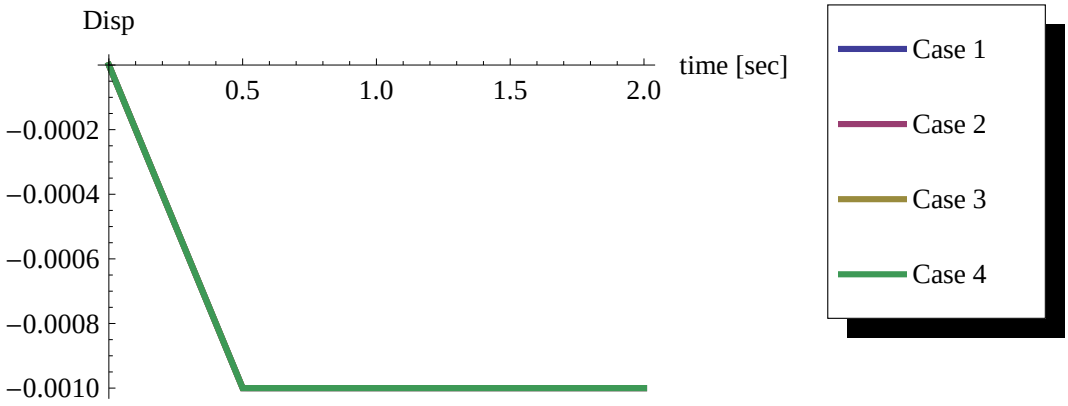

(a) Displacement BC

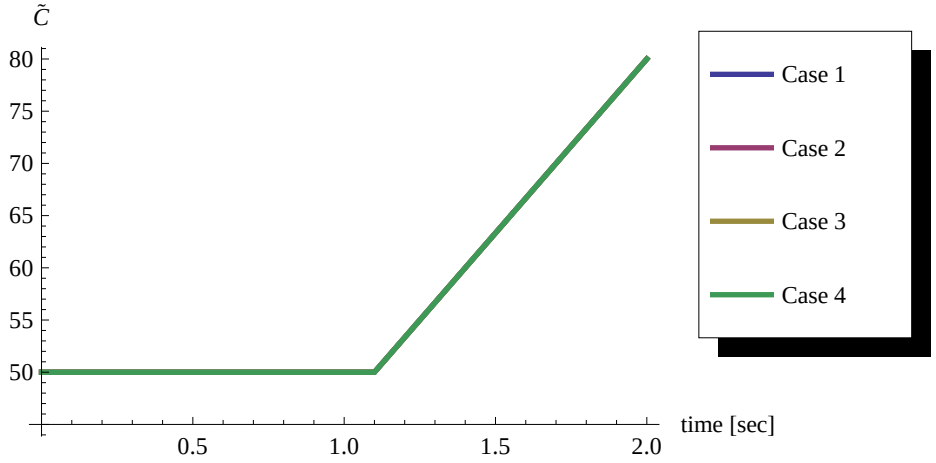

(b) Concentration BC

Figure 6.31: Plots of the concentration and displacement boundary conditions as functions of time

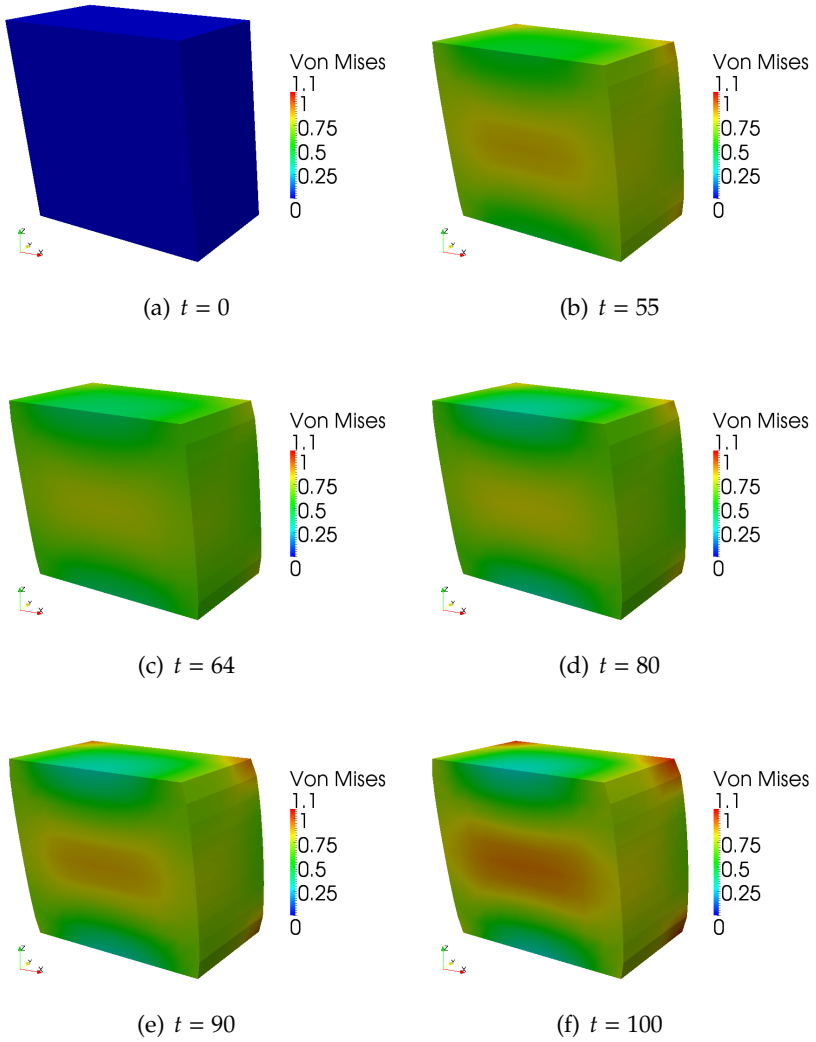

(a) $t = 0$ (b) $t = 55$

(c) $t = 64$ (d) $t = 80$

(e) $t = 90$ (f) $t = 100$

Figure 6.32: Plots of the Von Mises stress at different time steps for Case 1. Each time step is 0.02 seconds. The cube is cut in the middle with a plane $\{0, 1, 0\}$ (displacements are magnified by a factor of 10)

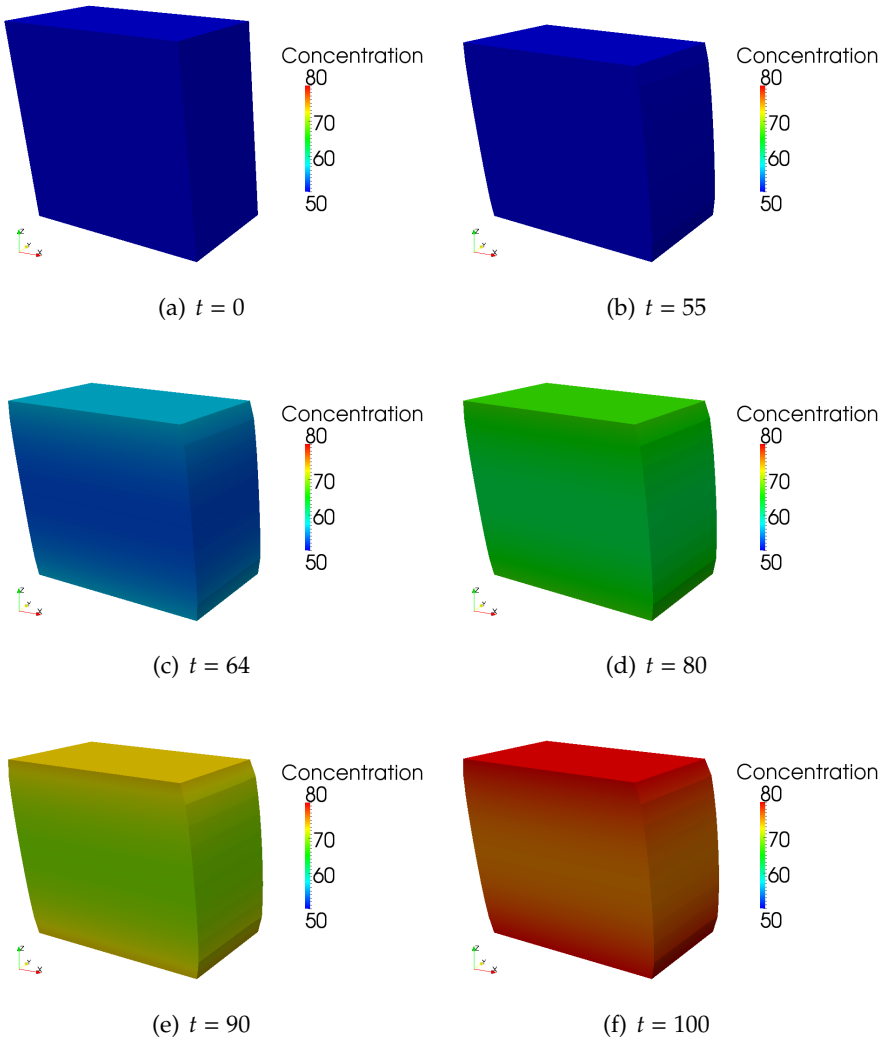

(a) $t = 0$ (b) $t = 55$

(c) $t = 64$ (d) $t = 80$

(e) $t = 90$ (f) $t = 100$

Figure 6.33: Plots of the concentration at different time steps for Case 1. Each time step is 0.02 seconds. The cube is cut in the middle with a plane $\{0, 1, 0\}$ (displacements are magnified by a factor of 10)

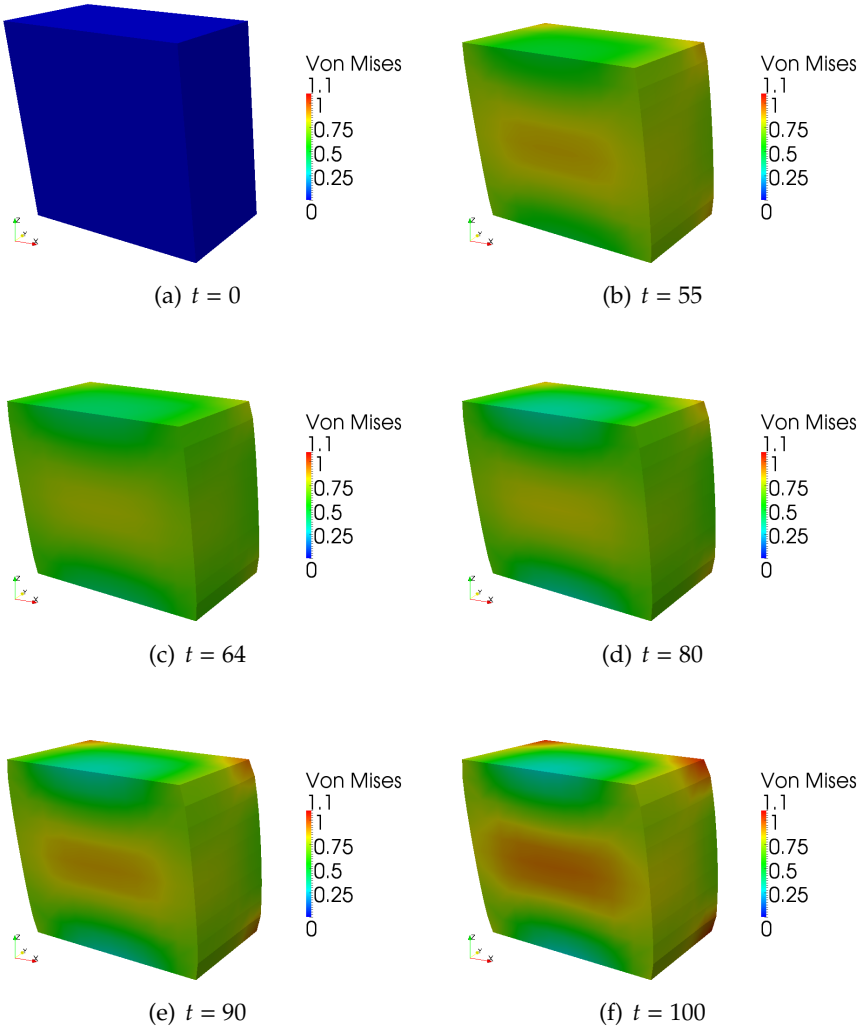

(a) $t = 0$ (b) $t = 55$

(c) $t = 64$ (d) $t = 80$

(e) $t = 90$ (f) $t = 100$

Figure 6.34: Plots of the Von Mises stress at different time steps for Case 2. Each time step is 0.02 seconds. The cube is cut in the middle with a plane $\{0, 1, 0\}$ (displacements are magnified by a factor of 10)

6.3.3 Case 3: Saturation

In this example we consider the following constitutive models:

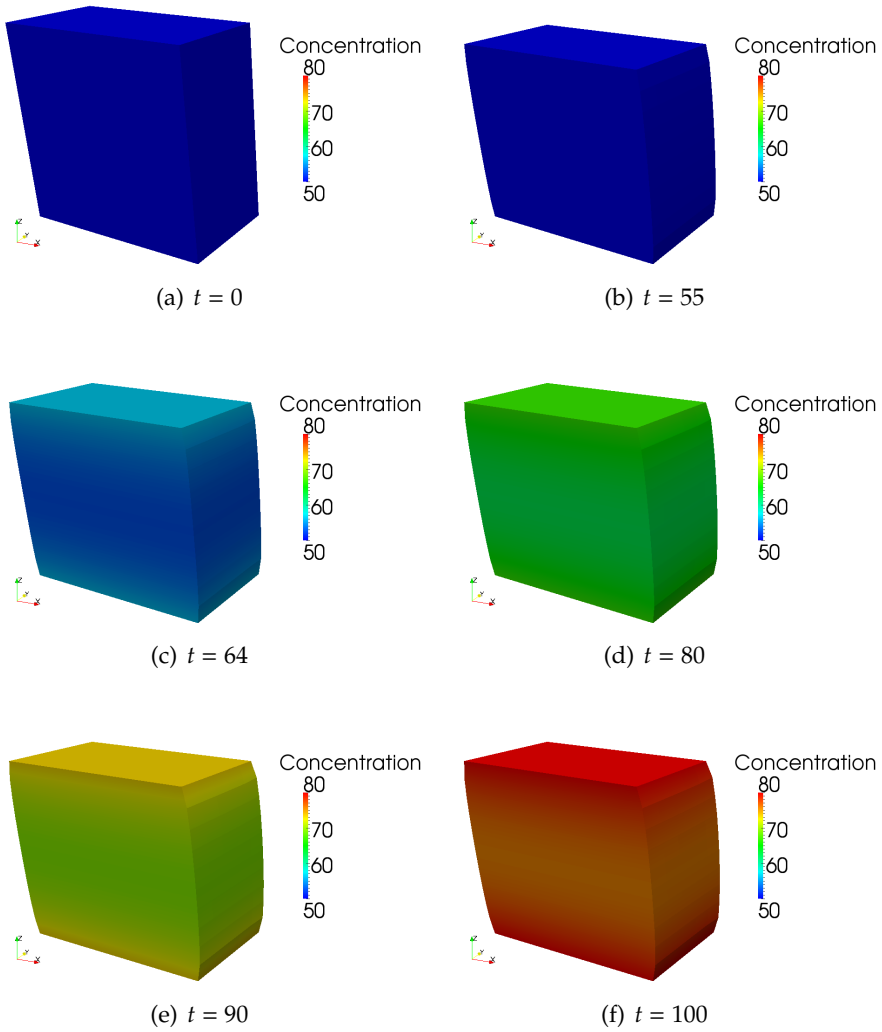

(a) $t = 0$ (b) $t = 55$

(c) $t = 64$ (d) $t = 80$

(e) $t = 90$ (f) $t = 100$

Figure 6.35: Plots of the concentration at different time steps for Case 2. Each time step is 0.02 seconds. The cube is cut in the middle with a plane $\{0, 1, 0\}$ (displacements are magnified by a factor of 10)

$$\begin{aligned}
\tilde{\mathbf{D}}(\tilde{C}) &= \tilde{\mathbf{D}}_0 - \frac{\tilde{\mathbf{D}}_0}{Exp((\frac{\tilde{C}_0+\tilde{C}_1}{2} - \tilde{C})/\alpha) + 1} \\
\mathbf{S} &= \mathbb{E} : (\mathbf{E} - \beta(1 - \frac{1}{Exp((-\frac{\tilde{C}_0+\tilde{C}_1}{2} + \tilde{C})/\alpha) + 1})\mathbf{I}) \\
\mathbb{E} &= \mathbb{E}_0 - \frac{\mathbb{E}_0 - \mathbb{E}_1}{Exp((-\frac{\tilde{C}_0+\tilde{C}_1}{2} + \tilde{C})/\alpha) + 1}
\end{aligned} \tag{6.3.3}$$

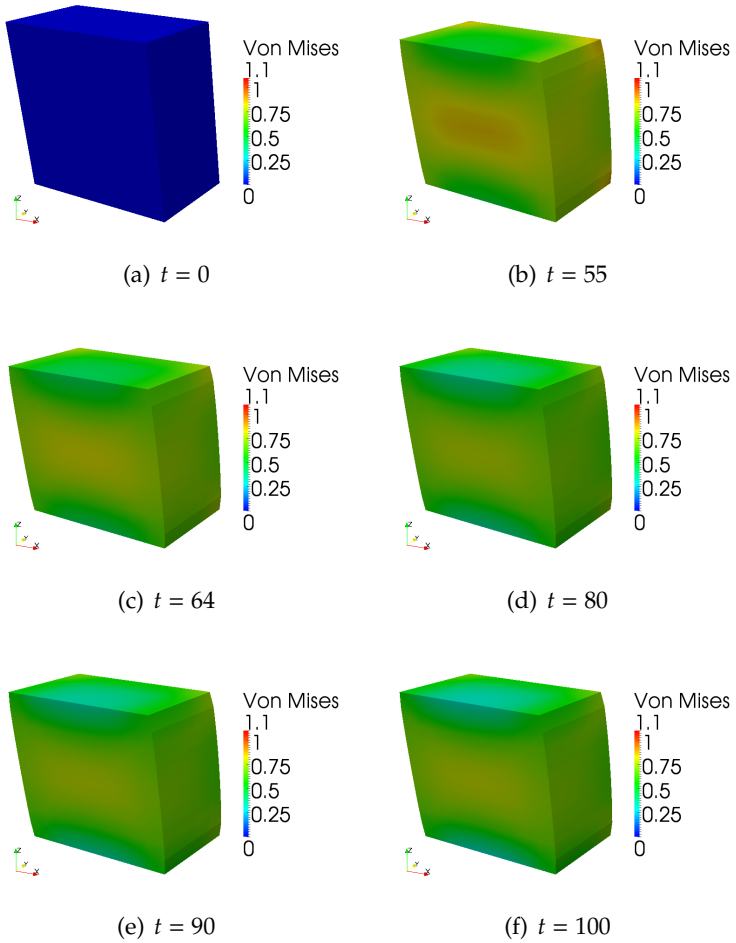

(a) $t = 0$ (b) $t = 55$

(c) $t = 64$ (d) $t = 80$

(e) $t = 90$ (f) $t = 100$

Figure 6.36: Plots of the Von Mises stress at different time steps for Case 3. Each time step is 0.02 seconds. The cube is cut in the middle with a plane $\{0, 1, 0\}$ (displacements are magnified by a factor of 10)

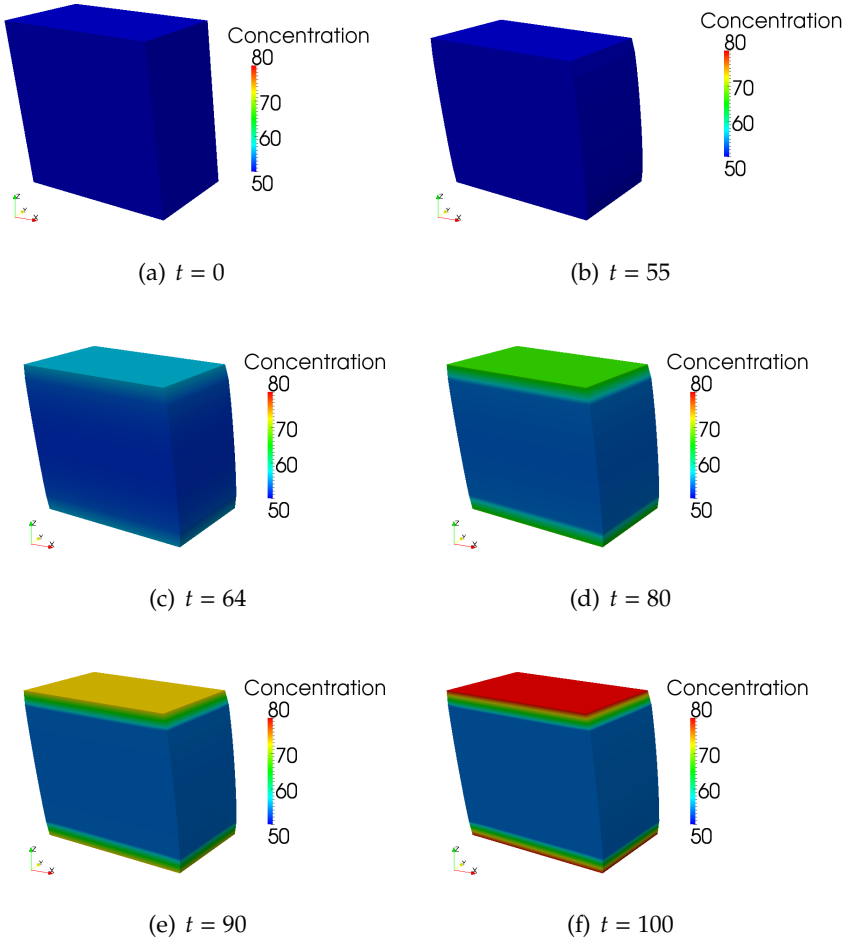

(a) $t = 0$ (b) $t = 55$

(c) $t = 64$ (d) $t = 80$

(e) $t = 90$ (f) $t = 100$

Figure 6.37: Plots of the concentration at different time steps for Case 3. Each time step is 0.02 seconds. The cube is cut in the middle with a plane $\{0, 1, 0\}$ (displacements are magnified by a factor of 10)

6.3.4 Case 4: Nonuniform diffusion induced strain

In this example we consider the following constitutive models:

$$\begin{aligned} \tilde{\mathbf{D}} &= \tilde{\mathbf{D}}_0 \\ \mathbf{S} &= \mathbb{E} : (\mathbf{E} - \beta(\tilde{C} - \tilde{C}_0)(\mathbf{I} - \mathbf{M} \otimes \mathbf{M})) \\ \mathbb{E} &= \mathbb{E}_0 - \frac{\mathbb{E}_0 - \mathbb{E}_1}{Exp((-\frac{\tilde{C}_0 + \tilde{C}_1}{2} + \tilde{C})/\alpha) + 1} \end{aligned} \tag{6.3.4}$$

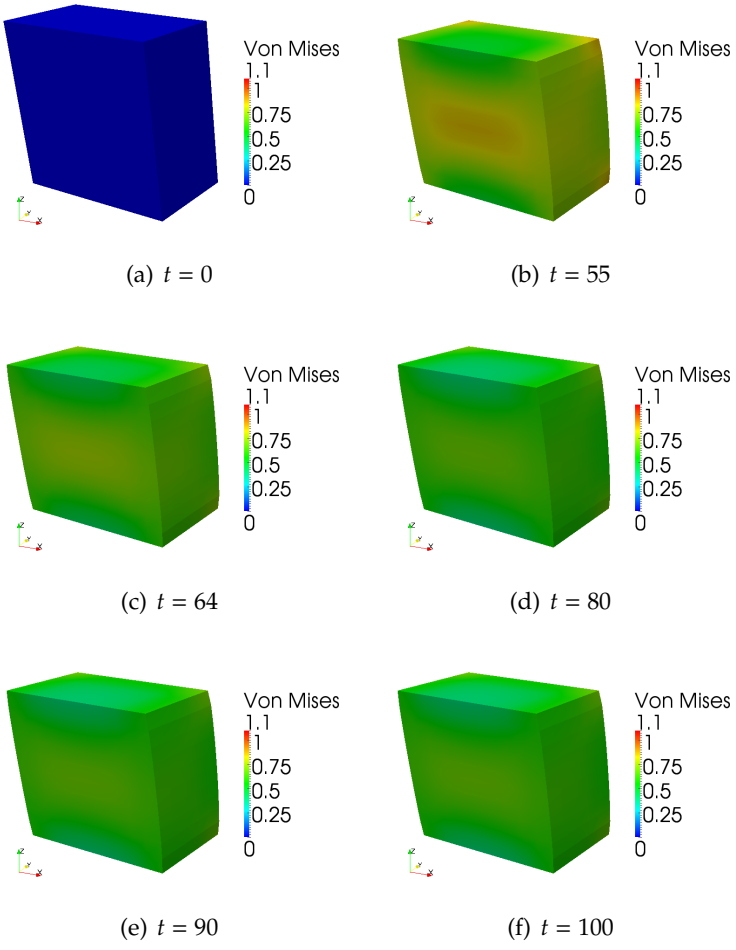

(a) $t = 0$ (b) $t = 55$

(c) $t = 64$ (d) $t = 80$

(e) $t = 90$ (f) $t = 100$

Figure 6.38: Plots of the Von Mises stress at different time steps for Case 4. Each time step is 0.02 seconds. The cube is cut in the middle with a plane $\{0, 1, 0\}$ (displacements are magnified by a factor of 10)

With all the cases introduced, we show several scalar physical quantities that can

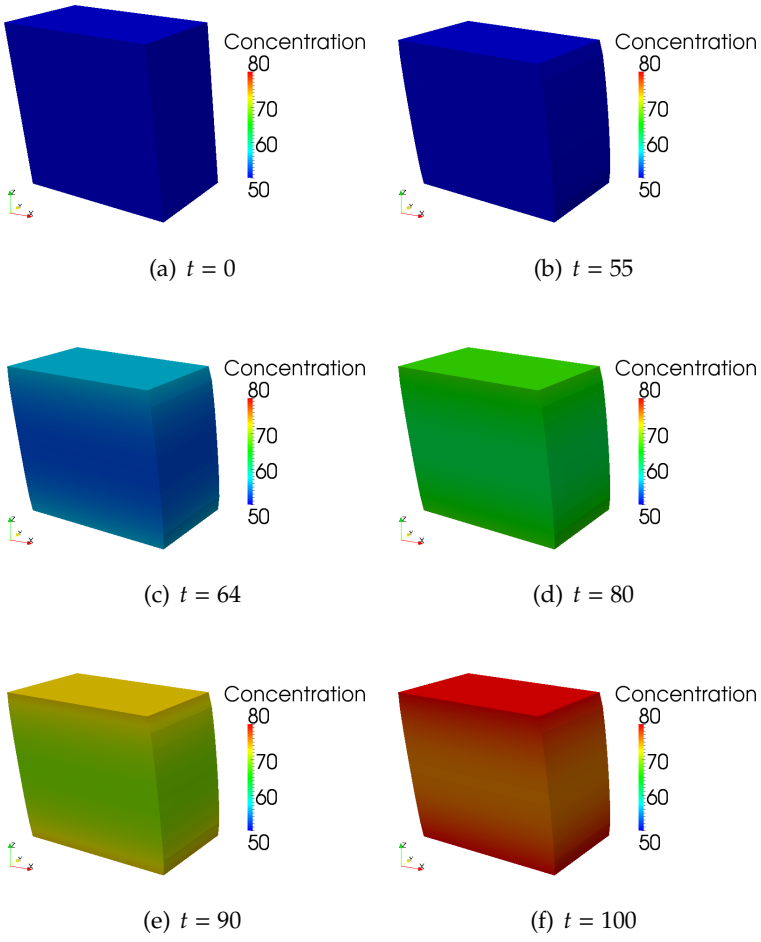

(a) $t = 0$ (b) $t = 55$

(c) $t = 64$ (d) $t = 80$

(e) $t = 90$ (f) $t = 100$

Figure 6.39: Plots of the concentration at different time steps for Case 4. Each time step is 0.02 seconds. The cube is cut in the middle with a plane $\{0, 1, 0\}$ (displacements are magnified by a factor of 10)

be use to compare and show differences between the cases.

Figure 6.40 (a) shows the change of non dimensional total mass of the body (divided by its initial mass) as a function of time. The plots of Cases 1, 2, and 4 lie one on top of the other. The curves rise in a linear manner after the concentration starts to ramp up on the boundaries. For Case 3 (saturation), we see that the curve does not rise in a linear manner, it seems to rise asymptotically to a constant value which is the saturation point of the body.

Figure 6.40 (b) shows the change of non dimensional total volume of the body (divided by its initial volume) as a function of time. The plots of Cases 1 and 2 lie one on top of the other. The curves rise in a linear manner after the concentration starts to ramp up on the boundaries. For Case 3 (saturation), we see that the curve does not rise in a linear manner, it seems to rise asymptotically to a constant value which is the saturation point of the body. For Case 4 (Non uniform diffusion induced strain), there is a very small change in the volume. That is due to the fact that the direction of the vector **M** is such that the deformation induced by diffusion is constrained by the boundary conditions.

Figure 6.41 (a) shows the change of the strain energy of the body, Ψ_m, as a function of time. The plots of Cases 1 and 2 lie one on top of the other. The value drops after the concentration starts to ramp up on the boundaries as a result of the softening effect (diffuso elasticity). After some time, the value starts to rise as a result of the deformations induced by the diffusion process. For Case 3 (saturation), we see that drops asymptotically to a constant value which is the saturation point of the body. It does not rise, because the concentration levels remain the same even though it changes on the boundary. For Case 4 (Nonuniform diffusion induced strain), the value drops similar to Cases 1 and 2, but it does not rise from that level. That is due to the fact that the direction of the vector **M** is such that the deformation induced by diffusion is constrained by the boundary conditions.

Figure 6.41 (b) shows the change of coupled energy term of the body, Ψ_{md}, as a function of time. The behavior is very similar to figure 6.41 (a).

Figure 6.41 (c) shows the change of diffusion energy of the body, Ψ_d, as a function of time. The plots of Cases 1, 2 and 4 lie one on top of each other. The curves rise as the concentration ramps up on the boundaries. For Case 3 (saturation), we see that the curve does not rise in a same manner, it seems to rise at a slower rate.

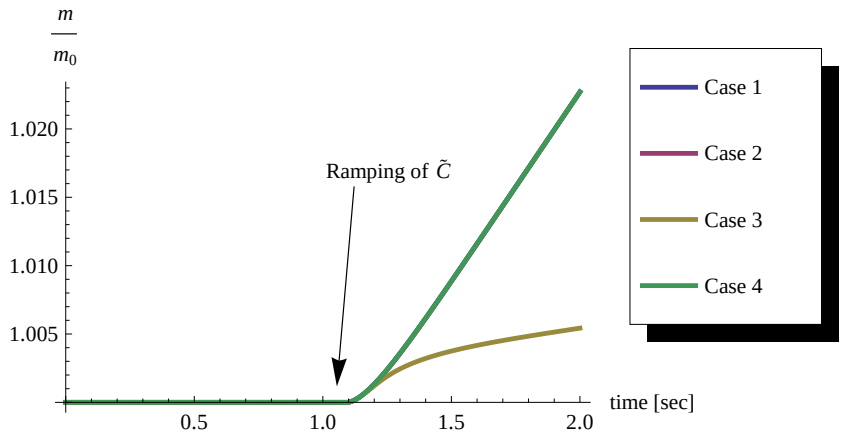

(a) Nondimensional mass as a function of time

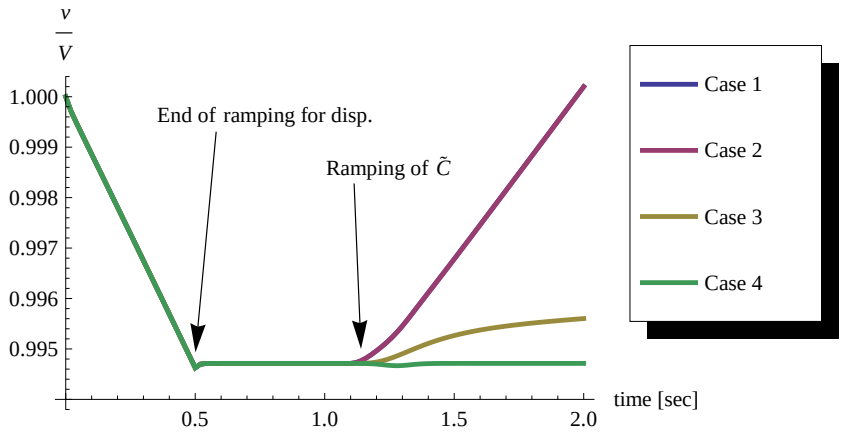

(b) Nondimensional volume as a function of time

Figure 6.40: Plots of the non dimensional mass and volume as functions of time

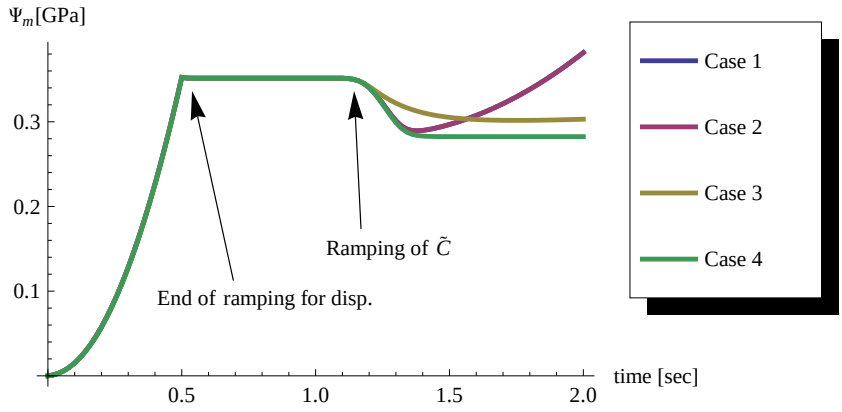

(a) The strain energy Ψ_m as a function of time

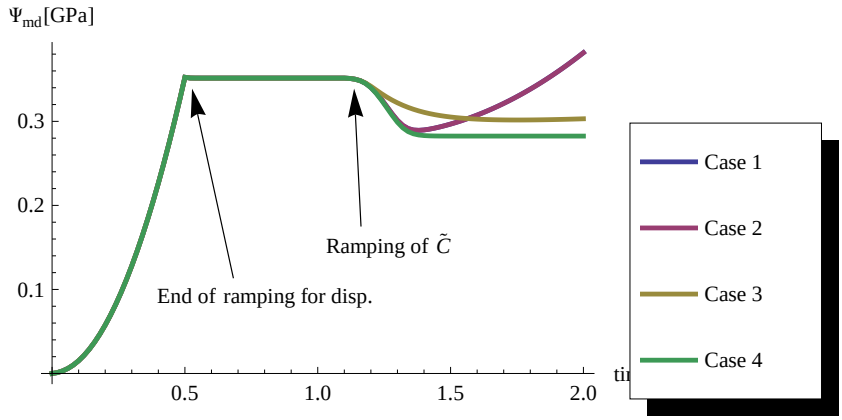

(b) The coupled term of internal energy Ψ_{md} as a function of time

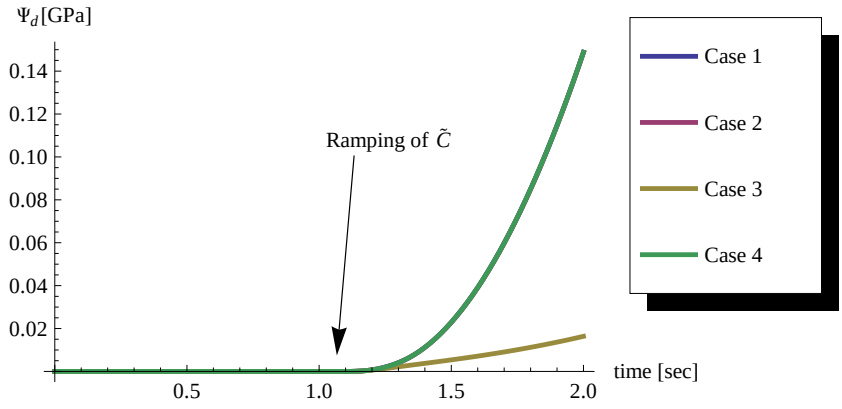

(c) The diffusion part of the internal energy Ψ_d as a function of time

Figure 6.41: Components of the internal energy in the body: Ψ_m, Ψ_{md} and Ψ_d

Chapter 7

Conclusions

To conclude the work presented here we summarize the analytical and numerical development done and discuss the results from the different examples that were shown here.

7.1 Analytical modeling

An analytical model of the coupling between the diffusion process and the deformation of a solid was developed, and the following new models were presented:
-Strain dependent diffusivity: The diffusion tensor depends on the volumetric strain $J = det(\mathbf{F})$. Therefore the diffusion processes is different for the same body in different configurations.
-Saturation: The diffusion tensor depends on the concentration and changes its values over a range of values of concentrations. Beyond a certain material constant, $\tilde{C}_1$, the diffusivity tensor reaches zero and causes the diffusion process to stop. This causes the body to saturate, even if the concentration boundary conditions are higher then within the body.
-Non uniform strains induced by diffusion: The strains induced by diffusion are not uniform and produce non uniform stresses. It should be noted that this is a material characteristic that is not related to the mechanical anisotropy of the material. This means that the material can deform in an isotropic manner due to mechanical loads, and deform in a non uniform manner due to the diffusion process.
-Diffuso-elasticity: Similar to thermoelasticity, the mechanical material constants can change in value due to a change in concentration. This change is constrained to a specific range in concentration, which is also a material specified quantity, after which the values of the constants plateau and remain constant for higher levels of concentrations.

7.2 Numerical modeling

With the analytical equations at hand, the time dependent equations are discretized using a finite difference scheme, and the spatial part is discretized using a non-linear finite element formulation. The coupling between the equations is solved using a

staggering method, which appeared to be of advantage since the equations are of different orders of magnitude. For the solution of the nonlinear algebraic equations the *fixed point iteration* scheme was implemented. This was easy to implement compared to Newton's method, because it does not require to compute a tangent stiffness. In terms of convergence, Newton's method has a higher order of convergence, but the computational cost of the tangent stiffness is also a factor to consider. Over all, the method performed well.

7.3 Results

Looking at the examples provided in this work, we observe the general behavior of the analytical and numerical models, and the difference between the different cases defined previously.

Free swelling of a homogeneous material

The main purpose of this section is to examine the effects of different constitutive models that were developed in this study, on a homogeneous material. In this case the body was able to reach a stress-free steady state, as a homogeneous level of concentration was reached. We looked at the Von Mises stresses, and the magnitude of the displacements for all the cases defined and compared them. We also looked at scalar quantities such as mass, volume, and energy. The results show how the models differ from each other, and how the coupling works. It also shows that the numerical modeling is working well.

Free swelling of a fiber composite material

The main purpose of this section is to see how a non-homogeneous material, like a fiber composite, is effected by the different constitutive models. We also looked at how the deformations and concentrations change compared to a homogeneous material. In this case the body was able to reach a stress-free steady state, only if the diffusion characteristics were identical for the fibers and the matrix. In addition to the results discussed for a homogeneous material, we also looked at the strain energy levels in the fibers and matrix, and the displacement of the fibers in relation to the matrix. The deformations are more complex, compared to a homogeneous material, and there are major differences in stresses and displacements. For the case where the fibers have the same coupling terms as the matrix, we saw that stresses were induced during the redistribution of the diffusing phase in the body, as expected, and that the deformations and stresses in the fibers were different than the matrix as a result of different mechanical properties. At steady state the body reached a point of zero stresses. For the case where the fibers and matrix have different coupling terms, the body reached a non-zero stresses at steady state, as expected.

Uniaxial Compression with diffusion of a homogeneous diffuso-elastic material

In this chapter, we looked at two different aspects: the first was another constitutive model, namely diffuso-elasticity, where material softening due to a change in

concentration was examined. The second was combined loading, where we examined the coupling between the mechanical loads and the diffusion process. We found that the constitutive models perform well, and that the coupling causes noticeable effects of loading and deformations on the concentrations, and vice versa. We saw that the mass, volume, and energy are affected by the combination of mechanical and diffusion loadings and that they are different for different cases (Cases 1-4).

7.4 General Remarks

It is worth noting here that most of the constitutive models shown here can be combined with each other, and create a more complex model that involves different physical phenomena. An example was shown in chapter 6.3, where diffuso-elasticity was combined with Cases 1-4. That created different models that combined, for example, diffuso-elasticity with saturation.
In general, the analytical models were able to successfully describe different physical phenomena, and the numerical tools were robust enough to simulate different cases, including homogeneous and non homogeneous materials, and combined loading.

Bibliography

[1] J.W. Gibbs. *Scientific papers of J. Willard Gibbs*. Longmans, Green and co., 1st edition, 1906.

[2] M.A. Biot. General theory of three-dimensional consolidation. *Journal of applied physics*, 12(2):155, 1941.

[3] C. Truesdell. Mechanical basis of diffusion. *The Journal of Chemical Physics*, 37:2336, 1962.

[4] AE Green and JE Adkins. A contribution to the theory of non-linear diffusion. *Archive for Rational Mechanics and Analysis*, 15(3):235–246, 1964.

[5] JE Adkins. Diffusion of fluids through aeolotropic highly elastic solids. *Archive for Rational Mechanics and Analysis*, 15(3):222–234, 1964.

[6] JE Adkins. Non-Linear Diffusion III. Diffusion through Isotropic Highly Elastic Solids. *Philosophical Transactions for the Royal Society of London. Series A, Mathematical and Physical Sciences*, 256(1071):301–316, 1964.

[7] DJ Unger and EC Aifantis. On the theory of stress-assisted diffusion, II. *Acta Mechanica*, 47(1):117–151, 1983.

[8] RK Wilson and EC Aifantis. On the theory of stress-assisted diffusion, I. *Acta Mechanica*, 45(3):273–296, 1982.

[9] EC Aifantis. On the problem of diffusion in solids. *Acta Mechanica*, 37(3):265–296, 1980.

[10] KR Rajagopal. Diffusion through polymeric solids undergoing large deformations. *Materials Science and Technology*, 19(9):1175–1180, 2003.

[11] S. Baek and AR Srinivasa. Diffusion of a fluid through an elastic solid undergoing large deformation* 1. *International Journal of Non-Linear Mechanics*, 39(2):201–218, 2004.

[12] W. Hong, X. Zhao, J. Zhou, and Z. Suo. A theory of coupled diffusion and large deformation in polymeric gels. *Journal of the Mechanics and Physics of Solids*, 56(5):1779–1793, 2008.

[13] H. Mehrer. *Diffusion in solids*. Springer Berlin, Heidelberg, New York, 2007.

[14] J. Crank. *The mathematics of diffusion*. Oxford University Press, USA, 1979.

[15] W. Hong, Z. Liu, and Z. Suo. Inhomogeneous swelling of a gel in equilibrium with a solvent and mechanical load. *International Journal of Solids and Structures*, 46(17):3282–3289, 2009.

[16] J. Zhang, X. Zhao, Z. Suo, and H. Jiang. A finite element method for transient analysis of concurrent large deformation and mass transport in gels. *Journal of Applied Physics*, 105:093522, 2009.

[17] MV Paukshto. Diffusion-induced stresses in solids. *International Journal of Fracture*, 97(1):227–236, 1999.

[18] X. Tang, J.D. Whitcomb, Y. Li, and H.J. Sue. Micromechanics modeling of moisture diffusion in woven composites. *Composites Science and Technology*, 65(6):817–826, 2005.

[19] Y.T. Yu and K. Pochiraju. Three-dimensional simulation of moisture diffusion in polymer composite materials. *Polymer-Plastics Technology and Engineering*, 42(5):737–756, 2003.

[20] TI Zohdi. Modeling and simulation of a class of coupled thermo-chemo-mechanical processes in multiphase solids. *Computer Methods in Applied Mechanics and Engineering*, 193(6-8):679–699, 2004.

[21] F.P. Duda, JMA Barbosa, L.J. Guimarães, A.C. Souza, C.U. PEM-COPPE, and RJ Rio de Janeiro. Modeling of Coupled Deformation-Diffusion-Damage in Elastic Solids. *International Journal of Modeling and Simulation for the Petroleum Industry*, 1(1), 2007.

[22] W. Wang, M. Sain, and PA Cooper. Study of moisture absorption in natural fiber plastic composites. *Composites science and technology*, 66(3-4):379–386, 2006.

[23] X. Chen, S. Zhao, and L. Zhai. Moisture absorption and diffusion characterization of molding compound. *Journal of Electronic Packaging*, 127:460, 2005.

[24] L. Li, Y. Chen, and S. Li. Water diffusion behavior in epoxy resins with various fluorine contents. *Applied spectroscopy*, 60(4):392–397, 2006.

[25] C. Wang, J. Wang, and T. Su. Determination of Water Diffusion Coefficients and Dynamics in Adhesive/Carbon Fiber–Reinforced Phenolic Resin Composite Joints. *The Journal of Adhesion*, 83(3):255–265, 2007.

[26] M. Al-Harthi, K. Loughlin, and R. Kahraman. Moisture diffusion into epoxy adhesive: testing and modeling. *Adsorption*, 13(2):115–120, 2007.

[27] EC Botelho. Evaluation by Free Vibration Method of Moisture Absorption Effects in Polyamide/Carbon Fiber Laminates. *Journal of Thermoplastic Composite Materials*, page 0892705709342614v1, 2009.

[28] S. Laurenzi, T. Albrizio, and M. Marchetti. Modeling of Moisture Diffusion in Carbon Braided Composites. *International Journal*, 2008.

[29] G. Sala. Composite degradation due to fluid absorption. *Composites Part B: Engineering*, 31(5):357–373, 2000.

[30] L.R. Bao and A.F. Yee. Moisture diffusion and hygrothermal aging in bismaleimide matrix carbon fiber composites: part II–woven and hybrid composites. *Composites Science and Technology*, 62(16):2111–2119, 2002.

[31] T.A. Bullions, AC Loos, and JE McGrath. Moisture sorption effects on and properties of a carbon fiber-reinforced phenylethynyl-terminated poly (etherimide). *Journal of Composite Materials*, 37(9):791, 2003.

[32] C. Hou, Y. Liang, and C.G. Wang. Determination of the Diffusion Coefficient of H 2 O in Polyacrylonitrile Fiber Formation. *Journal of Polymer Research*, 12(1):49–52, 2005.

[33] MH Shirangi, XJ Fan, and B. Michel. Mechanism of moisture diffusion, hygroscopic swelling and adhesion degradation in epoxy molding compounds. In *Proceedings of forty-first international symposium on microelectronics (IMAPS)*, pages 917–23, 2008.

[34] NL Post, F. Riebel, A. Zhou, T. Keller, SW Case, and JJ Lesko. Investigation of 3D Moisture Diffusion Coefficients and Damage in a Pultruded E-glass/Polyester Structural Composite. *Journal of Composite Materials*, 2008.

[35] SB Kumar, I. Sridhar, and S. Sivashanker. Influence of humid environment on the performance of high strength structural carbon fiber composites. *Materials Science and Engineering: A*, 498(1-2):174–178, 2008.

[36] Gerhard A. Holzapfel. *Nonlinear Solid Mechanics*. Wiley, 1st edition, 2007.

[37] O. C. Zienkiewicz and R. L. Taylor. *The Finite Element Method*, volume 1. McGraw Hill Book Company, London, 5th edition, 2000.

[38] Ted Belytschko, Wing Kam Liu, and Brian Moran. *Nonlinear Finite Elements for Continua and Structures*. Wiley, 1st edition, 2004.

[39] Dietrich Braess. *Finite elements Theory, fast solvers, and applications in solid mechanics*. Cambridge, 2nd edition, 2001.

[40] E. Hairer, S.P. Nørsett, and G. Wanner. *Solving ordinary differential equations: Nonstiff problems*. Springer, 1993.

[41] E. Hairer and G. Wanner. *Solving ordinary differential equations II: Stiff and differential-algebraic problems*. Springer, 2010.